5-9-2024

αB-Crystallin Phosphorylation Induces a Condensatopathy to Worsen Post-Myocardial Infarction Cardiomyopathy

Md Moydul Islam
Washington University in St. Louis

WASHINGTON UNIVERSITY IN ST. LOUIS

Department of Chemistry

Dissertation Examination Committee:
Kevin Moeller, Chair
Douglas Covey
Abhinav Diwan
Michael Gross
Xiucui Ma
Yusuke Okuno

αB-Crystallin Phosphorylation Induces a Condensatopathy to Worsen Post-Myocardial Infarction Cardiomyopathy

by

Md Moydul Islam

A dissertation presented to
Washington University in St. Louis
in partial fulfillment of the
requirements for the degree
of Doctor of Philosophy

May 2024
St. Louis, MO

Table of Contents

List of Figures

List of Tables

Acknowledgments

I would like to express my deepest gratitude to my family, friends, and lab members whose unwavering support and encouragement sustained me throughout the challenging journey of completing this doctoral thesis. Their belief in my abilities and constant encouragement provided the foundation for my success. I am immensely grateful to my thesis supervisor, Professor Abhinav Diwan, for his guidance, expertise, and continuous support. His insightful feedback and constructive criticism were invaluable in shaping the direction of my research. I would also like to extend my appreciation to my thesis committee members, Dr. Kevin Moeller, Dr. Michael Gross, Dr. Douglas Covey, Dr. Yusuke Okuno, and Dr. Xiucui Ma, for their time, expertise, and valuable contributions to this work.

After the challenging time of the global COVID-19 pandemic in the year 2020, the passing of my father in May 2021 deeply affected me, adding an extra layer of complexity to the doctoral journey. However, the unwavering support I received from my Bangladeshi friends in St. Louis and my lab members played a crucial role in helping me navigate through this difficult period and stay strong. Their empathy, kindness, and understanding created a supportive environment that allowed me to focus on my research despite the personal challenges. My younger brother, Masrur, provided continuous mental support to my mother in my absence. Both my mother and younger brother have taught me how to stay strong as a family and take care of each other during the times of challenge.

Additionally, the sense of camaraderie within the academic community in the Center for Cardiovascular Research at Wash U Medical School and the compassion extended by my department colleagues further contributed to my ability to stay motivated during the challenging period of my doctoral journey. This journey has been made meaningful and fulfilling by the collective support of my loved ones, mentors, and the academic community.

Md Moydul Islam

Washington University in St. Louis

May 2024

Dedicated to my parents.

ABSTRACT OF THE DISSERTATION

CRYAB Phosphorylation Induces a Condensatopathy to Worsen Post-Myocardial Infarction Cardiomyopathy

by

Md Moydul Islam

Doctor of Philosophy in Chemistry

Washington University in St. Louis, 2024

Professor Abhinav Diwan, Advisor

Rare genetic mutations in proteins expressed in cardiomyocytes lead to proteotoxic cardiomyopathies which are characterized by widespread protein-aggregate pathology. However, the mechanistic link between proteotoxicity and protein-aggregates in the more common ischemic cardiomyopathy remains unclear. Our study revealed the mis-localization of desmin, actin, and α-actinin to protein-aggregates in the myocardium of patients with ischemic cardiomyopathy and in mice hearts undergoing post-myocardial infarction ventricular remodeling. These findings mimic observations in autosomal-dominant cardiomyopathy resulting from the R120G mutation in the chaperone protein CRYAB where desmin is mis-localized into the aggregates. Importantly, we observed increased phosphorylation of CRYAB at serine-59 (pS59CRYAB) and its accumulation in the NP40-insoluble aggregate-rich fraction. Further investigation showed that CRYAB undergoes phase separation, and mimicking phosphorylation at serine-59 with an aspartate substitution reduced the fluidity of CRYAB condensates, promoting protein-aggregate formation and increased cell death. Conversely,

substituting serine-59 with alanine, by preventing phosphorylation, restored the fluidity of CRYAB condensates and reduced protein aggregation. Moreover, introducing a phospho-deficient S59A mutation, but not the phospho-mimetic S59D mutation, at the CRYAB locus in mice rescued adverse left ventricular remodeling after ischemia reperfusion injury. Treatment with 25-Hydroxycholesterol attenuated serine-59 phosphorylation, increasing the fluidity of R120G-CRYAB condensates, and ameliorating post-myocardial infarction cardiac dysfunction. Experimental interventions aimed at preventing aggregate formation or promoting disaggregation exacerbated post-myocardial infarction cardiomyopathy, highlighting the importance of pS59CRYAB sequestration in aggregates to attenuate disease progression. These findings suggest that modulating CRYAB phase separation could offer a promising approach to mitigating ischemic cardiomyopathy.

Chapter 1: Introduction

1.1 Membrane-less compartmentalization in cells

Eukaryotic cells contain membrane-bound compartments or organelles so that specific biochemical reactions and metabolism can occur in a specified and controlled manner[1]. Lysosomes[2], endosomes[3], endoplasmic reticulum[4], Golgi[5], and Mitochondria[6] are some of the membrane-bound organelles. For example: lysosomes are membrane-enclosed organelles harboring hydrolytic enzymes that can degrade nucleic acids, proteins, carbohydrates, and lipids[2] and they are crucial in protein quality control. Mitochondria are crucial in multiple biological functions such as ATP production, regulation of intracellular communication, apoptotic cell death regulation, production and scavenging of reactive oxygen species [6]. Exchange of signaling molecules or materials between the membrane-bound organelles and the environment surrounding them includes various cellular activities such as transport facilitated by transmembrane proteins, diffusion, vesicle trafficking etc[1]. Interestingly, in addition to the membrane-bound compartments, presence of membrane-less organelles or compartments or condensates in the eukaryotic cells are also observed[1]. One of the earliest examples of membrane-less compartment discovery was done by Ramon y Cajal at the beginning of the 20th century[7]. Since then, different types of membrane-less compartments such as stress granules, nuclear stress bodies, nuclear speckles, nucleolus, etc. have been characterized[8]. Membrane-less compartments are typically within 0.2–2 μm in size, comprised of different shapes, and can contain both nucleic acids and proteins[1]. Interestingly, membrane-less compartments behave similar to liquid droplets when biophysical properties are considered[9]. Like membrane-bound organelles, membrane-less organelles are also functional compartments. Cellular functions such

as cell division[10], cell adhesion[11], autophagy[12], endocytosis[13], mRNA splicing[14], DNA repair[15], innate and adaptive immune signaling[16,17] have been implicated in membrane-less compartments similar to membrane bound compartments. In summary, biomolecular condensates regulate both cellular structure and biochemistry[18]. However, owing to the liquid-droplet-like nature of biomolecular condensates, they can be dynamic, short-lived, and might form in a contextual-based manner. One of the examples is stress granules which are formed when cells are required to deal with stress[8]. They are 0.1-2 μm in size, localize in the cytoplasm, and function in RNA storage, decay, and translation.

In addition to having physiological functions in the cells, membrane-less compartments are also associated with disease states[19]. Physiological condensates transform into pathological condensates by several mechanisms such as disruption, dissolution, or alteration[18]. Interestingly, de-novo pathological condensates can also form by aberrant signaling. For example, altered expression of ribosomal proteins in nucleolus was observed in cancer[19]. Another example is the formation of FUS CHOP by aberrant transcriptional activity[20]. FUS CHOP is the fusion oncoprotein in Myxoid Sarcoma[20]. Studies have shown that knockdown of FUS CHOP can show therapeutic benefit[21]. Condensates are observed to have pathological effects by forming protein aggregates or misfolded peptide complexes[22]. Protein aggregates are less dynamic or exist in solid-like state that may include the transition from a liquid-like state[22]. Protein aggregates show a loss of physiological protein function, and the transition into aggregate-like condensate is irreversible in most cases[22]. Therefore, the intriguing combination of physiological functions and disease associations renders membrane-less compartments a compelling subject for study.

1.2 Factors that influence biomolecular condensate formation

It is known that the interaction between the participating constituents and their numbers both affect the formation of polymer structures,[23] and these interactions apply to phase-separated condensates. Biomolecular condensates form when a homogenous mixture of a single phase separates into condensed and dilute phases[24]. Across the biological spectrum, liquid-like, solid-like, or gel-like condensates can be formed from a one-phase regime in an increasing concentration or interaction strength-dependent manner[24]. Both homotypic and heterotypic multivalent interactions have been observed in biomolecular condensate formation[9]. In cells, the interactions between protein-protein, RNA-protein, RNA-RNA, Protein-DNA, and DNA-DNA are observed to undergo phase separation[18]. The traditional concept of protein and its biological function asserts that proteins are a folded structure, and their native folded conformation is needed for the biological function. However, recent studies of a specific class of proteins known as intrinsically disordered proteins (IDPs) show that proteins may not always be folded in a physiologic state. IDPs are made of intrinsically disordered regions (IDRs) which are disordered and cannot be fully folded or crystallized[25]. Interestingly, most proteins have both folded domains and IDRs (~58%)[26]. Fully folded proteins make up 1/3 of the total number of the proteins, and IDPs make up 5%. Phase separation is observed for the physiologic state[27] in proteins that contain IDRs. According to several studies, IDRs typically have repeated structural elements[9], and the weaker but higher number of multivalent interactions within the repeated elements can form a membrane-less compartment[26]. This interesting phenomenon of multivalent interaction and the association of biomolecular condensates in both health and disease led to multiple studies on understanding the molecular grammar of condensate formation. For example, a study done with Amyotrophic Lateral Sclerosis (ALS)-associated protein Fused in

Sarcoma (FUS) showed that FUS Prion-Like Domain (PLD) is mainly comprised of tyrosine residues. Condensate formation in PLD is driven by pi-pi interaction between tyrosine residues with a saturation concentration of 120 mM[28]. FUS full-length protein also has a number of positively charged amino acids, such as arginine in addition to the aromatic residues. The pi-cation interaction formed between an aromatic and positively charged amino acid is stronger than the pi-pi interaction and thus the saturation concentration of FUS full-length protein is 60-fold lower at 2 mM[28]. It is also observed that IDR mutations shift the phase separation threshold; these mutations are sometimes pathogenic[26]. Pathological states such as cancer[29], neurodegeneration[29], and viral infections[30] are associated with abnormal condensate formation. The formation of abnormal condensates typically includes a concentration of the constituents above the threshold limit of physiologic state maintenance, known as saturation concentration. However, additional pieces of evidence show that extrinsic factors like oxidative stress can also drive abnormal protein condensate formation in the ALS-associated protein TDP-43[31]. In addition, mutations in patients and post-translational modifications such as phosphorylation can also drive the formation of pathologic amyloid-like or solid-like condensates from liquid condensates[29]. One such example is Alzheimer's disease and Frontotemporal dementia-associated protein tau where disease-associated mutations and phosphorylation both can lead to aberrant and pathogenic biomolecular condensate formation[32,33]. Another example is FUS protein for which aging, and disease-associated mutants influence the formation of abnormal solid-like pathological condensates[34]. An interplay between pathological condensates across multiple diseases is also observed. Alzheimer's disease-associated tau and Parkinson's disease-associated Alpha-synuclein (α-syn) affect each other's biophysical properties and contribute to a α-syn:tau synergistic pathology[35]. In conclusion, it is crucial to comprehend the mechanisms

underlying condensate formation in both physiological and pathological states and explore how this understanding can be leveraged for therapeutic purposes in disease.

1.3 Chaperones assist in protein quality control likely by forming condensates

Cardiomyocytes are unique cell types that are structural and functional units of the heart. They are crucial for maintaining a healthy physiological state because cardiomyocytes need to beat throughout the lifetime of an individual. Studies have shown that cardiac function declines with aging, and it is associated with a gradual decline of cardiomyocyte protein quality control (PQC). Both extrinsic and intrinsic factors such as oxidative stress, inflammation, metabolism, and post-translational modification have been implicated in cardiac aging[36]. Thus, maintaining PQC in cardiac myocytes is crucial. Cardiomyocytes are a huge structure with a network of sarcomeres, cytoskeletons, and various organelles. Most processes of the PQC are thought to occur in the perinuclear region in other cells. However, PQC occurring only in the perinuclear region is not ideal in a huge cell such as cardiomyocytes. This is because synthesis and degradation of proteins will become inefficient owing to distances between all sarcomeres and perinuclear region, particularly in acute stress. Thus, to explain PQC in cardiac myocytes, one study postulated that the protein synthesis, repair, and degradation mechanisms in the sarcomere require a functional compartmentalization by forming condensates right next to the sarcomere known as ‘Sarcostat’[37]. Chaperone proteins are a crucial part of quality control because they help other proteins to fold. In addition to that, chaperones help in protein stabilization, degradation, trafficking, and translocation. Typically, both mechanical and oxidative stresses are observed in heart during cardiac pathology with a change in internal pH[38]. This might provide the environment for proteins to fold improperly, and the gradual accumulation gives rise to protein

aggregates. Molecular chaperones such as Hsp70 or Hsp90 family and co-chaperones such as BAG-3 and CHIP are instrumental in preventing protein aggregation by providing the appropriate environment for proper protein folding in the heart[38]. Thus, cardiac chaperone proteins are important to study to gain a better understanding of their effect on cardiac myocytes and their quality control.

Even though there are only about 180 chaperones in humans, they help to fold and quality control ~20,000 client proteins. Thus, the chaperone-client interaction is likely to be of a degenerate specificity. We speculate that the function of chaperones could be achieved by condensate formation because condensates have liquid-like properties, which gives them a flexible and dynamic nature. Chaperone proteins can interact with their client proteins to maintain protein homeostasis and avoid abnormal protein aggregation[39]. Studies have shown that small heat shock proteins Hsp27, Hsp40, and Hsp 70 can undergo phase separation showing liquid-like properties and helping proteins such as Fu sed in Sarcoma (FUS) to maintain their physiological state[40-42]. The chaperone protein HSPB8 can prevent aberrant phase transitions of FUS proteins by preventing hardening of FUS and by maintaining a dynamic liquid-like state[43]. These examples demonstrate that chaperone proteins could behave like biomolecular condensates and help client proteins maintain their native structure and functions. Thus, it would be interesting to see whether cardiac chaperone proteins can also undergo phase separation and how interaction with their client proteins lead to protein quality control in the heart.

1.4 αB-crystallin is an important chaperone in sarcomeres

αB-crystallin is one of the small heat shock proteins of 175 amino acids long[44]. It is a member of the alpha crystallin superfamily of chaperone proteins. As a chaperone, αB-crystallin

prevents irreversible aggregation of partially unfolded proteins. αB-crystallin is found mostly in eye lenses, but it takes part in many pathological conditions including cardiomyopathy, multi system neurological disorders and cataract formation[45-49]. The important functional domain of αB-crystallin is the α-crystallin domain (ACD). Chaperone function of αB-crystallin is mediated by the α-crystallin domain through its interaction with BAG3 and other small heat shock proteins[50]. Both D109 and R120 residues of ACD are crucial for the homodimerization and interestingly mutations in both residues induce the formation of protein aggregates[47,51-53]. Also, post-translational modification, specifically, phosphorylation, has been associated with influencing the activities of αB-crystallin[54]. There are three major serine phosphorylation sites of αB-crystallin-S19, S45, and S59[54]. S59 is most crucial for the function of αB-crystallin[54] which is phosphorylated by p38 MAPK. Increased phosphorylation in αB-crystallin is observed in aging, stress, and disease[55]. Specifically, upon ischemic stress, CRYAB translocate from cytosol to myofibrils[50]. Phosphorylation in S59 residue destabilizes CRYAB because it induces the ~24-32 mer wild-type state to form a 6-mer state causing increased partitioning in the insoluble fraction[55]. S59 phosphorylation causes CRYAB toxicity in breast cancer cells by downregulating its anti-apoptotic function[56]. A mutation from arginine to glycine at residue 120 has been associated with human cardiomyopathy, skeletal myopathy, and cataract formation[51,52]. Interestingly, we observed the abundance of phospho59-αB-crystallin is increased in the cardiomyopathy-associated R120G mutation in mice. Thus, studying how phosphorylation of the serine-59 residue of CRYAB can

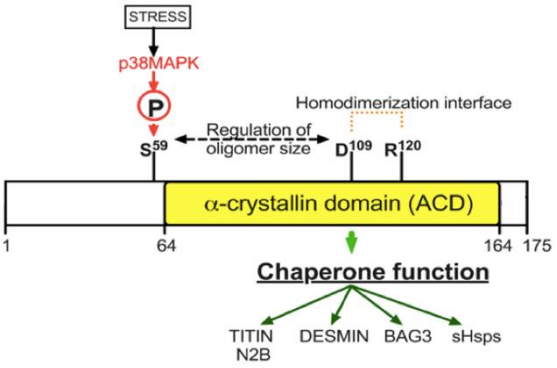

Figure 1.1. Domain structure of CRYAB.

be associated with modulating CRYAB function and its association in cardiomyopathy aren interesting topics to explore.

1.5 Protein aggregation in cardiomyopathy

Heart disease is the leading causes of death occurring at about 17.7 million people worldwide in 2015, representing 31% of all deaths globally[57]. Cardiomyopathy leads to heart failure[58]. In cardiomyopathy, the pumping function of the heart is impaired. Dilated cardiomyopathy is one of the most common cardiomyopathies where the heart chambers dilate causing wall thinning. As a consequence, the heart cannot pump efficiently, and the rest of the body does not get sufficient supply of blood for normal physiological function. Mutations in several proteins are associated in DCM, such as alpha myosin heavy chain (MYH6), alpha cardiac actin (ACTC1), cardiac troponin T (cTnT), titin, α-actinin 2 (ACTN2), αB-crystallin (CRYAB), desmin, phospholamban (PLN), RNA-binding protein 20 (RBM20), BCL2-associated athanogene 3, (BAG3), filamin C (FLNC) [59]. Specifically, CRYAB, desmin, and PLN mutations induce protein aggregate pathology in the heart, giving rise to abnormal protein quality control in cardiomyopathy[60]. The presence of protein aggregates in neurodegenerative diseases and cancer is widely studied, but its association with cardiovascular disease is now beginning to be understood. Atherosclerotic cardiovascular disease, cardiomyopathy, cardiac hypertrophy, and heart failure are associated with impaired protein quality control[61]. Thus, improving protein quality control and reducing aggregate pathology may be protective against cardiac diseases. Desmin is a known client protein of CRYAB. As a cardiac filament protein, desmin, is crucial to maintain the cardiac structure and function as it scaffolds sarcomere and mitochondria. CRYAB co-localizes with desmin in cultured myocytes and CRYAB prevents desmin aggregation by the interaction[62]. Interestingly, abnormal desmin function and mis-localization were observed in

patients with CRYAB R120G missense mutation [53], this abnormality can be recapitulated in mouse models[52]. Two separate studies showed that the removal of aggregates by intermittent fasting[63] or exercise[64] in mice rescued cardiomyopathy of CRYAB R120G missense mutation. These findings represent the importance of improving protein quality control in the heart by restoring or improving CRYAB function. As mutant CRYAB results in mis-localization of desmin, it is important to focus on whether the CRYAB interaction with desmin or other client proteins is crucial for maintaining structure and function in cardiomyocytes.

1.6 In-vitro tools to perform protein-protein phase separation and observing the physical attributes of the protein of interest

In vitro tools for investigating protein-protein phase separation, both within cellular environments and utilizing purified proteins and markers, have undergone remarkable advancements, revolutionizing our understanding of this intricate biological phenomenon. These methodologies not only facilitate the understanding of the underlying mechanisms governing phase separation but also offer invaluable insights into its physiological and pathological implications. OptoDroplet, a technique utilizing light-induced protein clustering, has emerged as a powerful tool for precisely controlling and studying phase transitions within cellular compartments[65]. In this experimental technique, the light inducible protein CRY2 from *Arabidopsis thaliana* is fused with mCh as the marker the IDR of the protein of interest. If the IDR is able to phase separate, blue light induction causes conformational change in CRY2-IDR interaction and forming condensates[65]. Droplet microfluidics, another innovative approach, enables the manipulation and characterization of phase-separated biomolecular condensates under precisely controlled conditions, facilitating a deeper understanding of their assembly and

behavior[66]. Cryogenic electron microscopy (cryo-EM) and nuclear magnetic resonance (NMR) spectroscopy have significantly advanced our understanding of phase separation by providing high-resolution structural information on the molecular architecture and the interactions that drive condensate formation[67,68]. Isotope labeling combined with mass spectrometry-based proteomics has also been instrumental in elucidating the composition and dynamics of phase-separated condensates, shedding light on their functional roles in cellular processes[69]. Moreover, computational modeling approaches, including molecular dynamics simulations and coarse-grained modeling, provide complementary insights into the thermodynamics and kinetics of phase separation, aiding in the interpretation of experimental observations[70,71]. Integrating these diverse methodologies offers a comprehensive toolkit for unraveling the complexity of protein-protein phase separation and its implications in health and disease. Fluorescence Recovery After Photobleaching (FRAP) is a valuable method for observing the dynamic behavior of protein-protein phase separation in cells. FRAP involves selectively photobleaching a fluorescently labeled region within a cellular structure, such as a biomolecular condensate, followed by monitoring the recovery of fluorescence intensity over time as unbleached fluorescent molecules diffuse back into the bleached region. This technique provides insights into the mobility and exchange dynamics of proteins within phase-separated condensates, shedding light on their stability, kinetics, and interactions. FRAP has been extensively applied in studies investigating biomolecular condensates, including stress granules, P-bodies, and nucleoli, to elucidate their biophysical properties and regulatory mechanisms[34,65,72]. By employing FRAP, researchers can quantify parameters such as diffusion coefficients and turnover rates, enabling a comprehensive understanding of the dynamic behavior of phase-separated assemblies and their functional implications in cellular processes and disease pathology.

1.7 Closed-chest ischemia-reperfusion as a tool to mimic human ischemic cardiomyopathy in the mouse

Two phenomena are important to study cardiomyopathy. Ischemia is the term where blood supply is obstructed, and O_2 and nutrient delivery is hindered. Reperfusion is the state where blood supply is restored. Ischemia-reperfusion injury is observed in several pathological states such as stroke and heart failure. These conditions continue to pose significant challenges in cardiovascular diseases which are the leading causes of global death. When oxygen and nutrient supply is hindered, their low levels induce tissue injury and cell death. This is also known as myocardial infarction (MI). The severity of the injury is typically proportional to the duration of ischemia. Reperfusion is the primary treatment of restoring function, but additional damage is observed during reperfusion stage in the heart. Prolonged ischemia induces a decline in ATP levels and intracellular pH owing to anaerobic metabolism and lactate accumulation[73]. As a result, dysfunctional ATPase-dependent ion transport mechanisms contribute to calcium overload, leading to increased intracellular and mitochondrial calcium levels, cell swelling, rupture, and cell death through necrotic, necroptotic, apoptotic, and autophagic pathways[73]. Although reperfusion restores oxygen levels, it triggers a surge in reactive oxygen species which are harmful for cells. When occlusion of blood flow to the heart occurs by plaque rupture in an individual, the person is are treated by reperfusion and stabilization of atherosclerotic plaque which caused the occlusion. However, upon the ischemia-reperfusion injury, most patients experience molecular, cellular, and interstitial changes that causes difference in size, mass, geometry and function of the heart known as cardiac remodeling.

To study cardiac remodeling, several experimental techniques have been employed. The best experimental technique that mimics myocardial infarction and heart failure is closed-chest ischemia-reperfusion injury in mice. This is a modified version of open-chest ischemia-reperfusion injury which are also used to mimic myocardial infarction. Open-chest ischemia-reperfusion poses higher risk of inflammation by the immune cells at the site of injury which can affect the infarct size. Closed-chest ischemia-reperfusion technique is an advancement over open-chest-reperfusion technique where the left anterior descending coronary artery is tied for 90-minutes causing ischemia, followed by 4-weeks of reperfusion[74]. After MI in the remote or uninjured portion of the heart, the heart undergoes cardiac remodeling and mimics cardiomyopathy in mice similar to humans[75]. Thus, studying the cellular changes occurring in cardiac myocytes after ischemia-reperfusion can give us a better understanding of how we can utilize the understanding to treat ischemic heart disease.

1.8 CRISPR gene editing technology to generate knock-in mouse models

CRISPR-Cas9 gene editing technology has revolutionized the generation of knock-in (KI) mouse models by adding unprecedented precision and efficiency. By harnessing the programmable nature of CRISPR-Cas9, researchers can introduce specific genetic modifications into the mouse genome, for example by using the Cas9 (CRISPR-associated) DNA endonuclease and a single guide RNA (sgRNA) to direct the introduction/deletion the new base at a selected site to precisely mimic human diseases or investigate gene function[76]. This approach has been extensively utilized in various fields of research, including neuroscience, oncology, developmental biology, and cardiology. In cardiology, CRISPR-mediated KI mouse models have been instrumental in elucidating the genetic basis of cardiovascular diseases and exploring

potential therapeutic targets. Studies have utilized CRISPR-Cas9 to engineer KI mouse models with mutations in genes encoding key cardiac proteins such as Titin and Mybpc3, implicated in dilated cardiomyopathy and familial hypertrophic cardiomyopathy, respectively[77,78]. Thus, CRISPR-Cas9-mediated generation of KI mouse models has emerged as a powerful tool for advancing our understanding of cardiovascular diseases and biological processes, with implications for the development of novel therapeutic interventions and precision medicine approaches.

1.9 25-hydroxycholesterol as a pharmacological chaperone reducing pathological αB-crystallin aggregates

25-hydroxycholesterol (25-HC) is a derivative of cholesterol that is obtained by enzyme catalyzed oxidation[79]. During the inflammatory responses, the generation of 25-hydroxycholesterol (25-HC) is markedly elevated in macrophages, dendritic cells, and microglia[80]. Additionally, the production of 25-HC can be augmented in certain neurological disorders, including Alzheimer's disease, and amyotrophic lateral sclerosis[80]. Nevertheless, it remains uncertain whether 25-HC exacerbates these pathologies or possesses protective characteristics. Interestingly, 25-HC showed antiviral properties in multiple studies[81,82]. Other protective functions of 25-HC such as lipid metabolism and cell survival are also reported[83]. αB-crystallin is mostly expressed in the heart and in the lens. When the soluble form of αB-crystallin becomes insoluble amyloid due to misfolding and aggregation, it forms cataracts in humans[84]. Interestingly, 25-HC has been found to act as a chaperone in solubilizing R120G mutation carrying αB-crystallin in mouse models of cataracts[85]. In in-vitro experiments, 25-HC improved the transparency of the lens following aggregation[85]. In-silico docking studies showed that 25-

HC is able to bind native CRYAB in its native form binding in a groove via multiple hydrogen bonds. Thus, studying how 25-HC and CRYAB interact and understanding the interactions on a molecular level are important for using this compound in therapeutic modalities for CRYAB-associated pathologies.

1.10 p62- the crucial autophagy adaptor

The term 'autophagy,' derived from the Greek meaning 'eating of self,'. It is the recycling mechanism of damaged organelles and proteins in our body[86]. Autophagy encompasses three distinct types: macro-autophagy, micro-autophagy, and chaperone-mediated autophagy[86]. All three types facilitate the proteolytic degradation of cytosolic components at the lysosome. In macro-autophagy, cytoplasmic cargo is delivered to the lysosome through the formation of a double membrane-bound vesicle known as an autophagosome. This autophagosome then fuses with the lysosome, forming an autolysosome[86]. The importance of autophagy becomes evident when considering its role in disease and aging. There is a growing body of evidence linking mutations or loss of function in key autophagy genes to conditions such as cancer, neuropathies, heart disease, autoimmune diseases, and other disorders. Understanding these connections provides valuable insights into the role of autophagy in maintaining cellular health and its impact on various pathological processes. One of the first selective autophagy receptors discovered is p62 or sequestosomes which are associated with the LIR (LC3 interacting region) domain that binds with LC3 (ATG8)

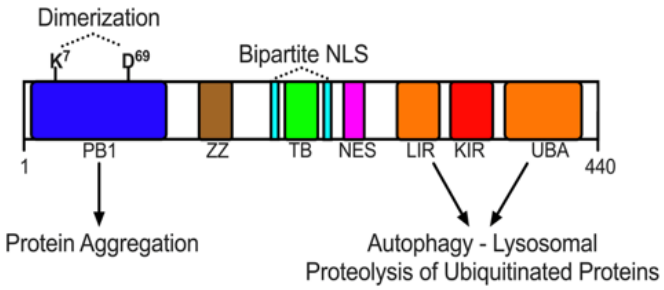

Figure 1.2. Domain structure of p62.

receptors of the autophagy cargo[87,88]. Human p62 is 440 amino acids long and contains N-terminal PB1 domain, zz domain, TRAF-6 binding domain (TB), Nuclear export signal (NES), nuclear localization signal (NLS), LC3 interacting region (LIR) and C-terminal ubiquitin associated domain (UBA) crucial for autophagy and then Keap-interacting region (KIR)[89]. The p62 binds to ubiquitinated proteins targeted for lysosomal degradation as well as to LC3-II. The p62 is ubiquitinylated at K7 by TRIM21[90]. Later, sequestosome (p62) like adaptors such as NBR1, NDP52, TAX1BP1, OPTN, BNIP3 were discovered. Those autophagy adaptors contain the LIR domains. LIR domains have a conserved sequence containing W/F/Y-xx-L/I/V which is crucial for the LIR-ATG8 interaction required for autophagy[89]. The p62 is required for the protein aggregate formation in macrophages and these aggregates sometime show an anti-inflammatory role. The role of both p62 overexpression and deletion both have been studied in disease association. In Huntington's disease, mutant huntingtin protein (*htt*) with expanded polyglutamine tracts have been found to have enhanced cytoplasmic inclusion when p62 is ablated[91]. The p62 ablation also enhances the pathology of Parkinson's disease-associated Alpha-synuclein protein by increasing the number of cytoplasmic inclusions[92]. Also, global knockout of p62 in mice showed abnormal metabolism at 34 weeks of age whereby the mouse develops obesity with insulin resistance and systemic inflammation. All these studies demonstrate the requirement of p62 to maintain protein quality control and metabolism. Interestingly, overexpression of p62 causes worsening outcome in diseases. As an example, p62 overexpression in liver induces fatty liver in mice[93]. The p62 overexpression in ALS-disease associated SOD1H46R mutated mice models shows compromised protein degradation and accelerates disease onset[94]. However, p62 overexpression improves mitochondrial functions, improves spatial learning and long-term memory function in mice[95]. Thus, p62 has contextual

based dual role in cell. However, as p62 is required for protein aggregate formation, targeting the ablation of p62 in the cardiac myocytes may give us a better understanding of how protein aggregates can be associated in ischemic heart disease and whether removal of protein aggregates could be an effective therapeutic strategy.

1.11 Yeast protein Hsp104 as a disaggregate to reduce proteotoxic aggregates

Amyloids are aggregates that are very stable and do not denature easily. Whereas amyloids may not always be fatal for an organism, their toxic effects often disrupt specific cellular functions. Consequently, it is anticipated that cell defense systems would be triggered in response to the accumulation of amyloids. Notably, the heat shock protein with a molecular mass of 104 kDa, Hsp104, has emerged as a pivotal player in induced thermotolerance in yeast. Thermotolerance refers to the ability of yeast cells to withstand severe heat shock exposure after undergoing pretreatment with mild heat shock[96]. In mutant yeast cells lacking Hsp104, the accumulation of protein aggregates occurs at elevated temperatures[96]. This observation suggests that Hsp104 may counteract protein aggregation, demonstrating its role as a molecular chaperone. Thus, understanding Hsp104 structure and function may harness the disaggregase properties to remove aggregates in associated disease models. Hsp104 couples ATP hydrolysis to the dissolution of various polypeptides that are trapped in toxic pre-amyloid oligomers, phase-transitioned gels, disordered aggregates, amyloids, and prions[97,98]. The interaction of the N-terminal domain of Hsp104 with substrates plays a regulatory role in protein disaggregation[99]. Engineered Hsp104 was reported to disaggregate neurodegenerative diseases associated with protein aggregates such as alpha-synuclein, TDP-43 and FUS[21,100,101]. As Hsp104 is not a yeast protein, it needs to be expressed in a transgenic way in mice or other mammals. A crossbreeding

experiment involving hsp104 transgenic mice and mice expressing the first 171 residues of mutant huntingtin showed a reduction in aggregate formation and an extension of the lifespan of the Huntington's disease (HD) mice by 20%[102]. Whereas the xenogeneic expression of Hsp104 significantly enhanced the viability of the neuronal mouse CAD cell line following exposure to heat shock, it proves inefficient in modulating the propagation of mammalian prions or mitigating neurodegeneration in the brains of scrapie-infected mice[103]. Thus, the gain-of-function of Hsp104 disaggregase may be harnessed to work on diverse proteotoxic aggregations and thus have tremendous therapeutic potential in cases where aggregates are directly related to pathology.

1.12 Current knowledge gaps and hypothesis

Protein aggregates that form self-assemblies serve context-dependent beneficial or harmful roles in prokaryotes, fungi, and invertebrates[104,56]. However, in human diseases and mammalian models, protein aggregates have been associated with 'proteotoxicity', the mechanism for which remains unexplored. In this thesis, I will study this knowledge gap in protein biology in a disease-relevant condition of cardiomyopathy. Cardiomyopathy is a condition where the heart muscle is unable to pump blood efficiently compared to healthy conditions. A rapidly fatal human cardiomyopathy that results from a genetic mutation (arginine to glycine residue mutation at position 120, R120G) in a muscle-enriched protein αB-crystallin, showed associated aggregate formation in mice model[3]. Desmin, which is a client protein of CRYAB, is an intermediate filament protein that is crucial for maintaining the basic structure of sarcomere, the contractile unit of cardiac myocytes. Desmin is mis-localized when R120G is overexpressed in mice[3]. When lysosomal degradative function was improved, clearance of the aggregate was achieved and

desmin localization was restored[3]. In genetic mutations such as R120G and stress conditions such as ischemia-reperfusion (return of blood supply after a period of lack of oxygen), abundance of phosphorylated αB-crystallin (in serine at position 59) increases in the protein aggregate enriched fraction. Phosphorylation of αB-crystallin makes it more aggregate-prone than the physiological form. Thus, I propose to close this knowledge gap of how phosphorylation of CRYAB can modulate its function and affect post myocardial infarction cardiomyopathy.

Furthermore, CRYAB is a chaperone protein that binds to multiple client proteins in the heart including desmin. As studies showed that chaperone proteins can reduce aggregation of abnormal protein condensates, it is unknown whether CRYAB can phase separate and reduce abnormal protein condensate formation of its client proteins. Also, phosphorylation in CRYAB is mediated by p38 MAPK upon ischemia, and it is unknown whether increased phosphorylation is also seen in more common ischemic cardiomyopathy like rare familial cardiomyopathy. *I hypothesize that phosphorylation in CRYAB make it aggregate-prone and toxic to worsen post-myocardial infarction cardiomyopathy.* Utilizing a genetic approach, I plan to study phospho-mimetic and deficient mutants of CRYAB using in-vitro and in-vivo approaches. An endogenous ligand of αB-crystallin (25-hydroxycholesterol, 25-HC) with anti-aggregation properties can be potentially used to reverse the protein aggregates. In-silico studies suggest that 25-HC binds CRYAB in its native form. Whether 25-HC is able to reduce CRYAB phosphorylation and can be used in therapeutic purposes similar to those that reduce cataract formation, is still unknown. As a pharmacological approach, I planned to use 25-HC and determine its effect in cardiac remodeling in ischemia reperfusion injury.

The p62 is an adaptor protein crucial for the clearance of aggregates by autophagy. Both overexpression and deletion of p62 is associated with pathologic outcomes, and it is unclear what

would be the effect of ablating protein aggregates in the heart by cardiac-specific deletion of p62 is unclear.

In parallel, the yeast disaggregase HSP104 overexpression removes protein aggregates in multiple pathologic models of neurodegenerative diseases showing protective effects but does not rescue prion protein pathogenesis in vivo models. Whether the overexpression of Hsp104 in the cardiac myocytes by targeting protein aggregates would have an effect in post-myocardial infarction, is still unknown. As an orthogonal approaches, I planned to use both of those strategies to determine how ablating or disaggregating protein aggregates will affect cardiac function after ischemia reperfusion injury. In this project, we tried to close these knowledge gaps with in in-vivo and in-vitro models to determine the role of CRYAB phosphorylation and protein aggregates in ischemic cardiomyopathy.

1.13 References

1. Zhao YG, Zhang H. Phase Separation in Membrane Biology: The Interplay between Membrane-Bound Organelles and Membraneless Condensates. *Dev Cell*. 2020;55:30-44. doi: 10.1016/j.devcel.2020.06.033
2. Saftig P, Klumperman J. Lysosome biogenesis and lysosomal membrane proteins: trafficking meets function. *Nat Rev Mol Cell Biol*. 2009;10:623-635. doi: 10.1038/nrm2745
3. Helenius A, Mellman I, Wall D, Hubbard A. Endosomes. *Trends in Biochemical Sciences*. 1983;8:245-250.
4. Anelli T, Sitia R. Protein quality control in the early secretory pathway. *The EMBO journal*. 2008;27:315-327.
5. Wang Y, Seemann J. Golgi biogenesis. *Cold Spring Harb Perspect Biol*. 2011;3:a005330. doi: 10.1101/cshperspect.a005330
6. Bhatti JS, Bhatti GK, Reddy PH. Mitochondrial dysfunction and oxidative stress in metabolic disorders - A step towards mitochondria based therapeutic strategies. *Biochim Biophys Acta Mol Basis Dis*. 2017;1863:1066-1077. doi: 10.1016/j.bbadis.2016.11.010
7. Ram6n y Cajal S. Un sencillo m6todo de coloraci6n selectiva del reticulo protopl~ smico. *Trab Lab Invest Biol*. 1903;2:129-221.
8. Spector DL. SnapShot: Cellular bodies. *Cell*. 2006;127:1071. doi: 10.1016/j.cell.2006.11.026
9. Banani SF, Lee HO, Hyman AA, Rosen MK. Biomolecular condensates: organizers of cellular biochemistry. *Nat Rev Mol Cell Biol*. 2017;18:285-298. doi: 10.1038/nrm.2017.7
10. Trivedi P, Palomba F, Niedzialkowska E, Digman MA, Gratton E, Stukenberg PT. The inner centromere is a biomolecular condensate scaffolded by the chromosomal passenger complex. *Nat Cell Biol*. 2019;21:1127-1137. doi: 10.1038/s41556-019-0376-4
11. Beutel O, Maraspini R, Pombo-García K, Martin-Lemaitre C, Honigmann A. Phase Separation of Zonula Occludens Proteins Drives Formation of Tight Junctions. *Cell*. 2019;179:923-936.e911. doi: 10.1016/j.cell.2019.10.011
12. Fujioka Y, Alam JM, Noshiro D, Mouri K, Ando T, Okada Y, May AI, Knorr RL, Suzuki K, Ohsumi Y, et al. Phase separation organizes the site of autophagosome formation. *Nature*. 2020;578:301-305. doi: 10.1038/s41586-020-1977-6
13. Bergeron-Sandoval LP, Kumar S, Heris HK, Chang CLA, Cornell CE, Keller SL, François P, Hendricks AG, Ehrlicher AJ, Pappu RV, et al. Endocytic proteins with prion-like domains form viscoelastic condensates that enable membrane remodeling. *Proc Natl Acad Sci U S A*. 2021;118. doi: 10.1073/pnas.2113789118
14. Zhang Y, Yan L, Zhou Z, Yang P, Tian E, Zhang K, Zhao Y, Li Z, Song B, Han J, et al. SEPA-1 mediates the specific recognition and degradation of P granule components by autophagy in C. elegans. *Cell*. 2009;136:308-321. doi: 10.1016/j.cell.2008.12.022
15. Kilic S, Lezaja A, Gatti M, Bianco E, Michelena J, Imhof R, Altmeyer M. Phase separation of 53BP1 determines liquid-like behavior of DNA repair compartments. *Embo j*. 2019;38:e101379. doi: 10.15252/embj.2018101379
16. Du M, Chen ZJ. DNA-induced liquid phase condensation of cGAS activates innate immune signaling. *Science*. 2018;361:704-709. doi: 10.1126/science.aat1022

17. Su X, Ditlev JA, Hui E, Xing W, Banjade S, Okrut J, King DS, Taunton J, Rosen MK, Vale RD. Phase separation of signaling molecules promotes T cell receptor signal transduction. *Science*. 2016;352:595-599. doi: 10.1126/science.aad9964
18. Roden C, Gladfelter AS. RNA contributions to the form and function of biomolecular condensates. *Nat Rev Mol Cell Biol*. 2021;22:183-195. doi: 10.1038/s41580-020-0264-6
19. Farley-Barnes KI, Ogawa LM, Baserga SJ. Ribosomopathies: Old Concepts, New Controversies. *Trends Genet*. 2019;35:754-767. doi: 10.1016/j.tig.2019.07.004
20. Owen I, Yee D, Wyne H, Perdikari TM, Johnson V, Smyth J, Kortum R, Fawzi NL, Shewmaker F. The oncogenic transcription factor FUS-CHOP can undergo nuclear liquid-liquid phase separation. *J Cell Sci*. 2021;134. doi: 10.1242/jcs.258578
21. Ryan JJ, Sprunger ML, Holthaus K, Shorter J, Jackrel ME. Engineered protein disaggregases mitigate toxicity of aberrant prion-like fusion proteins underlying sarcoma. *J Biol Chem*. 2019;294:11286-11296. doi: 10.1074/jbc.RA119.009494
22. Franzmann TM, Alberti S. Protein Phase Separation as a Stress Survival Strategy. *Cold Spring Harb Perspect Biol*. 2019;11. doi: 10.1101/cshperspect.a034058
23. Flory PJ. *Principles of polymer chemistry*. Cornell university press; 1953.
24. Conti BA, Oppikofer M. Biomolecular condensates: new opportunities for drug discovery and RNA therapeutics. *Trends Pharmacol Sci*. 2022;43:820-837. doi: 10.1016/j.tips.2022.07.001
25. Chakrabarti P, Chakravarty D. Intrinsically disordered proteins/regions and insight into their biomolecular interactions. *Biophys Chem*. 2022;283:106769. doi: 10.1016/j.bpc.2022.106769
26. Tsang B, Pritišanac I, Scherer SW, Moses AM, Forman-Kay JD. Phase Separation as a Missing Mechanism for Interpretation of Disease Mutations. *Cell*. 2020;183:1742-1756. doi: 10.1016/j.cell.2020.11.050
27. Brangwynne CP, Tompa P, Pappu RV. Polymer physics of intracellular phase transitions. *Nature Physics*. 2015;11:899-904.
28. Wang J, Choi JM, Holehouse AS, Lee HO, Zhang X, Jahnel M, Maharana S, Lemaitre R, Pozniakovsky A, Drechsel D, et al. A Molecular Grammar Governing the Driving Forces for Phase Separation of Prion-like RNA Binding Proteins. *Cell*. 2018;174:688-699.e616. doi: 10.1016/j.cell.2018.06.006
29. Alberti S, Hyman AA. Biomolecular condensates at the nexus of cellular stress, protein aggregation disease and ageing. *Nat Rev Mol Cell Biol*. 2021;22:196-213. doi: 10.1038/s41580-020-00326-6
30. Geiger F, Acker J, Papa G, Wang X, Arter WE, Saar KL, Erkamp NA, Qi R, Bravo JP, Strauss S, et al. Liquid-liquid phase separation underpins the formation of replication factories in rotaviruses. *Embo j*. 2021;40:e107711. doi: 10.15252/embj.2021107711
31. Yan X, Kuster D, Mohanty P, Nijssen J, Pombo-García K, Rizuan A, Franzmann TM, Sergeeva A, Passos PM, George L, et al. Intra-condensate demixing of TDP-43 inside stress granules generates pathological aggregates. *bioRxiv*. 2024. doi: 10.1101/2024.01.23.576837
32. Wegmann S, Eftekharzadeh B, Tepper K, Zoltowska KM, Bennett RE, Dujardin S, Laskowski PR, MacKenzie D, Kamath T, Commins C, et al. Tau protein liquid-liquid phase separation can initiate tau aggregation. *Embo j*. 2018;37. doi: 10.15252/embj.201798049

33. Ainani H, Bouchmaa N, Ben Mrid R, El Fatimy R. Liquid-liquid phase separation of protein tau: An emerging process in Alzheimer's disease pathogenesis. *Neurobiol Dis*. 2023;178:106011. doi: 10.1016/j.nbd.2023.106011
34. Patel A, Lee HO, Jawerth L, Maharana S, Jahnel M, Hein MY, Stoynov S, Mahamid J, Saha S, Franzmann TM, et al. A Liquid-to-Solid Phase Transition of the ALS Protein FUS Accelerated by Disease Mutation. *Cell*. 2015;162:1066-1077. doi: 10.1016/j.cell.2015.07.047
35. Siegert A, Rankovic M, Favretto F, Ukmar-Godec T, Strohäker T, Becker S, Zweckstetter M. Interplay between tau and α-synuclein liquid-liquid phase separation. *Protein Sci*. 2021;30:1326-1336. doi: 10.1002/pro.4025
36. Bernhard D, Laufer G. The aging cardiomyocyte: a mini-review. *Gerontology*. 2008;54:24-31.
37. Islam M, Diwan A, Mani K. Come Together: Protein Assemblies, Aggregates and the Sarcostat at the Heart of Cardiac Myocyte Homeostasis. *Front Physiol*. 2020;11:586. doi: 10.3389/fphys.2020.00586
38. Ranek MJ, Stachowski MJ, Kirk JA, Willis MS. The role of heat shock proteins and co-chaperones in heart failure. *Philos Trans R Soc Lond B Biol Sci*. 2018;373. doi: 10.1098/rstb.2016.0530
39. Li D, Liu C. Spatiotemporal dynamic regulation of membraneless organelles by chaperone networks. *Trends Cell Biol*. 2022;32:1-3. doi: 10.1016/j.tcb.2021.08.004
40. Li Y, Gu J, Wang C, Hu J, Zhang S, Liu C, Zhang S, Fang Y, Li D. Hsp70 exhibits a liquid-liquid phase separation ability and chaperones condensed FUS against amyloid aggregation. *iScience*. 2022;25:104356. doi: 10.1016/j.isci.2022.104356
41. Gu J, Liu Z, Zhang S, Li Y, Xia W, Wang C, Xiang H, Liu Z, Tan L, Fang Y, et al. Hsp40 proteins phase separate to chaperone the assembly and maintenance of membraneless organelles. *Proc Natl Acad Sci U S A*. 2020;117:31123-31133. doi: 10.1073/pnas.2002437117
42. Liu Z, Zhang S, Gu J, Tong Y, Li Y, Gui X, Long H, Wang C, Zhao C, Lu J, et al. Hsp27 chaperones FUS phase separation under the modulation of stress-induced phosphorylation. *Nat Struct Mol Biol*. 2020;27:363-372. doi: 10.1038/s41594-020-0399-3
43. Boczek EE, Fürsch J, Niedermeier ML, Jawerth L, Jahnel M, Ruer-Gruß M, Kammer KM, Heid P, Mediani L, Wang J, et al. HspB8 prevents aberrant phase transitions of FUS by chaperoning its folded RNA-binding domain. *Elife*. 2021;10. doi: 10.7554/eLife.69377
44. Banerjee PR, Pande A, Shekhtman A, Pande J. Molecular mechanism of the chaperone function of mini-α-crystallin, a 19-residue peptide of human α-crystallin. *Biochemistry*. 2015;54:505-515. doi: 10.1021/bi5014479
45. Simon S, Fontaine JM, Martin JL, Sun X, Hoppe AD, Welsh MJ, Benndorf R, Vicart P. Myopathy-associated alphaB-crystallin mutants: abnormal phosphorylation, intracellular location, and interactions with other small heat shock proteins. *J Biol Chem*. 2007;282:34276-34287. doi: 10.1074/jbc.M703267200
46. Cortese A, Currò R, Ronco R, Blake J, Rossor AM, Bugiardini E, Laurà M, Warner T, Yousry T, Poh R, et al. Mutations in alpha-B-crystallin cause autosomal dominant axonal Charcot-Marie-Tooth disease with congenital cataracts. *Eur J Neurol*. 2024;31:e16063. doi: 10.1111/ene.16063

47. Brodehl A, Gaertner-Rommel A, Klauke B, Grewe SA, Schirmer I, Peterschröder A, Faber L, Vorgerd M, Gummert J, Anselmetti D, et al. The novel αB-crystallin (CRYAB) mutation p.D109G causes restrictive cardiomyopathy. *Hum Mutat*. 2017;38:947-952. doi: 10.1002/humu.23248
48. Ha C, Kim D, Bak M, Park JH, Kim YG, Jang JH, Kim JW, Choi JO, Jang MA. CRYAB stop-loss variant causes rare syndromic dilated cardiomyopathy with congenital cataract: expanding the phenotypic and mutational spectrum of alpha-B crystallinopathy. *J Hum Genet*. 2024. doi: 10.1038/s10038-023-01218-1
49. Sadeh M, Rahat D, Meiner V, Fellig Y, Arad M, Schueler-Furman O, Hu Y, Li Y, Bönnemann CG, Lossos A. Multi-system neurological disorder associated with a CRYAB variant. *Neurogenetics*. 2021;22:117-125. doi: 10.1007/s10048-021-00640-x
50. Golenhofen N, Ness W, Koob R, Htun P, Schaper W, Drenckhahn D. Ischemia-induced phosphorylation and translocation of stress protein alpha B-crystallin to Z lines of myocardium. *Am J Physiol*. 1998;274:H1457-1464. doi: 10.1152/ajpheart.1998.274.5.H1457
51. Wang X, Osinska H, Klevitsky R, Gerdes AM, Nieman M, Lorenz J, Hewett T, Robbins J. Expression of R120G-alphaB-crystallin causes aberrant desmin and alphaB-crystallin aggregation and cardiomyopathy in mice. *Circ Res*. 2001;89:84-91. doi: 10.1161/hh1301.092688
52. Rajasekaran NS, Connell P, Christians ES, Yan LJ, Taylor RP, Orosz A, Zhang XQ, Stevenson TJ, Peshock RM, Leopold JA, et al. Human alpha B-crystallin mutation causes oxido-reductive stress and protein aggregation cardiomyopathy in mice. *Cell*. 2007;130:427-439. doi: 10.1016/j.cell.2007.06.044
53. Vicart P, Caron A, Guicheney P, Li Z, Prévost MC, Faure A, Chateau D, Chapon F, Tomé F, Dupret JM, et al. A missense mutation in the alphaB-crystallin chaperone gene causes a desmin-related myopathy. *Nat Genet*. 1998;20:92-95. doi: 10.1038/1765
54. Ciano M, Allocca S, Ciardulli MC, Della Volpe L, Bonatti S, D'Agostino M. Differential phosphorylation-based regulation of αB-crystallin chaperone activity for multipass transmembrane proteins. *Biochem Biophys Res Commun*. 2016;479:325-330. doi: 10.1016/j.bbrc.2016.09.071
55. Bakthisaran R, Akula KK, Tangirala R, Rao Ch M. Phosphorylation of αB-crystallin: Role in stress, aging and patho-physiological conditions. *Biochim Biophys Acta*. 2016;1860:167-182. doi: 10.1016/j.bbagen.2015.09.017
56. Launay, N., Tarze, A., Vicart, P., & Lilienbaum, A. (2010). Serine 59 phosphorylation of {alpha}B-crystallin down-regulates its anti-apoptotic function by binding and sequestering Bcl-2 in breast cancer cells. *The Journal of biological chemistry*, *285*(48), 37324–37332. https://doi.org/10.1074/jbc.M110.124388
57. Organization WH. Cardiovascular diseases (cvds). *http://www who int/mediacentre/factsheets/fs317/en/index html*. 2009.
58. Benjamin EJ, Virani SS, Callaway CW, Chamberlain AM, Chang AR, Cheng S, Chiuve SE, Cushman M, Delling FN, Deo R, et al. Heart Disease and Stroke Statistics-2018 Update: A Report From the American Heart Association. *Circulation*. 2018;137:e67-e492. doi: 10.1161/cir.0000000000000558
59. McNally EM, Mestroni L. Dilated Cardiomyopathy: Genetic Determinants and Mechanisms. *Circ Res*. 2017;121:731-748. doi: 10.1161/circresaha.116.309396

60. Bloom MW, Gorevic PD. Cardiac Amyloidosis. *Ann Intern Med*. 2023;176:Itc33-itc48. doi: 10.7326/aitc202303210
61. Gouveia M, Xia K, Colón W, Vieira SI, Ribeiro F. Protein aggregation, cardiovascular diseases, and exercise training: Where do we stand? *Ageing Res Rev*. 2017;40:1-10. doi: 10.1016/j.arr.2017.07.005
62. Wang K, Spector A. alpha-crystallin prevents irreversible protein denaturation and acts cooperatively with other heat-shock proteins to renature the stabilized partially denatured protein in an ATP-dependent manner. *Eur J Biochem*. 2000;267:4705-4712. doi: 10.1046/j.1432-1327.2000.01521.x
63. Ma X, Mani K, Liu H, Kovacs A, Murphy JT, Foroughi L, French BA, Weinheimer CJ, Kraja A, Benjamin IJ, et al. Transcription Factor EB Activation Rescues Advanced αB-Crystallin Mutation-Induced Cardiomyopathy by Normalizing Desmin Localization. *J Am Heart Assoc*. 2019;8:e010866. doi: 10.1161/jaha.118.010866
64. Maloyan A, Gulick J, Glabe CG, Kayed R, Robbins J. Exercise reverses preamyloid oligomer and prolongs survival in alphaB-crystallin-based desmin-related cardiomyopathy. *Proc Natl Acad Sci U S A*. 2007;104:5995-6000. doi: 10.1073/pnas.0609202104
65. Shin Y, Berry J, Pannucci N, Haataja MP, Toettcher JE, Brangwynne CP. Spatiotemporal Control of Intracellular Phase Transitions Using Light-Activated optoDroplets. *Cell*. 2017;168:159-171.e114. doi: 10.1016/j.cell.2016.11.054
66. Banani SF, Rice AM, Peeples WB, Lin Y, Jain S, Parker R, Rosen MK. Compositional Control of Phase-Separated Cellular Bodies. *Cell*. 2016;166:651-663. doi: 10.1016/j.cell.2016.06.010
67. Alberti S, Gladfelter A, Mittag T. Considerations and Challenges in Studying Liquid-Liquid Phase Separation and Biomolecular Condensates. *Cell*. 2019;176:419-434. doi: 10.1016/j.cell.2018.12.035
68. Babinchak WM, Surewicz WK. Liquid-Liquid Phase Separation and Its Mechanistic Role in Pathological Protein Aggregation. *J Mol Biol*. 2020;432:1910-1925. doi: 10.1016/j.jmb.2020.03.004
69. Lu H, Yu D, Hansen AS, Ganguly S, Liu R, Heckert A, Darzacq X, Zhou Q. Phase-separation mechanism for C-terminal hyperphosphorylation of RNA polymerase II. *Nature*. 2018;558:318-323. doi: 10.1038/s41586-018-0174-3
70. Boeynaems S, Alberti S, Fawzi NL, Mittag T, Polymenidou M, Rousseau F, Schymkowitz J, Shorter J, Wolozin B, Van Den Bosch L, et al. Protein Phase Separation: A New Phase in Cell Biology. *Trends Cell Biol*. 2018;28:420-435. doi: 10.1016/j.tcb.2018.02.004
71. Posey AE, Holehouse AS, Pappu RV. Phase Separation of Intrinsically Disordered Proteins. *Methods Enzymol*. 2018;611:1-30. doi: 10.1016/bs.mie.2018.09.035
72. Brangwynne CP, Eckmann CR, Courson DS, Rybarska A, Hoege C, Gharakhani J, Jülicher F, Hyman AA. Germline P granules are liquid droplets that localize by controlled dissolution/condensation. *Science*. 2009;324:1729-1732. doi: 10.1126/science.1172046
73. Wu MY, Yiang GT, Liao WT, Tsai AP, Cheng YL, Cheng PW, Li CY, Li CJ. Current Mechanistic Concepts in Ischemia and Reperfusion Injury. *Cell Physiol Biochem*. 2018;46:1650-1667. doi: 10.1159/000489241

74. Javaheri A, Bajpai G, Picataggi A, Mani S, Foroughi L, Evie H, Kovacs A, Weinheimer CJ, Hyrc K, Xiao Q, et al. TFEB activation in macrophages attenuates postmyocardial infarction ventricular dysfunction independently of ATG5-mediated autophagy. *JCI Insight*. 2019;4. doi: 10.1172/jci.insight.127312
75. Kim SC, Boehm O, Meyer R, Hoeft A, Knüfermann P, Baumgarten G. A murine closed-chest model of myocardial ischemia and reperfusion. *J Vis Exp*. 2012:e3896. doi: 10.3791/3896
76. Hall B, Cho A, Limaye A, Cho K, Khillan J, Kulkarni AB. Genome Editing in Mice Using CRISPR/Cas9 Technology. *Curr Protoc Cell Biol*. 2018;81:e57. doi: 10.1002/cpcb.57
77. Tucker NR, McLellan MA, Hu D, Ye J, Parsons VA, Mills RW, Clauss S, Dolmatova E, Shea MA, Milan DJ, et al. Novel Mutation in FLNC (Filamin C) Causes Familial Restrictive Cardiomyopathy. *Circ Cardiovasc Genet*. 2017;10. doi: 10.1161/circgenetics.117.001780
78. Fraysse B, Weinberger F, Bardswell SC, Cuello F, Vignier N, Geertz B, Starbatty J, Krämer E, Coirault C, Eschenhagen T, et al. Increased myofilament Ca2+ sensitivity and diastolic dysfunction as early consequences of Mybpc3 mutation in heterozygous knock-in mice. *J Mol Cell Cardiol*. 2012;52:1299-1307. doi: 10.1016/j.yjmcc.2012.03.009
79. Russell DW. Oxysterol biosynthetic enzymes. *Biochimica et Biophysica Acta (BBA)-Molecular and Cell Biology of Lipids*. 2000;1529:126-135.
80. Odnoshivkina UG, Kuznetsova EA, Petrov AM. 25-Hydroxycholesterol as a Signaling Molecule of the Nervous System. *Biochemistry (Mosc)*. 2022;87:524-537. doi: 10.1134/s0006297922060049
81. Zhang J, Zhu Y, Wang X, Wang J. 25-hydroxycholesterol: an integrator of antiviral ability and signaling. *Front Immunol*. 2023;14:1268104. doi: 10.3389/fimmu.2023.1268104
82. Zang R, Case JB, Yutuc E, Ma X, Shen S, Gomez Castro MF, Liu Z, Zeng Q, Zhao H, Son J, et al. Cholesterol 25-hydroxylase suppresses SARS-CoV-2 replication by blocking membrane fusion. *Proc Natl Acad Sci U S A*. 2020;117:32105-32113. doi: 10.1073/pnas.2012197117
83. Cao Q, Liu Z, Xiong Y, Zhong Z, Ye Q. Multiple Roles of 25-Hydroxycholesterol in Lipid Metabolism, Antivirus Process, Inflammatory Response, and Cell Survival. *Oxid Med Cell Longev*. 2020;2020:8893305. doi: 10.1155/2020/8893305
84. Andley UP, Hamilton PD, Ravi N, Weihl CC. A knock-in mouse model for the R120G mutation of αB-crystallin recapitulates human hereditary myopathy and cataracts. *PLoS One*. 2011;6:e17671. doi: 10.1371/journal.pone.0017671
85. Makley LN, McMenimen KA, DeVree BT, Goldman JW, McGlasson BN, Rajagopal P, Dunyak BM, McQuade TJ, Thompson AD, Sunahara R, et al. Pharmacological chaperone for α-crystallin partially restores transparency in cataract models. *Science*. 2015;350:674-677. doi: 10.1126/science.aac9145
86. Klionsky DJ, Abeliovich H, Agostinis P, Agrawal DK, Aliev G, Askew DS, Baba M, Baehrecke EH, Bahr BA, Ballabio A, et al. Guidelines for the use and interpretation of assays for monitoring autophagy in higher eukaryotes. *Autophagy*. 2008;4:151-175. doi: 10.4161/auto.5338
87. Pankiv S, Clausen TH, Lamark T, Brech A, Bruun JA, Outzen H, Øvervatn A, Bjørkøy G, Johansen T. p62/SQSTM1 binds directly to Atg8/LC3 to facilitate degradation of

ubiquitinated protein aggregates by autophagy. *J Biol Chem*. 2007;282:24131-24145. doi: 10.1074/jbc.M702824200

88. Bjørkøy G, Lamark T, Brech A, Outzen H, Perander M, Overvatn A, Stenmark H, Johansen T. p62/SQSTM1 forms protein aggregates degraded by autophagy and has a protective effect on huntingtin-induced cell death. *J Cell Biol*. 2005;171:603-614. doi: 10.1083/jcb.200507002
89. Birgisdottir Å B, Lamark T, Johansen T. The LIR motif - crucial for selective autophagy. *J Cell Sci*. 2013;126:3237-3247. doi: 10.1242/jcs.126128
90. Pan JA, Sun Y, Jiang YP, Bott AJ, Jaber N, Dou Z, Yang B, Chen JS, Catanzaro JM, Du C, et al. TRIM21 Ubiquitylates SQSTM1/p62 and Suppresses Protein Sequestration to Regulate Redox Homeostasis. *Mol Cell*. 2016;61:720-733. doi: 10.1016/j.molcel.2016.02.007
91. Kurosawa M, Matsumoto G, Kino Y, Okuno M, Kurosawa-Yamada M, Washizu C, Taniguchi H, Nakaso K, Yanagawa T, Warabi E, et al. Depletion of p62 reduces nuclear inclusions and paradoxically ameliorates disease phenotypes in Huntington's model mice. *Hum Mol Genet*. 2015;24:1092-1105. doi: 10.1093/hmg/ddu522
92. Tanji K, Odagiri S, Miki Y, Maruyama A, Nikaido Y, Mimura J, Mori F, Warabi E, Yanagawa T, Ueno S, et al. p62 Deficiency Enhances α-Synuclein Pathology in Mice. *Brain Pathol*. 2015;25:552-564. doi: 10.1111/bpa.12214
93. Tybl E, Shi FD, Kessler SM, Tierling S, Walter J, Bohle RM, Wieland S, Zhang J, Tan EM, Kiemer AK. Overexpression of the IGF2-mRNA binding protein p62 in transgenic mice induces a steatotic phenotype. *J Hepatol*. 2011;54:994-1001. doi: 10.1016/j.jhep.2010.08.034
94. Mitsui S, Otomo A, Nozaki M, Ono S, Sato K, Shirakawa R, Adachi H, Aoki M, Sobue G, Shang HF, et al. Systemic overexpression of SQSTM1/p62 accelerates disease onset in a SOD1(H46R)-expressing ALS mouse model. *Mol Brain*. 2018;11:30. doi: 10.1186/s13041-018-0373-8
95. Seibenhener ML, Zhao T, Du Y, Calderilla-Barbosa L, Yan J, Jiang J, Wooten MW, Wooten MC. Behavioral effects of SQSTM1/p62 overexpression in mice: support for a mitochondrial role in depression and anxiety. *Behav Brain Res*. 2013;248:94-103. doi: 10.1016/j.bbr.2013.04.006
96. Parsell DA, Lindquist S. The function of heat-shock proteins in stress tolerance: degradation and reactivation of damaged proteins. *Annu Rev Genet*. 1993;27:437-496. doi: 10.1146/annurev.ge.27.120193.002253
97. Shorter J, Southworth DR. Spiraling in Control: Structures and Mechanisms of the Hsp104 Disaggregase. *Cold Spring Harb Perspect Biol*. 2019;11. doi: 10.1101/cshperspect.a034033
98. Sathyanarayanan U, Musa M, Bou Dib P, Raimundo N, Milosevic I, Krisko A. ATP hydrolysis by yeast Hsp104 determines protein aggregate dissolution and size in vivo. *Nat Commun*. 2020;11:5226. doi: 10.1038/s41467-020-19104-1
99. Harari A, Zoltsman G, Levin T, Rosenzweig R. Hsp104 N-terminal domain interaction with substrates plays a regulatory role in protein disaggregation. *Febs j*. 2022;289:5359-5377. doi: 10.1111/febs.16441
100. Jackrel ME, DeSantis ME, Martinez BA, Castellano LM, Stewart RM, Caldwell KA, Caldwell GA, Shorter J. Potentiated Hsp104 variants antagonize diverse proteotoxic misfolding events. *Cell*. 2014;156:170-182. doi: 10.1016/j.cell.2013.11.047

101. Mack KL, Kim H, Barbieri EM, Lin J, Braganza S, Jackrel ME, DeNizio JE, Yan X, Chuang E, Tariq A, et al. Tuning Hsp104 specificity to selectively detoxify α-synuclein. *Mol Cell*. 2023;83:3314-3332.e3319. doi: 10.1016/j.molcel.2023.07.029
102. Vacher C, Garcia-Oroz L, Rubinsztein DC. Overexpression of yeast hsp104 reduces polyglutamine aggregation and prolongs survival of a transgenic mouse model of Huntington's disease. *Hum Mol Genet*. 2005;14:3425-3433. doi: 10.1093/hmg/ddi372
103. Dandoy-Dron F, Bogdanova A, Beringue V, Bailly Y, Tovey MG, Laude H, Dron M. Infection by ME7 prion is not modified in transgenic mice expressing the yeast chaperone Hsp104 in neurons. *Neurosci Lett*. 2006;405:181-185. doi: 10.1016/j.neulet.2006.05.066
104. Mogk A, Ruger-Herreros C, Bukau B. Cellular Functions and Mechanisms of Action of Small Heat Shock Proteins. *Annu Rev Microbiol*. 2019;73:89-110. doi: 10.1146/annurev-micro-020518-115515

Chapter 2: CRYAB undergoes phase separation and stress-induced phosphorylation at S59 alters phase separation properties.

2.1 Introduction

Chaperone proteins play a pivotal role not only in facilitating the folding of other proteins but also in various functions such as stabilization, degradation, trafficking, translocation, complex assembly, ligand binding, evolution, and post-translational modifications such as phosphorylation[1]. Approximately 180 chaperones are responsible for assisting in the folding and quality control of ~20,000 client proteins[1]. This suggest that the chaperone-client interaction may have a degenerate specificity. We have postulated the possibility of chaperones achieving these functions through the formation of condensates, inspired by the observation within cells of various phase-separated condensates that lack membranes yet serve specific cellular functions similar to membrane-bound organelles[2]. In the context of cardiomyocytes, which is the fundamental units of cardiac tissue, a balanced protein quality control is crucial owing to their continuous rhythmic contractions throughout an individual's lifespan. In a huge structure such as cardiomyocyte, protein quality control is inefficient if it occurs only in perinuclear region. Thus, we speculate that perhaps, subcellular functions in cardiomyocytes need subcellular compartmentalization so that biochemical reactions can occur in an efficient manner.

Consequently, our focus shifts towards condensates as potential facilitators of compartmentalization within cardiomyocytes. We previously introduced the concept of a 'sarcostat,' suggesting that synthesis, repair, and degradation machinery operate proximally to the sarcomere[3]. Given the significance of the chaperone protein CRYAB in cardiac function, our

investigation initially centers on its phase separation properties. Whereas phase separation has been extensively studied in the context of protein aggregate formation in neurodegenerative diseases, its role in cardiac pathologies is emerging. Several factors influence phase separation across liquid-like or solid-like biomolecular condensates. Of them, mutations in patients and post-translational modifications such as phosphorylation are commonly found[4]. It has been observed that CRYAB phosphorylation is associated with autosomal dominant genetic human cardiomyopathy and forms protein aggregates in the mouse heart[5]. Thus, we aimed to elucidate whether phosphorylation impacts the aggregation and phase separation behavior of CRYAB. Studies suggest that proteins that are rich in positively charged and aromatic amino acids, with intrinsically disordered regions, exhibit multivalent interactions crucial for condensate formation[6]. Here, we examined the molecular grammar of CRYAB and evaluated the bioinformatics analysis of CRYAB phase separation propensity by using the program ParSe[7]. Subsequently, we engineered phospho-mimetic and deficient mutations of CRYAB and expressed them in HEK 293A cells to evaluate their effects on aggregation and toxicity. As we observed that hyperphosphorylation and protein aggregation formation are correlated in the CRYAB genetic human cardiomyopathy mutation, phase separation and FRAP analyses were then conducted to elucidate how phosphorylation influences the physical properties of CRYAB.

2.2 Results

2.2.1. Bioinformatics analysis show CRYAB has the molecular grammar to form condensates in physiological form

CRYAB protein is 175 aa long and has three different domains[8]. We evaluated the molecular grammar of the CRYAB protein in all the domains and saw 29.14% (n=51) of

positively charged (n=33) and aromatic side chain containing (n=18) amino acids (Fig. 1.1 A). Studies have shown that higher number of positively charged and aromatic side chains of amino acids influences condensate formation for proteins that contain intrinsically disordered regions[6]. Thus, we performed the bioinformatics analysis ParSe[7] and found that CRYAB could have intrinsically disordered regions (IDRs) in the 40-60 aa and then in 130-150aa range that might have the physical attributes to form condensates (Fig. 1.1 B). The IDR in the 40-60 aa is particularly interesting because studies have shown that CRYAB undergoes phosphorylation of the S59 residue upon ischemic stress by p38MAPK[9], demonstrating that this residue is crucial in modulating the phase separation properties of CRYAB.

2.2.2. Phosphorylation at serine-59 is necessary and sufficient to make CRYAB aggregate-prone

To examine the functional relevance of serine-59 phosphorylation, we generated CRYAB mutants that mimic a phosphorylation-deficient state by replacing serine with alanine (S59A) or a phospho-mimetic state with a change to aspartic acid (S59D). We also generated the CRYAB-R120G mutant with the S59A change and expressed these mutants with a N-terminal GFP tag in HEK293 cells to examine the relevance of serine-59 phosphorylation in regulating its aggregation potential. Despite being expressed at equivalent levels (Fig. 1.2 A), the S59D change resulted in formation of GFP-positive CRYAB aggregates mimicking the observations with the R120G mutant (Fig. 1.2 B). By contrast, the S59A change markedly reduced the aggregation of the CRYAB-R120G mutant protein indicating that serine-59 phosphorylation is necessary for its aggregate-prone behavior (Fig. 1.2 C-D). As we previously demonstrated, aggregate-prone CRYAB-R120G is toxic and induced cell death [10] (Fig. 1.2 C-D). The S59D mutant was indeed sufficient to induce increased cytotoxicity as compared with wild-type CRYAB, whereas the

S59A mutant attenuated the toxicity of the CRYAB-R120G mutant, paralleling the observations of their aggregate-prone behavior (Fig. 1.2 C-D). We also have generated S19A, S45A and S59A triple phospho-deficient mutants in CRYAB R120G variant, and observed similar magnitude of reduction in cell death (Fig. 1.3 A-C) that we observed in Fig 1.2 B-D. This further confirms that S59 residue is crucial for the aggregate-prone behavior of CRYAB, and s also suggest that cellular toxicity and aggregation are correlated in CRYAB phosphorylation.

2.2.3 Phosphorylation at serine-59 alters the phase separation behavior and dynamicity of CRYAB

An emerging body of evidence indicates that phase separation of proteins regulates their ability to form biomolecular assemblies termed as 'condensates' to modulate their biophysical properties that determine the dynamicity and fluidity of condensates and regulate their aggregation potential [4,11]. Accordingly, to examine whether CRYAB can phase separate in living cells, we adapted the OptoDroplet system [12] and expressed full-length CRYAB, as well as its N-terminus, C-terminus and alpha-crystallin domain (ACD) separately (Fig. 1.4 A). We employed the N-terminal domain of FUS (a condensate forming protein implicated in neurodegeneration as a positive control and Cry2 as a negative control) [12] and examined their propensity to phase separate after light activation. As shown, light activation resulted in dynamic phase separation of CRYAB into condensates mimicking the observations with N-terminal fragment of FUS protein, whereas Cry2 protein by itself did not phase separate, as previously described [12] (Fig. 1.4 C). Remarkably, CRYAB full-length protein and each of CRYAB's N-terminus, C-terminus and alpha-crystallin domain (ACD) domains have the propensity to phase separate (Fig. 1.5). Whereas some spherical CRYAB condensates were observed in unstressed state prior to blue light activation, the average number of condensates doubled after light activation (Fig. 1.4 D).

Interestingly, a S59A or S59D change in the full-length protein completely abrogated light-induced condensate formation (Fig. 1.4 D). However, like the observations with GFP-tagged proteins (Fig. 1.2 A-D), the mCherry-tagged optoIDR constructs induced protein-aggregate formation in cells expressing S59D and CRYAB-R120G mutant proteins (Fig. 1.4 C) even prior to light activation, with markedly larger and irregular protein-aggregates in S59D transfected cells, mimicking the R120G mutant (Fig. 1.4 A-D). In agreement with the observations with the GFP-tagged CRYAB-R120G-S59A vs. the CRYAB-R120G constructs (Fig. 1.2 A-D), the S59A change reduced the size of R120G optoDroplet construct aggregates (Fig. 1.4 E); but did not result in a noticeable light-induced increase in condensate formation (Fig. 1.4 D).

These findings suggest that similar to the R120G mutation, the S59D mutation reduces the fluidity of condensates, making CRYAB aggregate prone. To examine this conclusion, we performed fluorescence recovery after photobleaching (FRAP). As shown in Fig. 1.6 A-C, WT CRYAB shows rapid recovery following photobleaching, indicating that these phase-separated condensates are dynamic and liquid-like. In contrast, the recovery of fluorescence was markedly reduced in S59D and R120G mutant proteins as compared with wild-type CRYAB (Fig. 1.6 A-C). Remarkably, the S59A change in R120G restored the fluorescent recovery to wild-type levels (Fig. 1.6 A-C). The recovery was comparable in the S59A mutant to wild-type CRYAB (Fig. 1.6 A-C). Taken together, these data indicate that serine-59 phosphorylation is both necessary and sufficient to alter the phase separation behavior of CRYAB, reducing their fluidity to convert them to a ‘gel-like’ state [4,13], as a potential explanation for formation of aggregates.

2.3 Discussion

Protein-aggregates are a hallmark of neurodegenerative pathologies and rare genetic cardiomyopathies. Our findings here demonstrate a mechanistic role for altered phase separation and aggregation of CRYAB, a cardiac-enriched chaperone, in driving progression of ischemic cardiomyopathy, which is the leading cause of heart failure worldwide. We are primarily interested on how CRYAB phosphorylation can affects its physical properties and eventually its chaperone properties because CRYAB S59 is phosphorylated upon ischemic stress[14] and ParSe program[7] predicted a possible IDR region in 40-60aa range in CRYAB. We hypothesized that as a chaperone protein in the heart, CRYAB forms condensates and performs its function by interacting with client proteins such as desmin, actin and α-actinin within the condensates. When CRYAB is phosphorylated, the condensate properties of CRYAB are altered. As a result, CRYAB client proteins are abnormally located into the aggreates[15] inducing dysregulation in cardiomyocyte structure and function. Evidence shows that CRYAB R120G mutation, which is associated with rapidly fatal genetic human cardiomyopathy and the presence of protein aggregates in the heart[16], is hyperphosphorylated. Thus, we are interested to see whether phosphorylation can affect the physical properties of CRYAB condensate formation. Using transient transfection into HEK cells, we observed similar expression of CRYAB variants, and toxic effect of phospho-CRYAB variants in aggregate formation and cell survival.

We used OptoDroplet construct[12] for live cell imaging of condensate formation and evaluated dynamicity by FRAP. CRYAB undergoes phase separation into ‘liquid-like’ dynamic condensates under physiologic conditions. Sustained stress, as with development of ischemic cardiomyopathy, results in increased phosphorylation of CRYAB at serine-59, or hyper-phosphorylated R120G mutation, alters its phase separation behavior. pS59CRYAB forms ‘gel-

like' condensates with reduced dynamicity, triggering aggregate formation and cellular toxicity. That shows us that if CRYAB is phosphorylated under stress by p38 MAPK targeting S59 residue, it can affect CRYAB properties by making it aggregate-prone and toxic. It will be interesting to see whether aggregate-prone properties alter CRYAB-client protein interactions. This potentially can represent a mechanism for abnormal cardiomyocyte structure and function. One potential limitation of this experiment is that we have not used a stable cell line expressing CRYAB variants. However, we have maintained similar experimental conditions for transfection, protein expression and imaging to reduce experimental variance.

2.4 Conclusion

These findings suggest that phosphorylation in CRYAB, specifically in S59 residue can make it aggregate-prone, toxic, and alter its chaperone function by changing phase separation properties. Thus, to understand the biology and to find a target for ischemic cardiomyopathy, we should evaluate the abundance of pS59CRYAB, its localization in the heart, and how it can affect the interaction with its client proteins.

2.5 Materials and Methods

Molecular grammar determination and Phase separation propensity analysis. Molecular grammar determination was done by using Prot-Param 1.0 program by EBiAn-Easy Bioinformatics Analysis program. Phase separation propensity analysis was performed using ParSe: predict phase-separating protein regions from the primary sequence program from the website- http://folding.chemistry.msstate.edu/utils/parse.html.

Generation of crystallin constructs. pHR-mCh-Cry2WT (Addgene #10221) and pHR-FUSN-mCh-Cry2WT (Addgene #10223) as generated by Dr. Clifford Brangwynne [12], were obtained

and verified by sequencing. For phase separation assay in the live cells, we have generated pHR-CRYAB-mCh-Cry2 construct using in-fusion® snap assembly kit (Takara, CAT#638945). CRYAB S59A, S59D and R120G+S59A mutations were introduced in pHR-CRYAB-mCh-Cry2 construct using QuikChange II site-directed mutagenesis kit (Agilent, CAT#200523). These constructs were subsequently cloned into pcDNA 3.1 mammalian vector for the expression in HEK293A cells. Constructs coding for eGFP-CRYAB, eGFP-CRYAB S59A, eGFP-CRYAB S59D and eGFP-CRYAB-R120G + S59A were generated as described above in a pcDNA3.1 backbone for protein aggregation studies and cell death assessment.

Assessment of protein aggregation and cell death. HEK293 cells were transfected with various GFP-tagged CRYAB constructs using Lipofectamine 3000 reagent (ThermoFisher, CAT#L3000) and cells imaged for GFP at 24 hours after transfection under Zeiss-700 confocal microscope for presence of protein aggregation. Cells were harvested at 48 hours for cell death assay. Cell death was assessed using a fluorometric assay with LIVE/DEAD™ Viability/Cytotoxicity Kit for mammalian cells (ThermoFisher, CAT#L3224), as we have previously described [10].

Studies with optoDroplet constructs. CRYAB constructs were transfected into HEK 293A cells using Effectene transfection reagent (Qiagen, CAT#301425) and live-cell imaging was performed using 35-mm glass-bottom dishes at 24-hours after transfection using 40x oil immersion objective of the Nikon A1R confocal imaging system (equipped with 37°C stage) at the Center for Cellular Imaging (WUCCI) at Washington University in St. Louis School of Medicine. Cells were imaged with two laser wavelengths (488 nm for Cry2 activation and 561 nm for mCherry imaging) with laser power of 10% for the 488 nm. Various parameters were quantified using imageJ (NIH) by adjusting the threshold to ensure uniform cut-off values at the

t=0 and t=300s time-point images. Average condensate area was determined by total area of the fluorescence signal divided by number of condensates before or after 300s of the blue light activation. Average number of condensates per cell was obtained by dividing total number of condensates divided by number of cells before or after 300s of the blue light activation.

Studies with fluorescence recovery after photobleaching (FRAP). FRAP was performed on OptoIDR[12] constructs as described above while imaging with100x objective lens of the Nikon A1R confocal imaging system, using 488nm laser at 50% intensity and 561 nm laser at 50% intensity for 1 minute selecting a region of interest of ~ 1 μm in diameter; and fluorescence recovery was monitored. Intensity traces were collected using imageJ and normalized to pre-bleaching intensity (set at 100%). Only condensates with reduction in intensity to <10% (as compared to pre-bleach) post-photobleaching were selected for further analysis.

Immunofluorescence analysis. We performed immuno-histochemistry on cells. Primary cultures of HEK 293A cells were fixed in 100% cold methanol for 20 minutes, followed by blocking with 1% normal serum in PBS for 1 hour at room temperature. Primary antibodies used was as follows: Anti-GFP (Abcam, CAT#ab290) with overnight incubation at 4°C. After serial washes, samples were stained with secondary antibody and mounted with fluorescent 4',6-diamidino-2-phenylindole mounting medium (Vector Labs, H-1200). Confocal imaging was performed on a Zeiss confocal LSM-700 laser scanning confocal microscope using 40×/1.3 oil immersion objectives, and images were processed using the Zen black software.

2.6 Figures

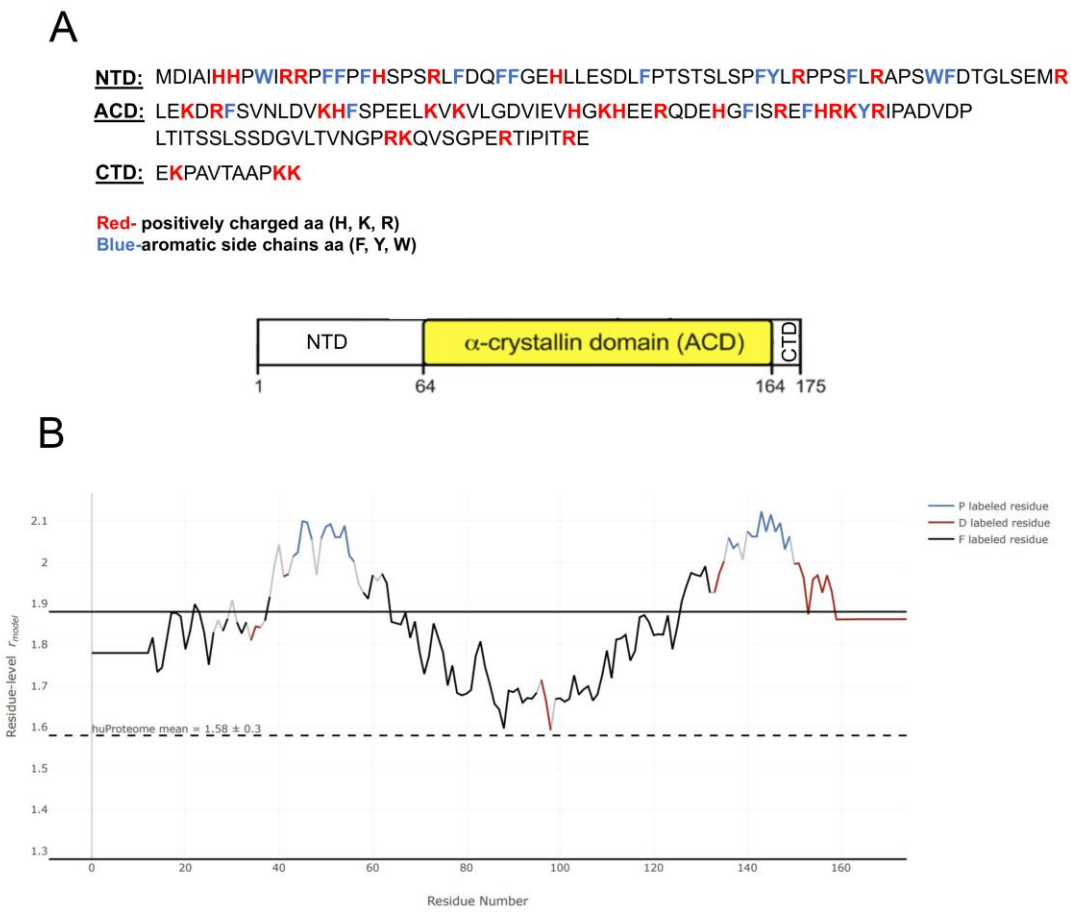

Figure 2.1: Molecular grammar and bioinformatics analysis predict phase separation properties in CRYAB. A) Schematic showing the molecular grammar of CRYAB protein and the domain structure. Red color shows positively charged amino acids and blue color shows aromatic side chain amino acids. **B)** ParSe bioinformatic analysis showing the propensity of CRYAB to phase separate. Blue color shows P regions (intrinsically disordered and prone to phase separate), red color shows D regions (intrinsically disordered and do not undergo condensate formation) and black color shows F regions (may or may not be intrinsically disordered and can fold to a stable conformation).

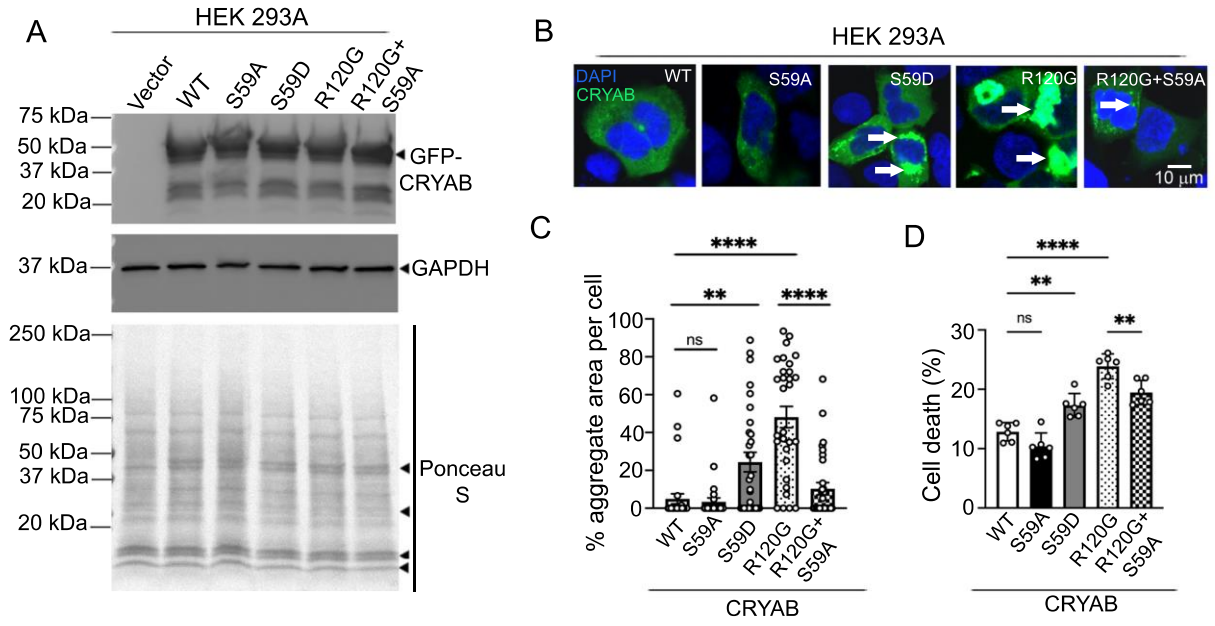

Figure 2.2: Phosphorylation of CRYAB at S59 makes it aggregate-prone and toxic. A) Immunoblot (A) demonstrating expression of GFP-fusion proteins in HEK293A cells transfected with GFP-tagged wild-type CRYAB, its phospho-mimetic mutant (S59D), phosphorylation-deficient mutant (S59A), R120G mutant or the R120G and S59A double mutant proteins. **B, C)** Representative immunofluorescence images (B) for detection of protein-aggregates with quantitation (C) of aggregate area per cell. ** indicates P<0.01 and **** indicates P<0.0001 by Tukey's post-hoc test after one-way ANOVA. Nuclei are blue (DAPI). **D)** Cell death in cells treated in A. ** indicates P<0.01 and **** indicates P<0.0001 by Tukey's post-hoc test after one-way ANOVA.

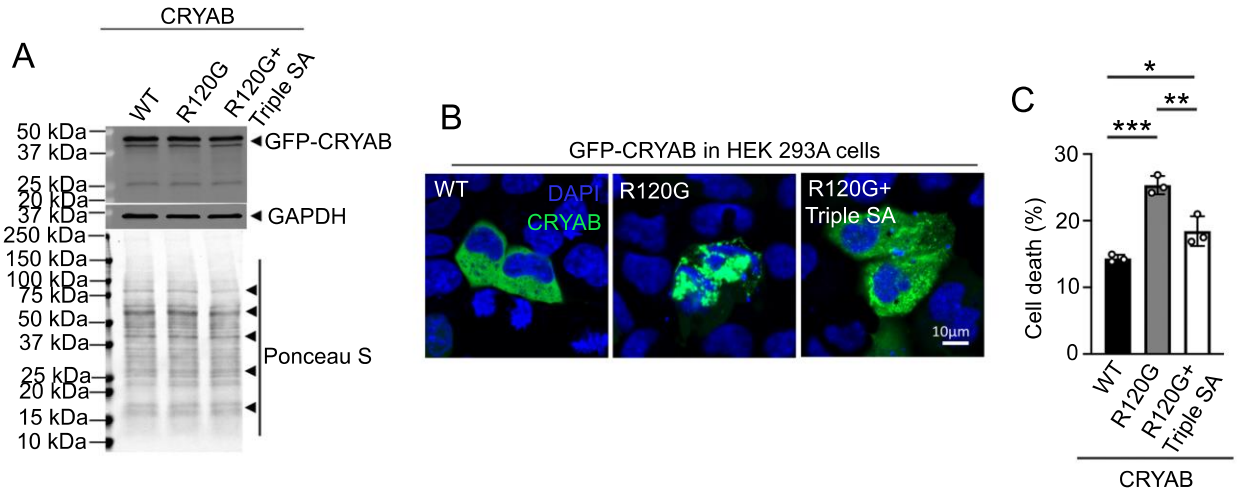

Figure 2.3. Phospho-deficient mutants of S19, S45 and S59 residue reduces cell death in CRYAB R120G. A) Immunoblot (A) demonstrating expression of GFP-fusion proteins in HEK293A cells transfected with GFP-tagged wild-type CRYAB, R120G mutant or the R120G and S19, S45, S59A triple mutant proteins. **B, C)** Representative immunofluorescence images (B) for detection of protein-aggregates with quantitation (C) of % cell death. * Indicates $p<0.05$, ** indicates $p<0.01$, and *** indicates $P<0.001$ by Tukey's post-hoc test after one-way ANOVA. Nuclei are blue (DAPI).

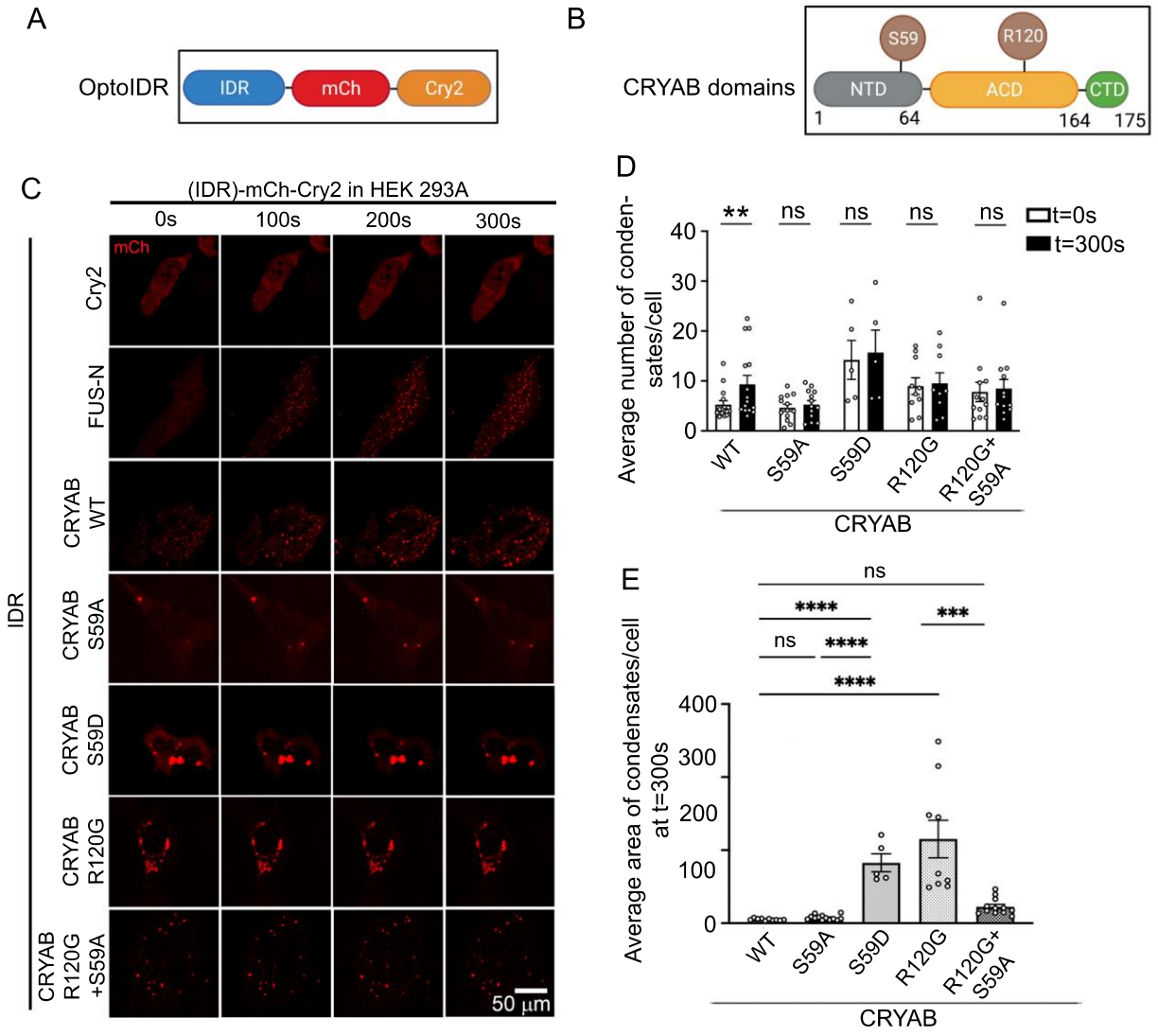

Figure 2.4. Phosphorylation alters phase separation properties of CRYAB. A) Schematic depicting generation of optoIDR constructs. 'IDR' indicates intrinsically disordered region, mCh indicates mCherry fluorophore and Cry2 encodes for *Arabidopsis thaliana* protein with light-activated phase separation characteristics. **B)** Various domains of CRYAB with localization of serine-59 and arginine 120 residues depicted. **C)** Representative time-lapse images at t=0s, 100s, 200s, and 300s after light activation in HEK293A cells transfected with constructs generated with CRYAB WT, its phosphorylation-deficient mutant (S59A), phospho-mimetic mutant (S59D), R120G mutant or the R120G and S59A double mutant proteins as the 'IDR' in the optoIDR constructs. Cry2 fused with mCherry without an IDR was used as the negative control and FUS-N fused with mCherry-Cry2 was studied as positive control. **D**) Average number of condensates/cells at t=0 vs. t=300s in cells treated as in E. ** indicates P<0.01 by Mann-Whitney

test. **E)** Average area of condensates/cell at t=300s in cells treated in E. *** indicates P<0.001 and **** indicates P<0.0001 by Tukey's post-hoc test after one-way ANOVA. 'ns' indicates not significant for all panels.

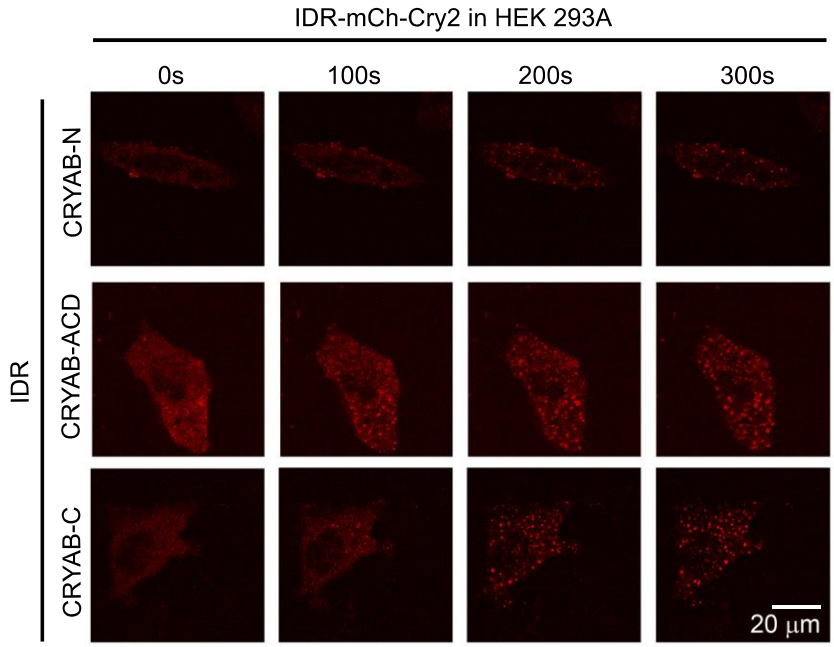

Figure 2.5. N-terminus, ACD, and C-terminus domains of CRYAB undergo phase separation. A) Representative time lapse images at t=0s, 100s, 200s, and 300s after light activation in HEK293A cells transfected with constructs generated with CRYAB N-terminus, Alpha-crystallin domain (ACD), and C-terminus domains as the 'IDR' in the optoIDR constructs.

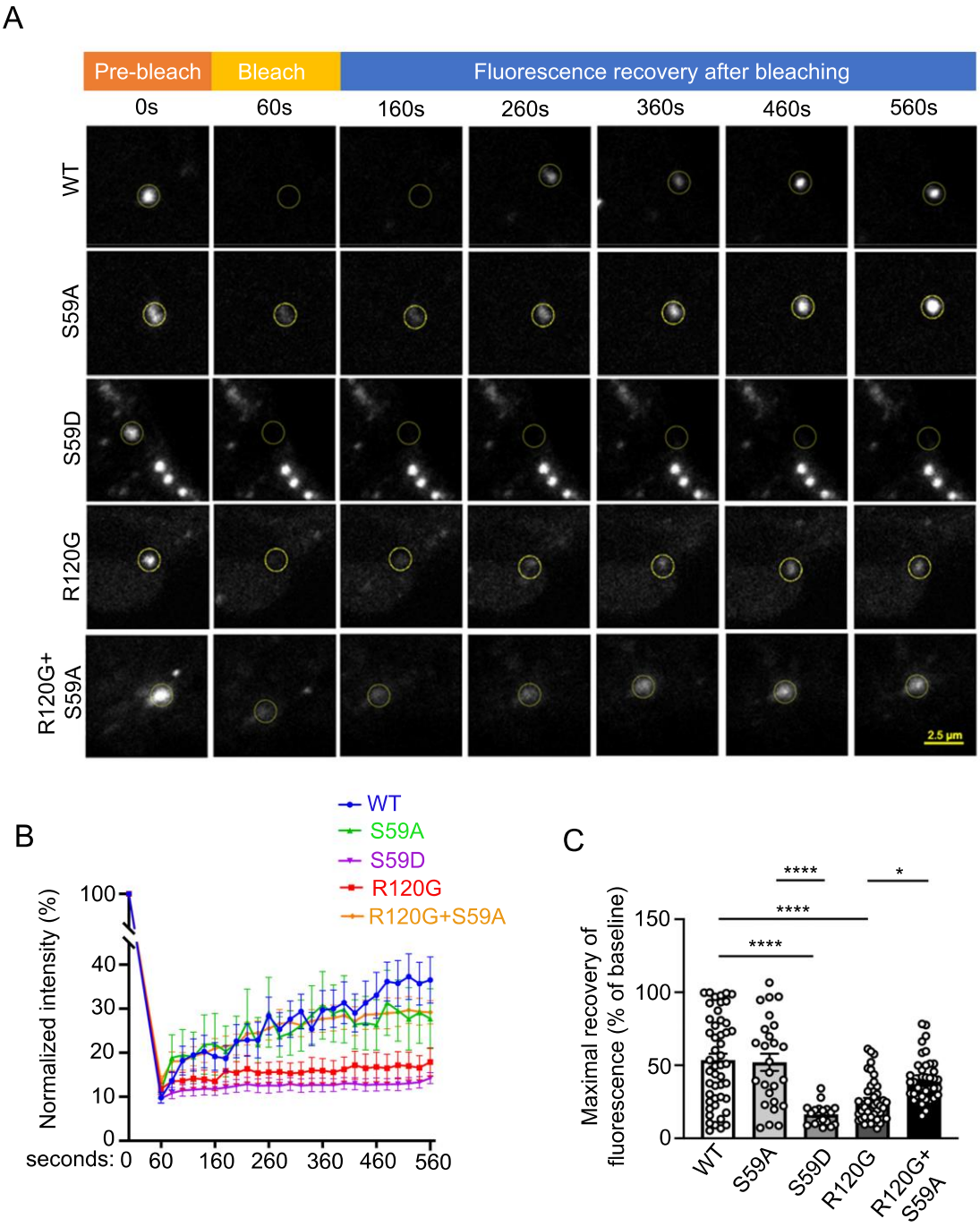

Figure 2.6. Phosphorylation of CRYAB at serine-59 reduces dynamicity of the condensates. A, B) Representative images demonstrating recovery of fluorescence after photobleaching in HEK 293A cells transfected with mCherry-Cry2 fused optoIDR constructs generated with CRYAB WT, its phosphorylation-deficient mutant (S59A), phospho-mimetic mutant (S59D), R120G mutant, or the R120G and S59A double mutant proteins. Representative images demonstrate area of photobleaching (marked with a dotted circle) prior to (pre-bleach),

immediately after, and at 100, 200, 300, 400 and 500 seconds (s) after photobleaching was terminated. Intensity at various time points is depicted as a fraction of intensity prior to bleaching (set at 100%). **C.** Quantitation of fluorescence recovery (maximum minus immediately post-bleach) in CRYAB variants indicated in A. * indicates $P<0.05$, and **** indicates $P<0.0001$ by Tukey's post-hoc test after one-way ANOVA.

2.7 References

1. Freilich R, Arhar T, Abrams JL, Gestwicki JE. Protein-Protein Interactions in the Molecular Chaperone Network. *Acc Chem Res*. 2018;51:940-949. doi: 10.1021/acs.accounts.8b00036
2. Banani SF, Lee HO, Hyman AA, Rosen MK. Biomolecular condensates: organizers of cellular biochemistry. *Nat Rev Mol Cell Biol*. 2017;18:285-298. doi: 10.1038/nrm.2017.7
3. Islam M, Diwan A, Mani K. Come Together: Protein Assemblies, Aggregates and the Sarcostat at the Heart of Cardiac Myocyte Homeostasis. *Front Physiol*. 2020;11:586. doi: 10.3389/fphys.2020.00586
4. Alberti S, Hyman AA. Biomolecular condensates at the nexus of cellular stress, protein aggregation disease and ageing. *Nat Rev Mol Cell Biol*. 2021;22:196-213. doi: 10.1038/s41580-020-00326-6
5. Rajasekaran NS, Connell P, Christians ES, Yan LJ, Taylor RP, Orosz A, Zhang XQ, Stevenson TJ, Peshock RM, Leopold JA, et al. Human alpha B-crystallin mutation causes oxido-reductive stress and protein aggregation cardiomyopathy in mice. *Cell*. 2007;130:427-439. doi: 10.1016/j.cell.2007.06.044
6. Wang J, Choi JM, Holehouse AS, Lee HO, Zhang X, Jahnel M, Maharana S, Lemaitre R, Pozniakovsky A, Drechsel D, et al. A Molecular Grammar Governing the Driving Forces for Phase Separation of Prion-like RNA Binding Proteins. *Cell*. 2018;174:688-699.e616. doi: 10.1016/j.cell.2018.06.006
7. Paiz EA, Allen JH, Correia JJ, Fitzkee NC, Hough LE, Whitten ST. Beta turn propensity and a model polymer scaling exponent identify intrinsically disordered phase-separating proteins. *J Biol Chem*. 2021;297:101343. doi: 10.1016/j.jbc.2021.101343
8. Rajagopal P, Tse E, Borst AJ, Delbecq SP, Shi L, Southworth DR, Klevit RE. A conserved histidine modulates HSPB5 structure to trigger chaperone activity in response to stress-related acidosis. *Elife*. 2015;4. doi: 10.7554/eLife.07304
9. Ma XL, Kumar S, Gao F, Louden CS, Lopez BL, Christopher TA, Wang C, Lee JC, Feuerstein GZ, Yue TL. Inhibition of p38 mitogen-activated protein kinase decreases cardiomyocyte apoptosis and improves cardiac function after myocardial ischemia and reperfusion. *Circulation*. 1999;99:1685-1691. doi: 10.1161/01.cir.99.13.1685
10. Ma X, Mani K, Liu H, Kovacs A, Murphy JT, Foroughi L, French BA, Weinheimer CJ, Kraja A, Benjamin IJ, et al. Transcription Factor EB Activation Rescues Advanced alphaB-Crystallin Mutation-Induced Cardiomyopathy by Normalizing Desmin Localization. *Journal of the American Heart Association*. 2019;8:e010866. doi: 10.1161/JAHA.118.010866
11. Choi JM, Holehouse AS, Pappu RV. Physical Principles Underlying the Complex Biology of Intracellular Phase Transitions. *Annu Rev Biophys*. 2020;49:107-133. doi: 10.1146/annurev-biophys-121219-081629
12. Shin Y, Berry J, Pannucci N, Haataja MP, Toettcher JE, Brangwynne CP. Spatiotemporal Control of Intracellular Phase Transitions Using Light-Activated optoDroplets. *Cell*. 2017;168:159-171.e114. doi: 10.1016/j.cell.2016.11.054
13. Zhang H. The glassiness of hardening protein droplets. *Science*. 2020;370:1271-1272. doi: 10.1126/science.abe9745

14. Zoncu R, Efeyan A, Sabatini DM. mTOR: from growth signal integration to cancer, diabetes and ageing. *Nat Rev Mol Cell Biol*. 2011;12:21-35. doi: 10.1038/nrm3025
15. Ma X, Mani K, Liu H, Kovacs A, Murphy JT, Foroughi L, French BA, Weinheimer CJ, Kraja A, Benjamin IJ, et al. Transcription Factor EB Activation Rescues Advanced αB-Crystallin Mutation-Induced Cardiomyopathy by Normalizing Desmin Localization. *J Am Heart Assoc*. 2019;8:e010866. doi: 10.1161/jaha.118.010866
16. Vicart P, Caron A, Guicheney P, Li Z, Prévost MC, Faure A, Chateau D, Chapon F, Tomé F, Dupret JM, et al. A missense mutation in the alphaB-crystallin chaperone gene causes a desmin-related myopathy. *Nat Genet*. 1998;20:92-95. doi: 10.1038/1765

Chapter 3: Impaired protein quality control is observed in both Human Ischemic Cardiomyopathy (ICM) and in mouse model of ICM.

3.1 Introduction

Cardiac muscle cells, which are the building blocks of the heart, depend on coordinated systems to maintain their structure and function. These systems ensure that the heart can contract and relax smoothly without interruption[1]. Certain mutations in proteins that helps other proteins to fold, i.e. chaperones like CRYAB, HSP27, HSPB6, HSPB8, and co-chaperones like BAG3 are linked to heart diseases by affecting the stability, position, or breakdown of proteins in the myocardium[2]. Dilated cardiomyopathy, where the left ventricle in the heart become enlarged (dilated), for example, show an accumulation of certain proteins that aren't folded properly, along with a decrease in a specific proteins such as BAG3 that appear to be required to maintain cardiac structure [2]. Similar issues are seen in mouse hearts after myocardial infarction, where boosting levels of BAG3 protein helps fix the problem with heart muscle contractions[2]. So, understanding how genetic heart conditions cause impaired protein quality control through dysfunction of the chaperone and co-chaperone proteins, could lead to new ways to prevent or treat heart failure in general.

In certain genetic conditions, proteins are mis-localized, leading to cardiac complications. This happens with mutations in genes like *DES*, which codes for a protein called Desmin [3,4] and in *CRYAB* [5], which codes for a chaperone protein called αB-crystallin. When these proteins are mis-localized, it causes cardiac complications similar to what's seen when these proteins are not sufficiently expressed in the heart[4].

In this study, we hypothesize that similar to genetic human cardiomyopathy[6], CRYAB is phosphorylated in its S59 residue in ischemic cardiomyopathy which makes CRYAB sticky and aggregate prone. To examine this function, we planned experiments to focus on CRYAB client proteins and observed their localization in ischemic cardiomyopathy hearts. To examine whether Desmin and other client proteins of CRYAB such as actin and α-actinin has altered localization in ischemic cardiomyopathy (ICM), we performed immunohistochemistry and biochemical subcellular fractionation on heart tissue obtained from humans with ICM and from donor hearts without known cardiac pathology, that were not used for transplantation (Table 3.1). In open-chest models of coronary ligation, surgical trauma through thoracotomy triggers an immune response, altering various mechanisms involved in ischemia and reperfusion and potentially changing the size of the infarct. Thus, we used closed-chest ischemia-reperfusion surgery in our study to overcome this which provides a better model to mimic human ischemic cardiomyopathy, by separating the MI from initial surgery. We evaluated WT C57BL6J mice that underwent closed-chest-ischemia reperfusion injury and performed immunoblotting and immunohistochemistry and read echocardiography to evaluate cardiac structure and function. Our goal was to observe how both in these models, CRYAB and its client proteins' localization in the cardiomyocytes and relative abundance in the aggregates are correlated with cardiac myocyte structure and function.

3.2 Results

3.2.1 Characteristics of individuals whose human heart samples were included in the study

We used n=8 human ICM hearts and n=8 non-failing donor hearts for our study (Table 3.1). We evaluated individual characteristics such as sex, age, BMI, Left Ventricle (LV) mass

index, LV End Diastolic Diameter (LVEDD), LV Ejection Fraction (LVEF), history of Diabetes, and other related medical histories. ICM hearts showed LV dilation (P<.01 in LVEDD (cm)), LV systolic dysfunction (P<0.0001 in LVEF (%)) and an increase in LV mass (P<0.0001 in LV mass index (g/kg). P values were obtained by two-tailed t-test for continuous variables and by Fisher's exact test for categorical variables. Most of the heart samples evaluated in both groups were males and with an average age of early to mid-50s.

3.2.2 Mis-localization and protein aggregates containing desmin and other CRYAB client proteins were observed in ICM human hearts

To examine whether CRYAB client proteins has altered localization in more common ischemic cardiomyopathy (ICM) similar to observations in the rare and fatal genetic cardiomyopathy, we performed immunohistochemistry in donor and ICM samples. When we evaluated the ICM human hearts, as shown in Fig. 3.1 A, Desmin was observed along the Z-discs and intercalated discs in donor hearts consistent with its physiologic localization. To characterize the mis-localization of Desmin and other client proteins of CRYAB, we developed a scoring strategy where we quantitated the striation of the proteins and presence of aggregates. We have found that Desmin was mis-localized to protein-aggregates in ICM hearts (Fig. 3.1 A) along with other CRYAB client proteins such as actin and α-actinin. This was accompanied by immunodetectable presence of increased polyubiquitin in ICM hearts and co-localization of desmin aggregates with polyubiquitin (Fig. 3.2). We also observed increased pre-amyloid oligomers in ICM hearts as detected by A11 antibody[7] staining (Fig. 3.3). These findings clearly suggest that similar to genetic human cardiomyopathy mutation R120G, CRYAB client proteins are also mis-localized in ischemic cardiomyopathy human hearts.

3.2.3 Protein aggregates containing increased pS59CRYAB was observed in human ischemic cardiomyopathy hearts

To examine potential mechanisms for Desmin mis-localization, we evaluated the localization of CRYAB, which plays a critical role in chaperoning desmin[8]; and observed increased partitioning of CRYAB to the detergent-insoluble aggregate-rich fraction (Fig. 3.4 A, E) with a reduction in CRYAB abundance in the soluble fraction (Fig. 3.4 F, I). Interestingly, prior studies indicate that CRYAB undergoes post-translational modifications, specifically phosphorylation at serine resides (at position 19, 45 and 59), under stress[9]. Of these, serine 45 and 59 are phosphorylated by stress-induced p38 MAPK kinase (Fig. 3.4)[9], as well as by protein kinase N, which are activated in cardiac ischemia-reperfusion injury[10,11]. Also, studies in cell-culture models show that R120G mutant of CRYAB is hyperphosphorylated at these three serine residues, which regulates its tendency to aggregate[12]. Our findings demonstrate increased abundance of phosphorylated CRYAB at residue serine-59 (pS59CRYAB), but not at serine 45 in the detergent-insoluble fraction (Fig. 3.4 A, E) with a concomitant decline in its abundance in the soluble fraction (Fig. 3.4 F, I), which parallels the partitioning of p62 and polyUb proteins to the aggregate-rich detergent-insoluble fraction. Importantly, we also detected increased abundance of p62, an adaptor protein that binds to and sequesters polyUb proteins in aggregates[13,14] (Fig. 3.4 A, B), accompanying increased polyUb proteins (Fig. 3.4 A, C) in the aggregate-rich NP-40 detergent-insoluble fraction. In parallel, we observed a trend in reduction in p62 abundance in detergent-soluble fraction (Fig. 3.4 F, G) in LV myocardial tissue from ICM patients as compared with donors, suggesting p62-mediated sequestration of polyubiquitinated proteins in aggregates.

3.2.4 Closed-chest cardiac ischemia-reperfusion (IR) injury modeling in C57BL6J mice mimics human ischemic cardiomyopathy phenotype observed in human

To examine if similar partitioning of pS59CRYAB is observed in mouse myocardium under stress, we performed closed-chest cardiac ischemia-reperfusion (IR) injury in young adult wild-type C57BL6J mice and evaluated them 4 weeks later. As shown in Fig. 3.5 A-D, IR injury induced a marked increase in left ventricular end-diastolic volume (EDV) with decline in left ventricular ejection fraction (EF) at 4 weeks post-MI, as compared with sham operated-mice, consistent with development of ischemic cardiomyopathy. Similar to the observations in human ICM (Fig. 3.1), this was accompanied by a significant increase in abundance of pS59CRYAB, with a trend towards increased p62 in the aggregate-rich NP40-insoluble fraction (Fig. 3.6 A-G) and mis-localization of desmin client proteins α-actinin and actin in the post-IR myocardium (Fig. 3.7 A, B). We also observed increased pS59CRYAB in CRYAB R120G transgenic mouse heart (Fig. 3.8). Taken together, these findings demonstrate that CRYAB is increasingly phosphorylated at serine-59 in the setting of genetic cardiomyopathy, as well as ischemic cardiomyopathy in mice and in humans, and partitions into aggregate-rich biochemical protein fraction. This is associated with mis-localization of CRYAB client proteins desmin, α-actinin and actin into the protein-aggregates, supporting the hypothesis that phosphorylation at serine-59 may render CRYAB aggregate-prone and sequester desmin and other client proteins within protein-aggregates in ischemic cardiomyopathy.

3.3 Discussion

Interestingly, many mutations linked to diseases affect proteins in the heart, causing them to clump together, which is known as protein-aggregates [5,15,16]. This has been observed in conditions like idiopathic dilated cardiomyopathy and hypertrophic cardiomyopathy[7,17,18]. However, it hasn't been looked into whether this happens in ischemic cardiomyopathy, a condition where blood flow to the heart is restricted. It's also unclear if these aggregates of proteins are helpful, harmful, or just a sign that the protein recycling system in the cell isn't working properly to get rid of damaged or misfolded proteins.

Desmin, a sarcomere-associated protein, plays a critical role in maintenance of sarcomere structure and subcellular organization by acting as a scaffold to hold the various structures in place. Mutations in Desmin or its chaperone CRYAB, result in Desmin associated cellular pathologies. Desmin or its helper protein CRYAB mutations can cause desmin to either not work properly or end up in aggregates, leading to a group of disorders known as 'desminopathies'[4]. Studies have shown that a specific mutation in CRYAB causes it to bind too tightly to desmin, trapping it in aggregates[8,19]; Boosting a process called autophagy, which helps clean up the cell, can help remove these aggregates and restore desmin localization[19,20]. This kind of protein aggregate isn't limited to desmin. Similar problems happen with another protein called BAG3, which is linked to restrictive cardiomyopathy in humans [21]. When a mutated form of BAG3, P209L is present, it causes other proteins in the heart to aggregate together, leading to heart muscle problems and cardiomyopathy[22].

Overall, this study shows how a chaperone protein in the heart can become aggregate-prone and induce ischemic cardiomyopathy by phosphorylation. Therefore, examining the

mechanisms by which cardiac proteins become aggregate-prone could offer therapeutic promise to prevent proteotoxic cardiac dysfunction.

3.4 Conclusion

This study demonstrates that CRYAB aggregates are present prone when it is phosphorylated (pS59CRYAB) in ischemic stress. Mis-localization of CRYAB client proteins such as actin, α-actinin and desmin are observed in ICM. Further understanding is needed to determine the effect of the presence of aggregates and increased abundance of pS59CRYAB in the aggregate-rich insoluble fractions. Further experiments, such as using both genetic and pharmacological approaches to modulate CRYAB phosphorylation and their effect on cardiac structure and functions after IR are needed in the future for a better understanding of this aspect.

3.5 Materials and Methods

Reagents and mice. C57BL6/J mice (strain #00664) from JAX [23] were employed. Both male and female mice were studied for subjecting them to IR injury model. All observers were blinded.

Closed-chest cardiac ischemia-reperfusion modeling. Mice were subjected to reversible left anterior descending coronary artery ligation for 90 min followed by reperfusion, in a closed-chest procedure, as described [24]. Overall surgical mortality was <5%. All surgeries were performed by two surgeons, Carla J. Weinheimer and Attila Kovacs from Mouse Cardiovascular Phenotyping Core at Washington University in St. Louis School of Medicine.

Human Heart tissues. De-identified frozen heart tissue samples were obtained from the Human Heart Tissue Bank at the University of Pennsylvania, and formalin-fixed paraffin-embedded left

ventricular myocardial tissue was obtained from the Translational Cardiovascular Biobank and Repository at Washington University School of Medicine. The hearts were procured from two separate patient groups: non-failing brain-dead organ donors with no history of heart failure (Donor, whose hearts were screened but not selected for transplantation) and heart transplant recipients with advanced ischemic cardiomyopathy (ICM), that were obtained at the time of orthotopic heart transplantation. Clinical characteristics of the subjects providing human tissue for these studies are summarized in Table 3.1.

Echocardiography. 2D–directed M-mode echocardiography was performed using a Vevo 2100 Imaging System (VisualSonics, Toronto, Canada) equipped with a 30-MHz linear-array transducer, as we have previously described [23,24]. Mice were anesthetized with isoflurane for studies obtained in unstressed mice and before I/R modeling (pre-ischemia echo study). Echocardiography during ischemia was performed under isoflurane anesthesia and at four weeks post ischemia-reperfusion injury was performed under avertin anesthesia. Cardiac images were obtained by a handheld technique. Area-at-risk, left ventricular dimensions, wall thickness, heart rate, fractional shortening, EF and volume calculations were performed by a blinded echocardiographer as described [24]. Histologic assessment with hematoxylin and eosin staining, and assessment of myocardial fibrosis with Masson's trichrome staining and transmission electron microscopy, was performed as previously described [19].

Biochemical fractionation into NP-40 detergent soluble and insoluble fractions. We subjected cardiac tissues obtained from human hearts and from the remote left ventricular myocardium of mice subjected to ischemia-reperfusion injury (non-injured basal one-third); and cell extracts from neonatal rat cardiac myocytes to obtain soluble-insoluble fractions as previously described [19]. Heart tissue was mechanically homogenized in homogenization buffer

(0.3 M KCl, 0.1 M KH_2PO_4, 50 mM K_2HPO_4, 10 mM EDTA, 4 mM Na Orthovanadate, 100 mM NaF, 1X Protease inhibitor, pH to 6.5). Homogenized samples were passed through mesh basket on ice, followed by collection of the lysate run-through which was incubated on ice for 30 minutes. An aliquot was transferred to another Eppendorf tube and 10% NP-40 was added to for a final concentration of 1% NP-40. Samples were then incubated on ice for 30 minutes and spun at 16,000g for 15 minutes at 4°C. Supernatant was collected as soluble fraction. The pellet was washed 3 times with cold PBS (following addition of 1ml PBS to each pellet, and spin down at 16,000g for 10 minutes) followed by resuspension in 1% SDS, 10mM Tris buffer to generate the insoluble fraction.

Immunofluorescence analysis. We performed immuno-histochemistry on cells and myocardial tissues as we have previously described [19]. Primary antibodies used were as follows: anti-desmin (Santa Cruz Biotechnology, Inc, SC-7559), anti-ubiquitin (Sigma-Aldrich, CAT#04-262), anti-actin (Millipore Sigma, A2066), anti-actinin (Abcam, ab9465) with overnight incubation at 4°C. As an example of desmin and polyubiquitin immunostaining, this protocol was followed: Paraffin-embedded heart sections (4 μm thick) were subjected to de-paraffinization using Xylene; serial 100%, 90%, 70% and 50% EtOH treatment followed by hydration using DI water and heat-induced epitope retrieval in Diva decloaker solution (Biocare medical, REF# DV2004MX). This was followed by blocking using 1% BSA (Sigma-Aldrich, CAT#A9647-100G), 0.1% Tween-20 (Sigma-Aldrich, CAT# P2287-500ML) in PBS (Corning, CAT# 21-040-CM) and 5% donkey serum. The slides were incubated overnight with primary antibody against Desmin (Santa Cruz Biotechnology, SC-7559), and Ubiquitin (Sigma-Aldrich, CAT#04-262). After serial washes, samples were stained with secondary antibody and mounted with fluorescent 4',6-diamidino-2-phenylindole mounting medium (Vector Labs, H-1200). For A11-staining

(ThermoFisher, CAT#AHB005), the protocol was revised according to vendors instructions. The antigen retrieval solution was 0.1M glycine/PBS, at pH 3.5. Anti-oligomer A-11 antibody was used at 1-5 ug/mL concentration in 1:1mixture of blocking solution (1%BSA, 0.1% Tween-20 in PBS) and PBS. Confocal imaging was performed on a Zeiss confocal LSM-700 laser scanning confocal microscope using 40×/1.3 oil immersion objectives, and images were processed using the Zen black software.

Striation and aggregate scoring. We focused on mis-localization of CRYAB client proteins desmin, actin and α-actinin and the presence of aggregates in human ICM samples to observe impaired protein quality control. We planned to represent mis-localization by performing a striation scoring and presence of aggregates by performing aggregate scoring. The scoring criteria was as follows:

For striation scoring: normal localization of proteins- a score of 0, abnormal striation or mis-localization of proteins- a score of 1,

For aggregate scoring: absence of aggregates- a score of 0, Presence of aggregates- a score of 2.

Then, all the individual scores of the cardiomyocytes in the total field of view were added and divided by total number of cardiomyocytes. We quantified at least 3 images per ICM or donor sample. Image acquisition and quantitation was done by different operators where scoring was done blindly (the operator had no information about individual samples and types).

Immunoblotting. Immunoblotting was performed as previously described [19] with antibodies listed below:

anti-SQSTM1/p62 antibody (Abcam, ab56416); αB-crystallin (CRYAB) polyclonal antibody (Enzo life sciences, CAT# ADI-SPA-223-F); Anti-Alpha B crystallin (pS59) antibody (Abcam, CAT#ab5577); Anti-Alpha B crystallin (pS45) antibody (Abcam, CAT#ab5598); Anti-ubiquitinylated proteins antibody, clone FK1 (Sigma-Aldrich, CAT#04-262) ; Anti-GAPDH antibody (Abcam, CAT#ab22555); LC3B antibody (Novus biologicals, CAT#NB100-2220SS); Anti-Actin antibody (Sigma, CAT#A2066).

Statistical analyses. Data presented as mean±SEM. All measurements were obtained from separate biological replicates. Statistical analyses were performed in GraphPad Prism version 9. Data were tested for assumptions of normality with Shapiro-Wilk normality test. Statistical significance was assessed with unpaired two-tailed Student's t-test for comparison between two groups, or one-way or two-way ANOVA for assessing differences across multiple groups followed by post-hoc testing. A non-parametric test was performed if data were not normally distributed. A two-tailed P value of <0.05 was considered statistically significant.

Study approval. All animal studies were approved by the IACUC at Washington University School of Medicine.

3.6 Figures

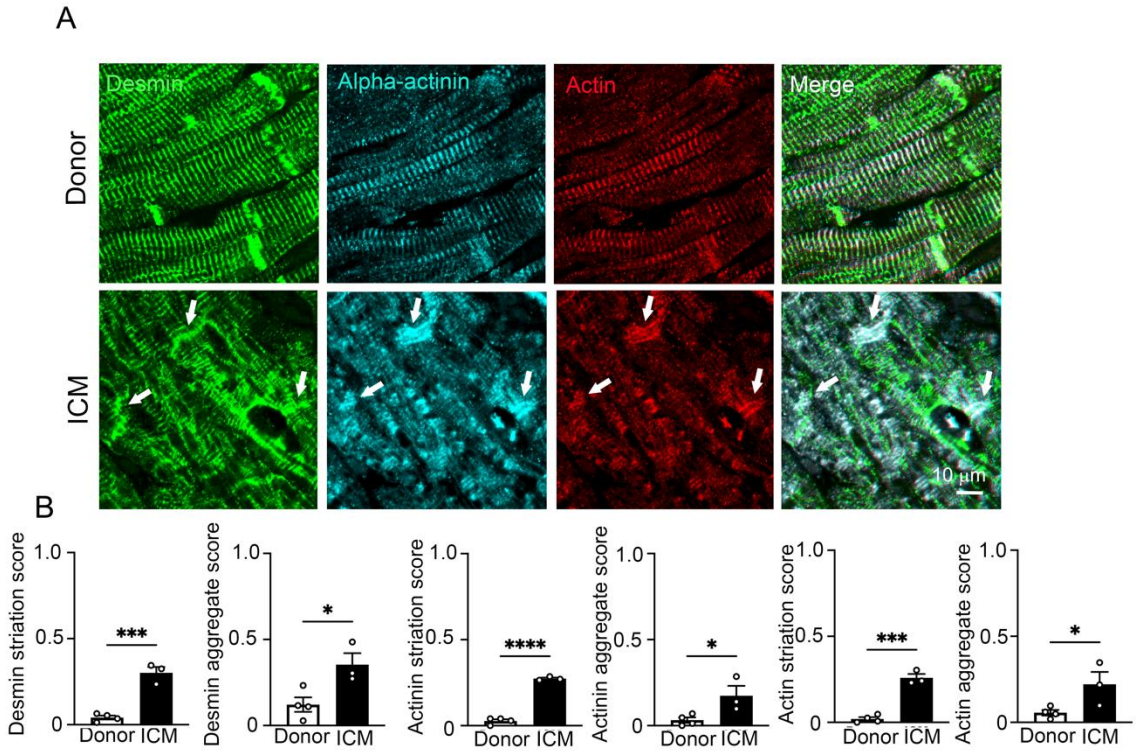

Figure 3.1: CRYAB client proteins such as desmin, actin, and α-actinin localize to protein-aggregates in human ischemic cardiomyopathy. **A**. Representative immunohistochemical images from left ventricular myocardium of individuals evaluated as controls (donor) or patients with end-stage ischemic cardiomyopathy (ICM) stained for desmin actin and α-actinin. Arrow points to desmin, actin and α-actinin aggregates which are mis-localized from its physiologic location on Z-discs and intercalated discs. DAPI stains nuclei. **B.** Quantitation of human ICM and donor samples that were presented in A. * indicates P <0.05, *** indicates P<0.001 and **** indicates P<0.0001 vs. control by t-test.

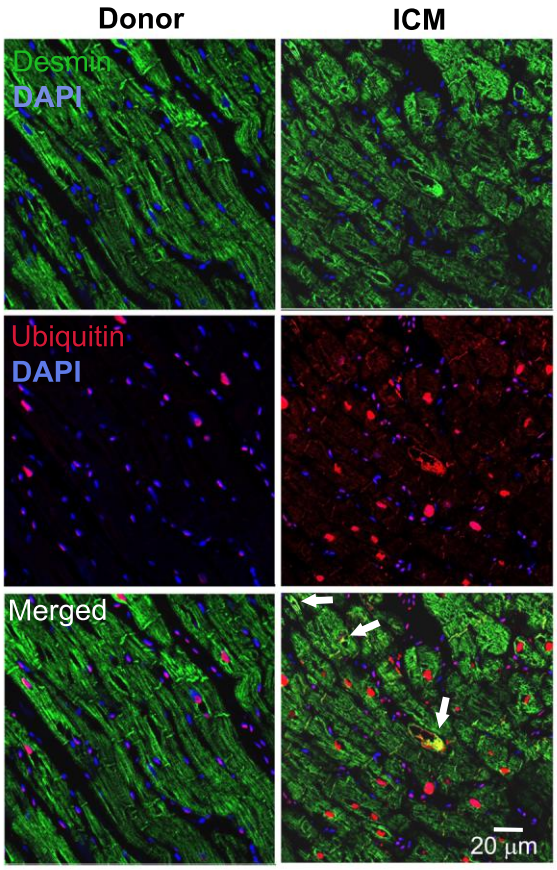

Figure 3.2: Increased polyubiquitin is observed with colocalization with desmin aggregates in ICM samples. Representative immunohistochemical images from left ventricular myocardium of individuals evaluated as controls (donor) or patients with end-stage ischemic cardiomyopathy (ICM) stained for desmin and polyUb. Arrow points to desmin and polyubiquitin co-localization showing the aggregates are marked for degradation.

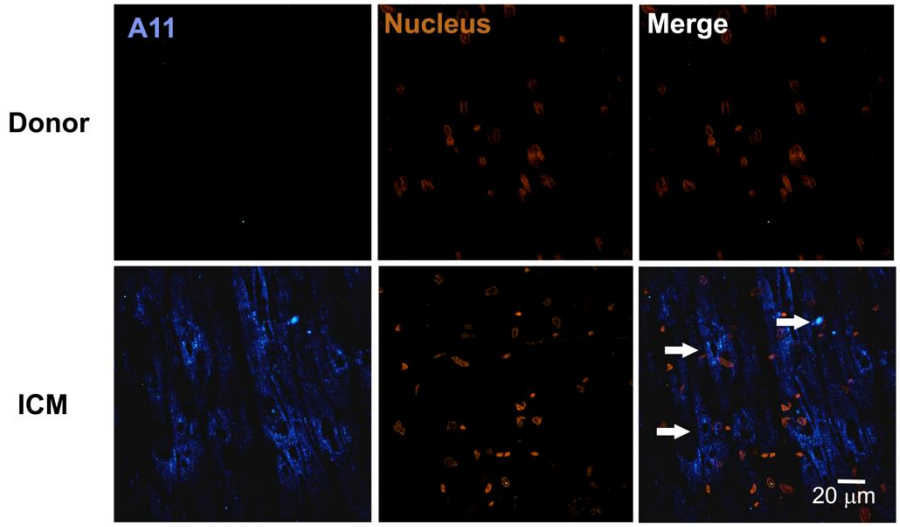

Figure 3.3: Increased presence of pre-amyloid oligomeric structures in ICM samples. Immunohistochemical staining for anti-oligomer A11 antibody in donor and ICM heart samples, demonstrating presence of pre-amyloid oligomers structures in ICM samples (pseudo-colored blue, arrows). DAPI stained nuclei are pseudo-colored orange. Representative of n=5 hearts/group.

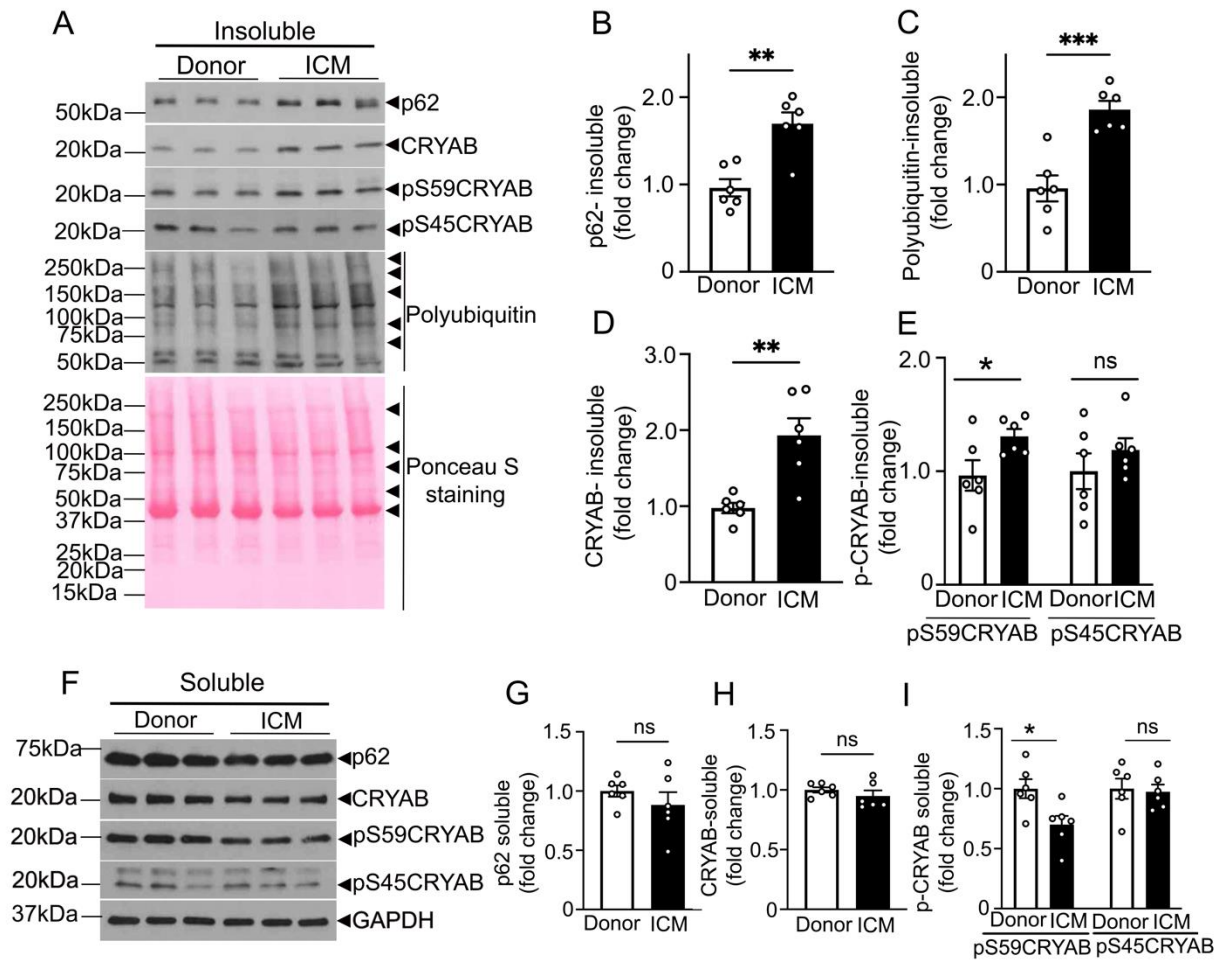

Figure 3.4: Increased presence of pS59CRYAB was observed in the detergent insoluble fraction in ICM samples. A-E. Immunoblot (A) and quantitation (fold change as compared to donor mean) depicting total p62 (B), polyubiquitinated proteins (C), CRYAB (D) and pS59CRYAB and pS45CRYAB (E) in NP40-detergent-insoluble fractions from human hearts from patients with ischemic cardiomyopathy (ICM) and donors. Ponceau S staining is shown as loading control. * Indicates P <0.05, ** indicates P<0.01 and *** indicates P<0.001 vs. donor as control by t-test. **F-I**. Immunoblot (F) and quantitation for p62 (G), CRYAB (H), and pS59CRYAB and pS45CRYAB (I) abundance in NP-40 detergent soluble biochemical fractions from human hearts as in A-E. GAPDH was used as loading control. * Indicates P <0.05 by t-test. 'ns' indicates not significant.

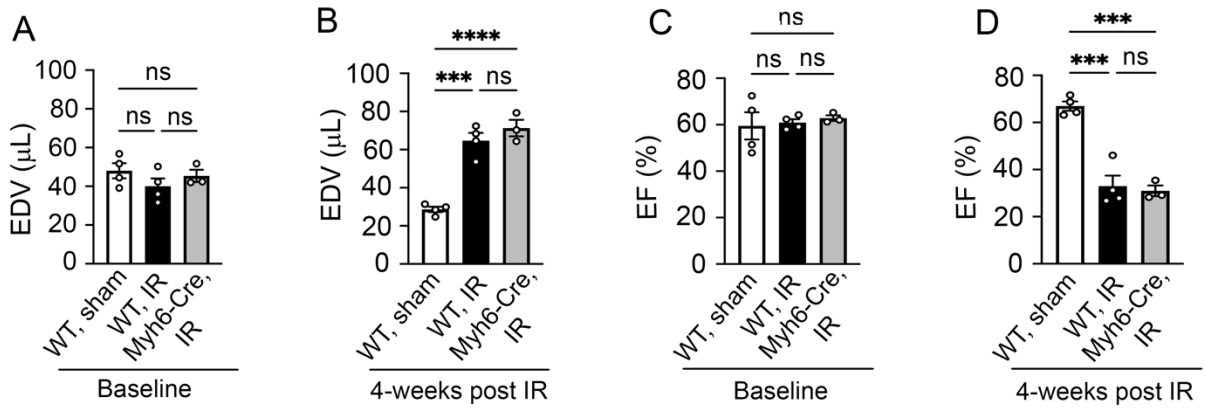

Figure 3.5: Young adult C57BL6J WT mouse subjected to closed chest ischemia-reperfusion (IR) mimicked human ischemic cardiomyopathy. A, B) Left ventricular end-diastolic volume (LVEDV) (A) at baseline and (B) at 4-weeks after IR in male C57BL6J WT young adult mice and in *Myh6*-Cre transgenic mice that were subjected to IR injury. **C, D)** Left ventricular end-diastolic volume (EDV, A, B) and ejection fraction (EF (%), C, D) at baseline (i.. prior to) and at 4-weeks after IR in C57BL6J WT young adult mice and in *Myh6*-Cre mice. *** indicates P value < 0.001 and **** indicates P value <0.0001 by Tukey's post-hoc test after one-way ANOVA.

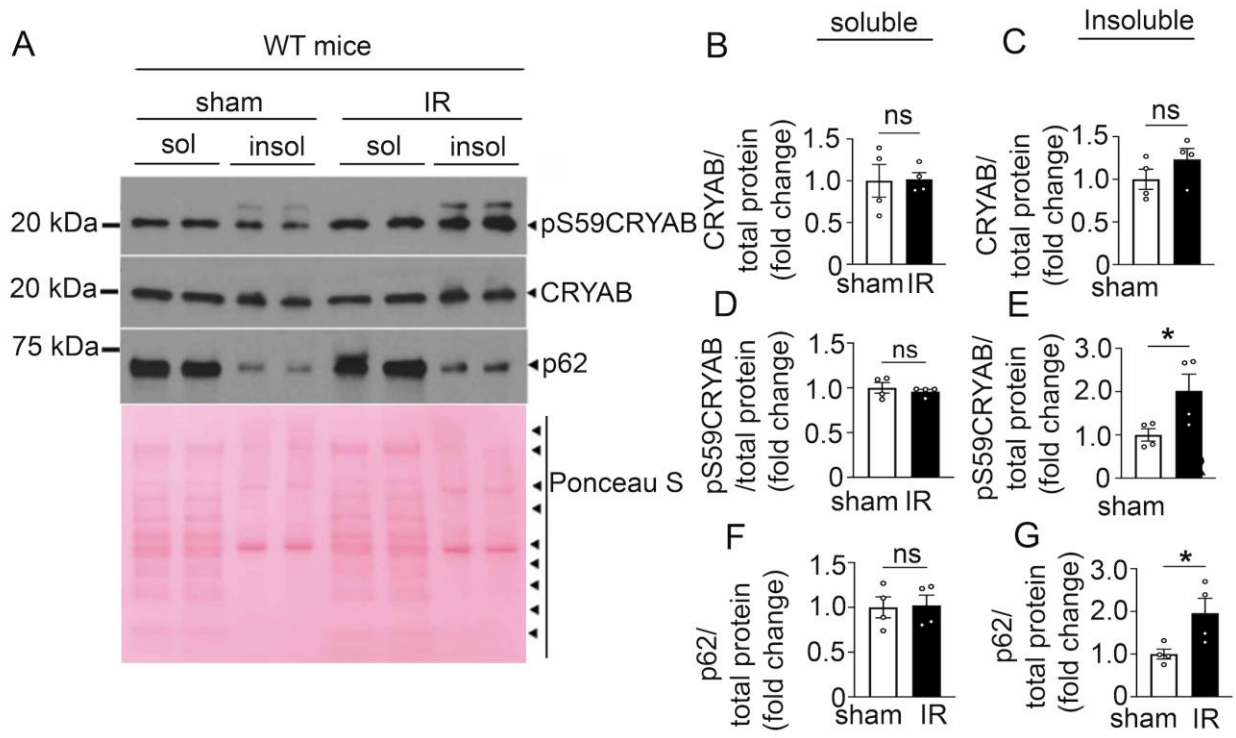

Figure 3.6: CRYAB phosphorylated at serine-59 partitions to the insoluble fraction in the myocardium of young adult C57BL6J WT mouse subjected to closed chest ischemia-reperfusion (IR) with development of ischemic cardiomyopathy. A-G) Representative (A) immunoblot and quantitation depicting the abundance of CRYAB (B, C) and pS59CRYAB (D, E) and p62 (F, G) in the soluble (*left* panels) and insoluble (*right* panels) biochemical fractions from myocardium of the C57BL6J WT young adult mice collected 4 weeks after IR or sham procedure as in A-D. Ponceau S is shown as loading control. * indicates P<0.05 by t-test.

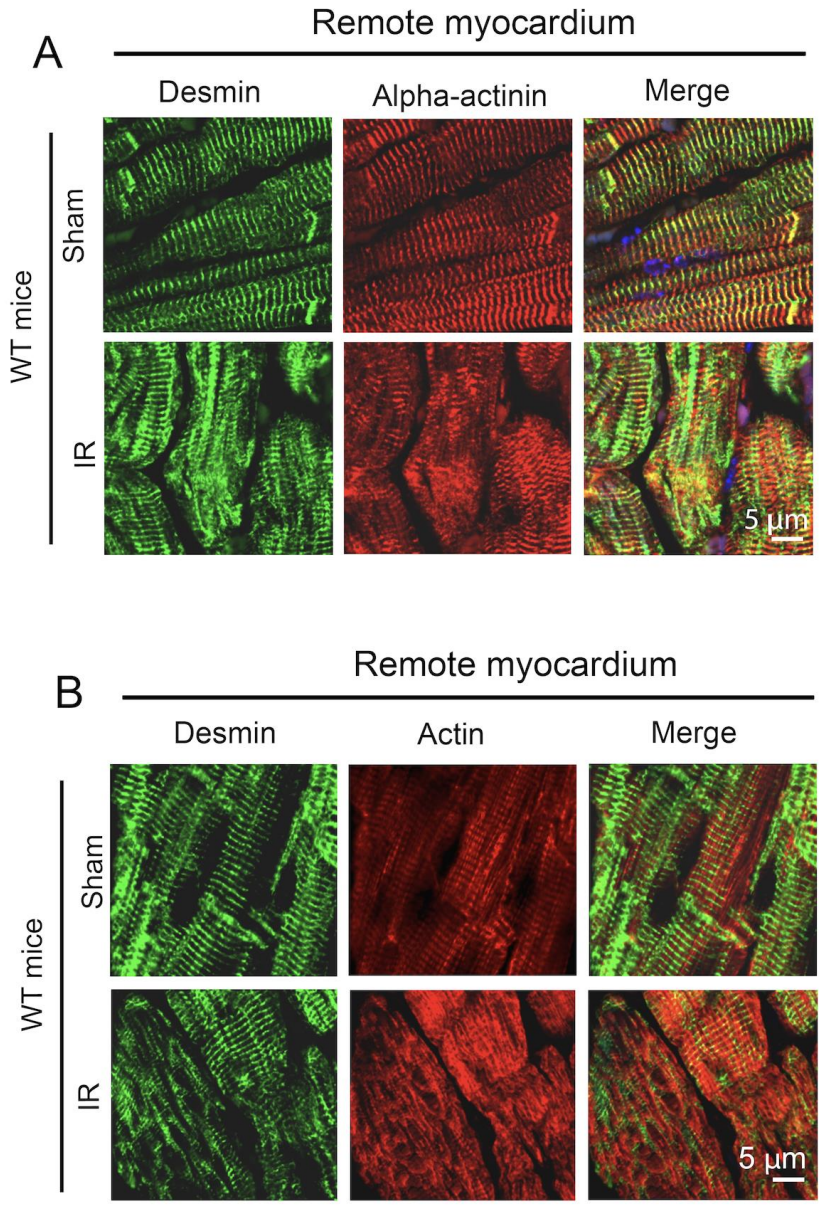

Figure 3.7: Mis-localization of desmin, actin and α-actinin was observed in WT mouse heart subjected to IR. A-B) Representative images A) demonstrating localization of desmin and α-actinin, and B) desmin and actin in the myocardium from C57BL6J mice 4 weeks after being subjected to IR injury that were presented in figure 3.5 and 3.6. Figure A shows desmin-actinin co-localization by yellow fluorescence signal as expected. Co-localization was not observed in figure B as theoretically expected.

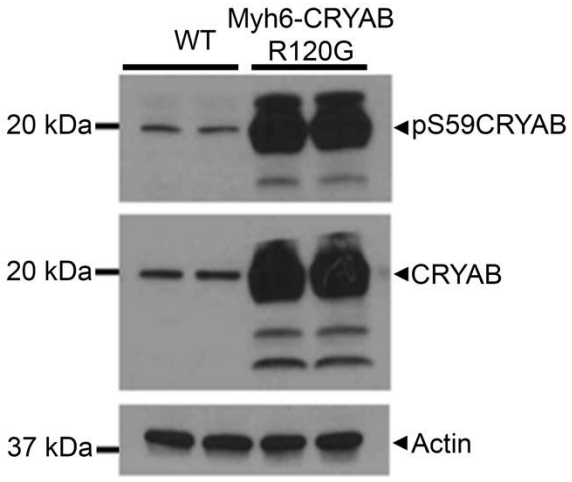

Figure 3.8: R120G protein is prominently phosphorylated at S59. Representative image showing expression of CRYAB and pS59CRYAB in crude extracts from 40-weeks old Myh6-CRYAB R120G mouse hearts or from C57BL6J WT mouse hearts as control. Actin is shown as the loading control.

3.7 References

1. Islam M, Diwan A, Mani K. Come Together: Protein Assemblies, Aggregates and the Sarcostat at the Heart of Cardiac Myocyte Homeostasis. *Frontiers in Physiology*. 2020;11. doi: 10.3389/fphys.2020.00586
2. Martin TG, Myers VD, Dubey P, Dubey S, Perez E, Moravec CS, Willis MS, Feldman AM, Kirk JA. Cardiomyocyte contractile impairment in heart failure results from reduced BAG3-mediated sarcomeric protein turnover. *Nature Communications*. 2021;12:2942. doi: 10.1038/s41467-021-23272-z
3. Dalakas MC, Park KY, Semino-Mora C, Lee HS, Sivakumar K, Goldfarb LG. Desmin myopathy, a skeletal myopathy with cardiomyopathy caused by mutations in the desmin gene. *NEnglJMed*. 2000;342:770-780. doi: 10.1056/NEJM200003163421104 [doi]
4. Goldfarb LG, Dalakas MC. Tragedy in a heartbeat: malfunctioning desmin causes skeletal and cardiac muscle disease. *JClinInvest*. 2009;119:1806-1813. doi: 38027 [pii];10.1172/JCI38027 [doi]
5. Vicart P, Caron A, Guicheney P, Li Z, Prevost MC, Faure A, Chateau D, Chapon F, Tome F, Dupret JM, et al. A missense mutation in the alphaB-crystallin chaperone gene causes a desmin-related myopathy. *NatGenet*. 1998;20:92-95. doi: 10.1038/1765 [doi]
6. Ma X, Mani K, Liu H, Kovacs A, Murphy JT, Foroughi L, French BA, Weinheimer CJ, Kraja A, Benjamin IJ, et al. Transcription Factor EB Activation Rescues Advanced αB-Crystallin Mutation-Induced Cardiomyopathy by Normalizing Desmin Localization. *J Am Heart Assoc*. 2019;8:e010866. doi: 10.1161/jaha.118.010866
7. Sanbe A, Osinska H, Saffitz JE, Glabe CG, Kayed R, Maloyan A, Robbins J. Desmin-related cardiomyopathy in transgenic mice: a cardiac amyloidosis. *Proceedings of the National Academy of Sciences of the United States of America*. 2004;101:10132-10136. doi: 10.1073/pnas.0401900101
8. Elliott JL, Der Perng M, Prescott AR, Jansen KA, Koenderink GH, Quinlan RA. The specificity of the interaction between alphaB-crystallin and desmin filaments and its impact on filament aggregation and cell viability. *Philos Trans R Soc Lond B Biol Sci*. 2013;368:20120375. doi: 10.1098/rstb.2012.0375
9. Ito H, Okamoto K, Nakayama H, Isobe T, Kato K. Phosphorylation of alphaB-crystallin in response to various types of stress. *The Journal of biological chemistry*. 1997;272:29934-29941. doi: 10.1074/jbc.272.47.29934
10. Takagi H, Hsu CP, Kajimoto K, Shao D, Yang Y, Maejima Y, Zhai P, Yehia G, Yamada C, Zablocki D, et al. Activation of PKN mediates survival of cardiac myocytes in the heart during ischemia/reperfusion. *Circ Res*. 2010;107:642-649. doi: 10.1161/circresaha.110.217554
11. Cook SA, Sugden PH, Clerk A. Activation of c-Jun N-terminal kinases and p38-mitogen-activated protein kinases in human heart failure secondary to ischaemic heart disease. *Journal of molecular and cellular cardiology*. 1999;31:1429-1434. doi: 10.1006/jmcc.1999.0979
12. den Engelsman J, Gerrits D, de Jong WW, Robbins J, Kato K, Boelens WC. Nuclear import of {alpha}B-crystallin is phosphorylation-dependent and hampered by hyperphosphorylation of the myopathy-related mutant R120G. *The Journal of biological chemistry*. 2005;280:37139-37148. doi: 10.1074/jbc.M504106200

13. Vadlamudi RK, Joung I, Strominger JL, Shin J. p62, a phosphotyrosine-independent ligand of the SH2 domain of p56lck, belongs to a new class of ubiquitin-binding proteins. *The Journal of biological chemistry*. 1996;271:20235-20237. doi: 10.1074/jbc.271.34.20235
14. Pan JA, Sun Y, Jiang YP, Bott AJ, Jaber N, Dou Z, Yang B, Chen JS, Catanzaro JM, Du C, et al. TRIM21 Ubiquitylates SQSTM1/p62 and Suppresses Protein Sequestration to Regulate Redox Homeostasis. *Molecular cell*. 2016;62:149-151. doi: 10.1016/j.molcel.2016.03.015
15. Brody MJ, Vanhoutte D, Bakshi CV, Liu R, Correll RN, Sargent MA, Molkentin JD. Disruption of valosin-containing protein activity causes cardiomyopathy and reveals pleiotropic functions in cardiac homeostasis. *The Journal of biological chemistry*. 2019;294:8918-8929. doi: 10.1074/jbc.RA119.007585
16. Dominguez F, Cuenca S, Bilinska Z, Toro R, Villard E, Barriales-Villa R, Ochoa JP, Asselbergs F, Sammani A, Franaszczyk M, et al. Dilated Cardiomyopathy Due to BLC2-Associated Athanogene 3 (BAG3) Mutations. *Journal of the American College of Cardiology*. 2018;72:2471-2481. doi: 10.1016/j.jacc.2018.08.2181
17. Gianni D, Li A, Tesco G, McKay KM, Moore J, Raygor K, Rota M, Gwathmey JK, Dec GW, Aretz T, et al. Protein aggregates and novel presenilin gene variants in idiopathic dilated cardiomyopathy. *Circulation*. 2010;121:1216-1226. doi: 10.1161/circulationaha.109.879510
18. Willis MS, Patterson C. Proteotoxicity and cardiac dysfunction. *The New England journal of medicine*. 2013;368:1755. doi: 10.1056/NEJMc1302511
19. Ma X, Mani K, Liu H, Kovacs A, Murphy JT, Foroughi L, French BA, Weinheimer CJ, Kraja A, Benjamin IJ, et al. Transcription Factor EB Activation Rescues Advanced alphaB-Crystallin Mutation-Induced Cardiomyopathy by Normalizing Desmin Localization. *Journal of the American Heart Association*. 2019;8:e010866. doi: 10.1161/JAHA.118.010866
20. Bhuiyan MS, Pattison JS, Osinska H, James J, Gulick J, McLendon PM, Hill JA, Sadoshima J, Robbins J. Enhanced autophagy ameliorates cardiac proteinopathy. *J Clin Invest*. 2013;123:5284-5297. doi: 10.1172/jci70877
21. Selcen D, Muntoni F, Burton BK, Pegoraro E, Sewry C, Bite AV, Engel AG. Mutation in BAG3 causes severe dominant childhood muscular dystrophy. *Annals of neurology*. 2009;65:83-89. doi: 10.1002/ana.21553
22. Kimura K, Ooms A, Graf-Riesen K, Kuppusamy M, Unger A, Schuld J, Daerr J, Lother A, Geisen C, Hein L, et al. Overexpression of human BAG3P209L in mice causes restrictive cardiomyopathy. *Nature Communications*. 2021;12:3575. doi: 10.1038/s41467-021-23858-7
23. Ma X, Rawnsley DR, Kovacs A, Islam M, Murphy JT, Zhao C, Kumari M, Foroughi L, Liu H, Qi K, et al. TRAF2, an Innate Immune Sensor, Reciprocally Regulates Mitophagy and Inflammation to Maintain Cardiac Myocyte Homeostasis. *JACC Basic Transl Sci*. 2022;7:223-243. doi: 10.1016/j.jacbts.2021.12.002
24. Javaheri A, Bajpai G, Picataggi A, Mani S, Foroughi L, Evie H, Kovacs A, Weinheimer CJ, Hyrc K, Xiao Q, et al. TFEB activation in macrophages attenuates postmyocardial infarction ventricular dysfunction independently of ATG5-mediated autophagy. *JCI Insight*. 2019;4. doi: 10.1172/jci.insight.127312

3.8 Supporting Materials

Table 3.1: Characteristics of individuals whose myocardial samples were included in the study.

Individual Characteristics	**Ischemic Cardiomyopathy (n=8)**	**Non-failing Donor (n=8)**	**Statistical Comparison**
Male Gender/Total Sample (N)	5/8	6/8	NS
Age (years)	57 ± 3	52 ± 2	NS
BMI	28 ± 1	29± 4	NS
LV Mass Index (g/kg)	176 ± 4	105 ± 2	P<0.0001
LVEDD (cm)	6.13 ± 0.3	4.03 ± 0.4	P<.01
LVEF (%)	23 ± 4	60 ± 3	P<0.0001
History of Diabetes	2/8	2/8	NS
History of HTN	4/8	1/8	NS
History of ACE-I/ARB use	4/8	0/8	NS
History of Beta-blocker use	4/8	0/8	NS

All data for continuous variables are mean ± SEM. P values reported are by two-tailed t-test for continuous variables and by Fisher's exact test for categorical variables. NS indicates not significant. LV Mass Index= Left Ventricular Mass Index, LVEDD= Left Ventricular End Diastolic Diameter, LVEF= Left Ventricular Ejection Fraction.

Chapter 4: Preventing Phosphorylation in S59 of CRYAB rescues post-myocardial infarction (MI) remodeling in mouse.

4.1 Introduction

Desmin mis-localization to protein-aggregates is observed desmin heritable mutations [1,2]. Desmin is a client protein of the chaperone αB-crystallin [3]. αB-crystallin helps desmin to fold in its native formation. Thus, desmin impaired protein quality control is associated with CRYAB impaired chaperone function. There are three serine resides at position 19, 45 and 59 that can be phosphorylated in αB-crystallin [4]. Of these, serine 45 and 59 are phosphorylated by stress-induced p38 MAPK kinase [4], as well as by protein kinase N, which are activated in cardiac ischemia-reperfusion injury [5,6]. Also, studies in cell-culture models show that R120G mutant of CRYAB is hyperphosphorylated at these three serine residues, which regulates its tendency to aggregate [7]. In our study, we previously observed that phosphorylation alters phase separation properties of CRYAB which is associated with inducing CRYAB as aggregate-prone and worsening of cardiomyopathy in mouse. Thus, we hypothesized that in-vivo, phosphorylation deficient mutant (S59A) in CRYAB will be protective and phosphorylation-mimetic mutation (S59D) will have an adverse effect in cardiac remodeling post-MI. To demonstrate that, we developed homozygous knock-in mouse models carrying either phospho-mimetic mutation S59D or phospho-deficient mutation S59A in the C57BL6J background and performed IR surgery in the young adult male and female mice (8-10 weeks). First, we performed baseline cardiac structure and function analysis, and then subjected closed-chest ischemia reperfusion injury to assess the effect of CRYAB phosphorylation. We evaluated cardiac function analysis by

evaluating area-at risk, ejection fraction, left ventricular end diastolic volume, and then scar size at 4-weeks post-MI. We also performed western blotting using NP-40 detergent soluble and insoluble fractions of the heart to observe relative abundance of CRYAB and aggregate markers into the aggregates. Proper chaperone function represents proper localization of proteins in myocardium. As a read out of the CRYAB chaperone function, we focused on the localization of CRYAB client proteins in cardiomyocytes. To observe whether the localization of CRYAB client proteins can be affected by their interactions with CRYAB, we planned to perform co-immunoprecipitation experiments. We performed immunostaining to observe the localization of CRYAB and its client proteins in the cardiomyocytes. Then, we evaluated how CRYAB-client protein interaction is altered in CRYAB phospho-deficient and phospho-mimetic mice by performing immunoprecipitation.

4.2 Results

4.2.1 CRYAB phospho-mimetic and phospho-deficient mice did not show cardiac function abnormality in the unstressed state

Our prior findings in this study predict a beneficial effect of phosphorylation deficiency in S59 residue on post-MI remodeling. Accordingly, we planned to set up a protocol, where we developed homozygous knock-in mice carrying either phospho-mimetic mutation S59D or phospho-deficient mutation S59A and planned to observe the effect after IR injury at 4-weeks in cardiac function. We observed that phospho-mimetic S59D or -deficient S59A KI/KI mice did not show any gross abnormality in cardiac structure or function at baseline (Table 4.1), prior to myocardial infarction modeling.

4.2.2 Phospho-mimetic CRYAB mouse showed desmin mis-localization with increased polyubiquitinated proteins in unstressed state

We did not observe any gross abnormalities in CRYAB KI/KI mice models using hematoxylin and eosin and Masson's trichrome staining (Fig. 4.1 A, B), we also did not observe any gross abnormalities. However, ultra-structure of S59D KI/KI mice using transmission electron microscopy showed presence of protein aggregates (white arrow, Fig. 4.1 C) and abnormal mitochondria (black arrow, Fig. 4.1 C). We then performed western blot using NP-40 detergent soluble-insoluble fractions of the heart (Fig. 4.2), and saw increased polyubiquitin, p62 and CRYAB in the protein aggregate-enriched fraction. This demonstrates that even in unstressed state, CRYAB phospho-mimetic mutation has aggregate-prone characteristics. Next, we ran a western blot using crude extract of the CRYAB WT, S59D and S59A mice hearts. Crude extract is obtained by the mild detergent NO-40 treatment. Thus, it is not enriched in protein aggregates. We observed decreased total CRYAB level in the S59D mice compared to WT and S59A mice (Fig. 4.3). This suggests that S59D CRYAB is in a pool that is not accessible by NP-40, where protein aggregates are enriched. This also show that S59D mutation alters CRYAB homeostasis, where CRYAB protein quality control is impaired.

4.2.3 Preventing serine-59 phosphorylation in CRYAB rescues post-MI cardiac remodeling

We subjected young adult mice to IR injury and performed baseline and 4-weeks after ischemia echo. (Fig. 4.4). After 4-weeks of the IR surgery, our data demonstrate a significant increase in LVEF in the S59A KI/KI mouse compared to the WT mice. This shows that after myocardial infarction, phospho-deficiency in S59 can be protective. We also observed decreased LVEF in S59D KI/KI mouse than S59A KI/KI (Fig. 4.4) with significant effect on LV dilation

(Fig. 4.4). This shows that S59 phosphorylation worsens cardiac function after myocardial infarction. In CRYAB S59A KI/KI mice, we also have seen a significant reduction in scar size compared to WT or S59D mice (Fig. 4.5 A, B) representing that cardiac remodeling is improved in S59A mouse. Overall, this data demonstrates that phosphorylation deficiency can be protective at 4-weeks after IR injury in cardiac function in mice.

4.2.4 Phospho-mimetic S59 change increases interaction between CRYAB and desmin

We immunostained the hearts of sham and IR treated mice and observed desmin, actin and α-actinin localization. We observed increased mis-localization of desmin after IR, but it was significantly reduced on S59A mice (Fig. 4.6 A-C). Even in the sham treated S59D hearts, we observed abnormal desmin striation with increased polyubiquitinated proteins (Fig. 4.6 A-C). To demonstrate how phosphorylation in CRYAB can affect its interaction with its client proteins such as desmin, we performed co-immunoprecipitation using CRYAB phospho-mimetic S59D and phospho-deficient S59A variants (Fig. 4.7 A-G). We observed increased interaction between desmin-CRYAB in phospho-mimetic setting and decreased interaction between desmin-CRYAB in phospho-deficient setting compared to CRYAB WT (Fig.4.7 A-G). This shows that CRYAB becomes sticky when phosphorylated in S59 residue and thus has increased interaction with its client proteins. Also, we observed reduced CRYAB-desmin interaction in S59A mouse, showing that decreased interaction can be protective after myocardial infarction.

4.3 Discussion

Serine-59 residue in CRYAB is phosphorylated by p38MAPK which is stress-induced. We observed that CRYAB interacts with its client proteins (such as desmin) more strongly when

phosphorylated. We observed worsening cardiac remodeling after IR in the S59D hearts, but not in the S59A hearts. In acute stress like ischemia, reversible interaction between CRYAB-client might be protective to preserve protein quality and keep the cardiomyocyte structure intact. However, persistent stress such as post-MI might induce sustained increase in CRYAB-client interaction which could be sufficient to cause mis-localization. Future studies on the effect of cardiac remodeling in S59D and S59A mice using shorter and longer timepoints than 4-weeks should be performed to have a better understanding of the role of phosphorylation in acute vs persistent stress. In future, in addition to ischemia reperfusion injury, we could evaluate if other stress in addition to ischemia such as aging can worsen cardiac function in S59D mice than S59A mice. As we know that, p38MAPK phosphorylates CRYAB S59, it could be a potential target candidate for improved cardiac remodeling. One of the effective strategies could be using pharmacological approaches to target p38MAPK and decrease stress-induced phosphorylation. Also, we observed decreased total CRYAB protein in S59D mice. This shows that further experiment is needed on CRYAB null mice to observe how loss of CRYAB can affect cardiac function after ischemia reperfusion injury, or aging. We observed increased interaction between CRYAB-desmin to be associated with worsening cardiac function after IR. It will be interesting to see whether other CRYAB clients such as actin or α-actinin also has increased interaction with CRYAB. This will demonstrate the mechanism for wider array of mis-localization between CRYAB clients.

4.4 Conclusion

Phosphorylation mimetic CRYAB S59D variant showed abnormal looking mitochondria, abnormal desmin striation and presence of aggregation at baseline without stress. However, this level of abnormal protein quality control is not sufficient to cause cardiac dysfunction.

Preventing phosphorylation is protective after ischemic injury in mouse which shows reduced desmin mis-localization and presence of aggregates, but future studies are needed to understand the mechanism.

4.5 Materials and Methods

Generating S59A and S59D KI/KI mice models using CRISPR/Cas9 strategy. A single active gRNA was used to introduce point mutations in the CRYAB locus of B6/CBA hybrids using homology-directed repairs (HDR) after the pro-nuclear introduction of both gRNA and Cas9 was done by electroporation. ZE electroporation was performed in four sessions where 2 different mice colonies, S59A (AGC to GCC) and S59D (AGC to GAC), were generated with a single electroporation mix (ie: both ssODNs in the same mix). The presence of the CRYAB point mutations was confirmed in each generation of mice colony by deep sequencing. We used both male and female C57BL/6J mice of minimum sixth generation for the experiment.

Closed-chest cardiac ischemia-reperfusion modeling. Mice were subjected to reversible left anterior descending coronary artery ligation for 90 minutes followed by reperfusion, in a closed-chest procedure, as described [8] and detailed methods presented in the earlier chapter of the thesis.

Echocardiography. 2D–directed M-mode echocardiography was performed using a Vevo 2100 Imaging System (VisualSonics, Toronto, Canada) equipped with a 30-MHz linear-array transducer, as we have previously described [8,9]. Detailed methods were presented in the earlier chapter of the thesis and as described [8]. Histologic assessment with hematoxylin and eosin staining, and assessment of myocardial fibrosis with Masson's trichrome staining and transmission electron microscopy, was performed as previously described [10].

Biochemical fractionation into soluble and insoluble fractions. We subjected cardiac tissues obtained from the remote left ventricular myocardium of mice subjected to ischemia-reperfusion injury (non-injured basal one-third) as previously described [10]. Detailed methods were presented in the earlier chapter of the thesis.

Co-Immunoprecipitation: Frozen hearts were placed in RIPA buffer (Cell Signaling 9806) containing Protease and Phosphatase Inhibitor (Thermo Fisher 78442) and homogenized with a mechanical homogenizer. Tissue lysis was pelleted at 600g for 5min. (Both supernatant and pellet were used for Co-IP). The pellet was dissolved with PBS containing 1% SDS and 5mM EDTA, and sonicated. The solution was centrifuged at 16000g for 5 min and the supernatant were diluted by 10 with PBS containing 5mM EDTA.

Protein A/G Sepharose (Abcam ab193262) were incubated with 5μg antibody or IgG in PBS for 30 min at room temperature with rotation. The immunocomplex was added to the lysis solution after 15min incubation with rotation at room temperature. The beads were washed with PBS for four times. The proteins were eluted by boiling in SDS sample buffer and analyzed by western blot. The antibodies used in this experiment were: Anti-desmin (Desmin (D93F5) XP® Rabbit mAb #5332), anti-CRYAB (Abcam, CAT# ab13496).

Immunofluorescence analysis. We performed immunohistochemistry on myocardial tissues as we have previously described [10]. Confocal imaging was performed on a Zeiss confocal LSM-700 laser scanning confocal microscope using 40×/1.3, and 63x oil immersion objectives, and images were processed using the Zen black software. Primary antibody used were as follows: anti-desmin (Santa Cruz Biotechnology, Inc, CAT#SC-7559), anti-ubiquitin (Sigma-Aldrich,

CAT#04-262), anti-actin (Millipore Sigma, CAT#A2066), anti-alpha-actinin (Abcam, CAT#ab9465).

Striation and aggregate scoring. We focused on mis-localization of CRYAB client proteins desmin, actin and α-actinin and the presence of aggregates in CRYAB WT, S59D KI/KI and S59A KI/KI mice models to observe impaired protein quality control. At least three images were taken per sample for quantitation. Striation and aggregate scoring were performed following the protocol stated in chapter 3.

Immunoblotting. Immunoblotting was performed as previously described [10] with antibodies listed below: p62 (Abcam, ab56416); polyubiquitin (Sigma-Aldrich CAT#04-262), CRYAB (Enzo life sciences, CAT#ADI-SPA-223-F), GAPDH (Abcam, CAT#ab22555), desmin (Santa Cruz Biotechnology, SC-7559).

Scar size analyses. Scar area analysis was performed on Trichrome staining photographs from CRYAB WT, S59A KI/KI and S59D KI/KI male and female mice. Fibrotic scar tissue was outlined using the freeform outline tool in ImageJ to produce a pixel-based area measurement that could then be converted to square micrometers. In a similar fashion, area of the total LV was determined. We presented the data as scar size/LV area (%).

Statistical analyses. Data presented as mean±SEM. All measurements were obtained from separate biological replicates. Statistical analyses were performed in GraphPad Prism version 9. Data were tested for assumptions of normality with Shapiro-Wilk normality test. Statistical significance was assessed with unpaired two-tailed Student's t-test for comparison between two groups, or one-way or two-way ANOVA for assessing differences across multiple groups

followed by post-hoc testing. A non-parametric test was performed if data were not normally distributed. A two-tailed P value of <0.05 was considered statistically significant.

Study approval. All animal studies were approved by the IACUC at Washington University School of Medicine. Studies on human tissue were performed under an exemption by the IRB at Washington University School of Medicine as only de-identified human samples were used and these studies were deemed exempt by the IRB at Washington University School of Medicine.

4.6 Figures

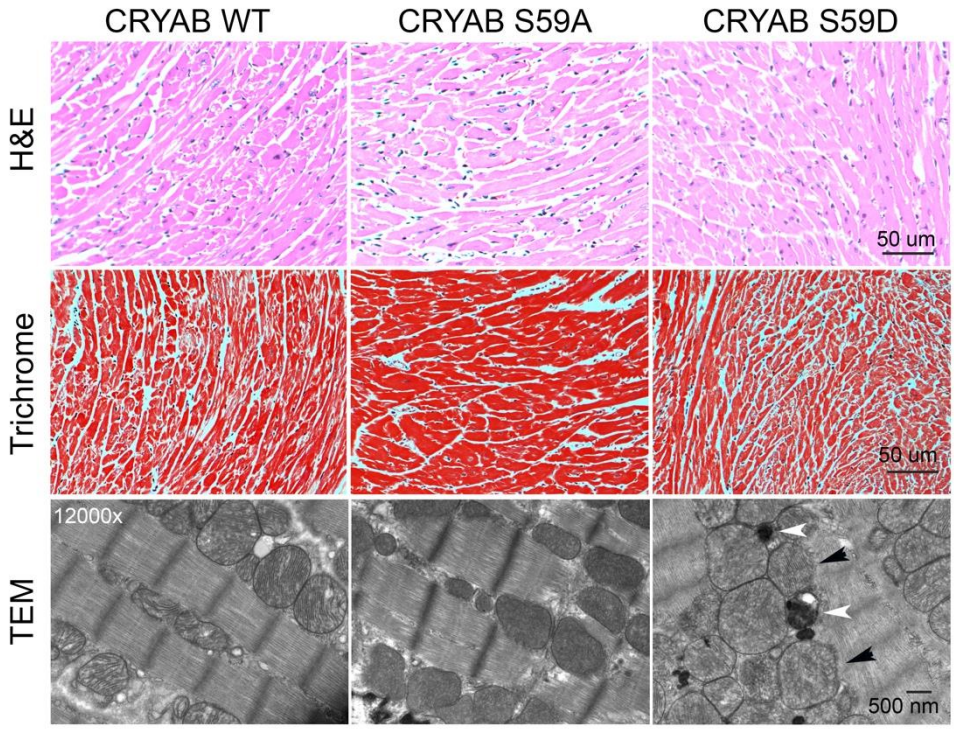

Figure 4.1: Phospho-mimetic S59D KI/KI mice did not show any gross abnormality in cardiac structure and function in unstressed state. Representative hematoxylin and eosin-stained images (*top panel*), Masson's trichrome stained images (*middle panel*), and transmission electron microscopy images (*bottom panel)* to demonstrate myocardial ultrastructure in CRYAB wild-type, S59A KI/KI and S59D KI/KI mice at 10-11 weeks of age.

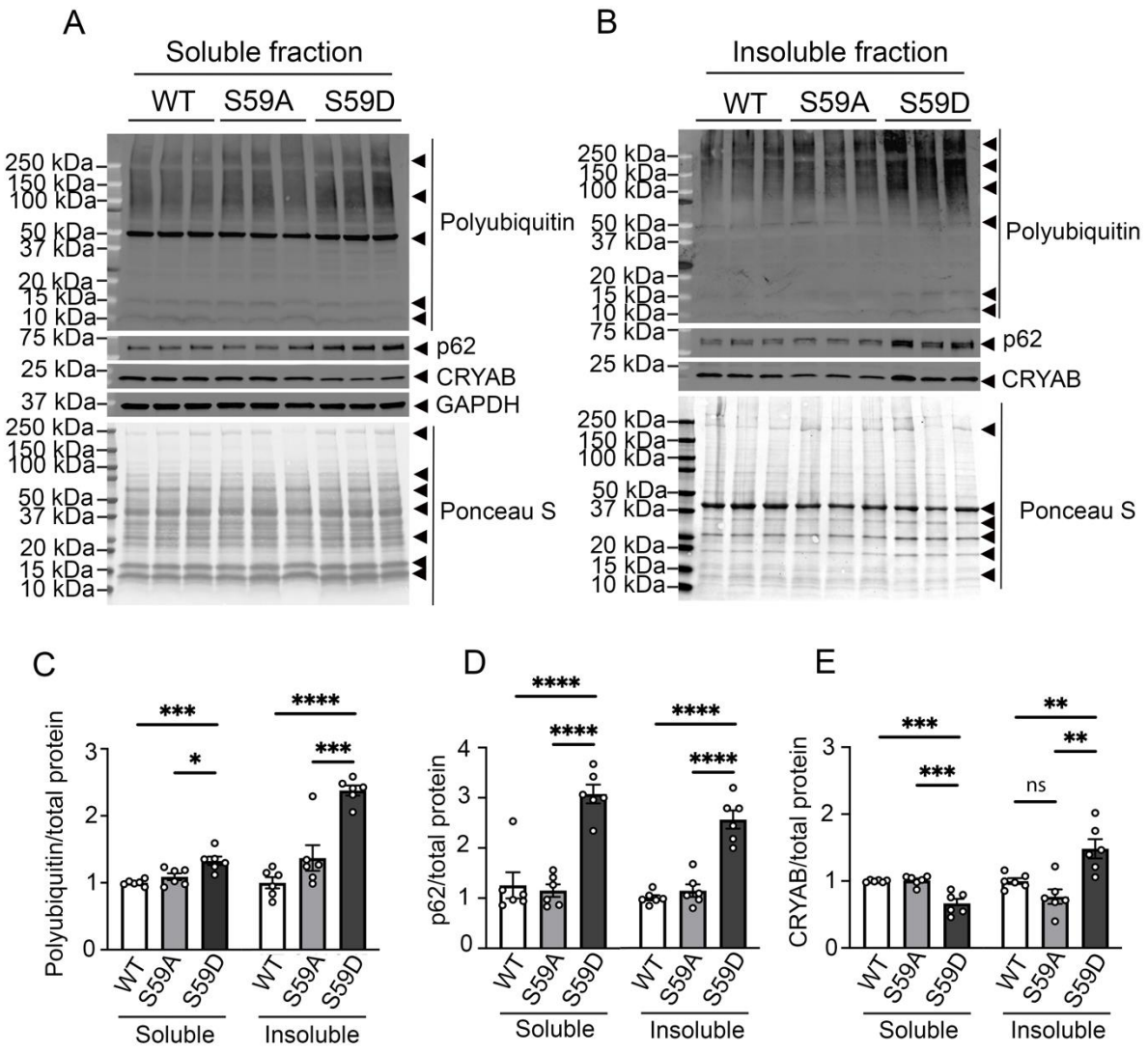

Figure 4.2: Phospho-mimetic S59D KI/KI mice have increased CRYAB, p62, and polyubiquitinated proteins in the insoluble fraction. A-E) Representative immunoblot (A, B) of detergent soluble (A) and insoluble (B) fractions and quantitation (C, D, E) depicting fold change of polyubiquitin (C), p62 (D) and CRYAB (E) in CRYAB wild-type, S59A KI/KI and S59D KI/KI mice at 10-11 weeks of age. GAPDH and Ponceau S staining were performed as loading controls. * denotes P < 0.05, ** denotes P <0.01, *** denotes P <0.001, and **** denotes P <0.0001 by Tukey's post-hoc testing after one-way ANOVA. 'ns' denotes as not significant.

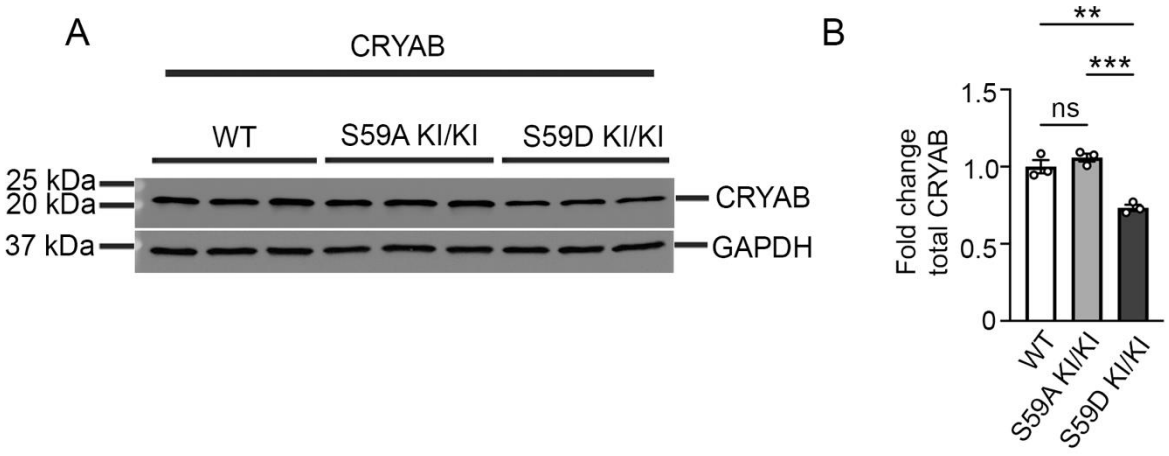

Figure 4.3: Phospho-mimetic S59D KI/KI mice have increased pS59CRYAB in the aggregate enriched insoluble fraction. A) Representative immunoblot (A) and quantitation (B) depicting fold change of CRYAB in CRYAB wild-type, S59A KI/KI and S59D KI/KI mice at 10-11 weeks of age. GAPDH was used as loading control. ** denotes P <0.01 and *** denotes P <0.001, by Tukey's post-hoc testing after one-way ANOVA. 'ns' denotes as not significant.

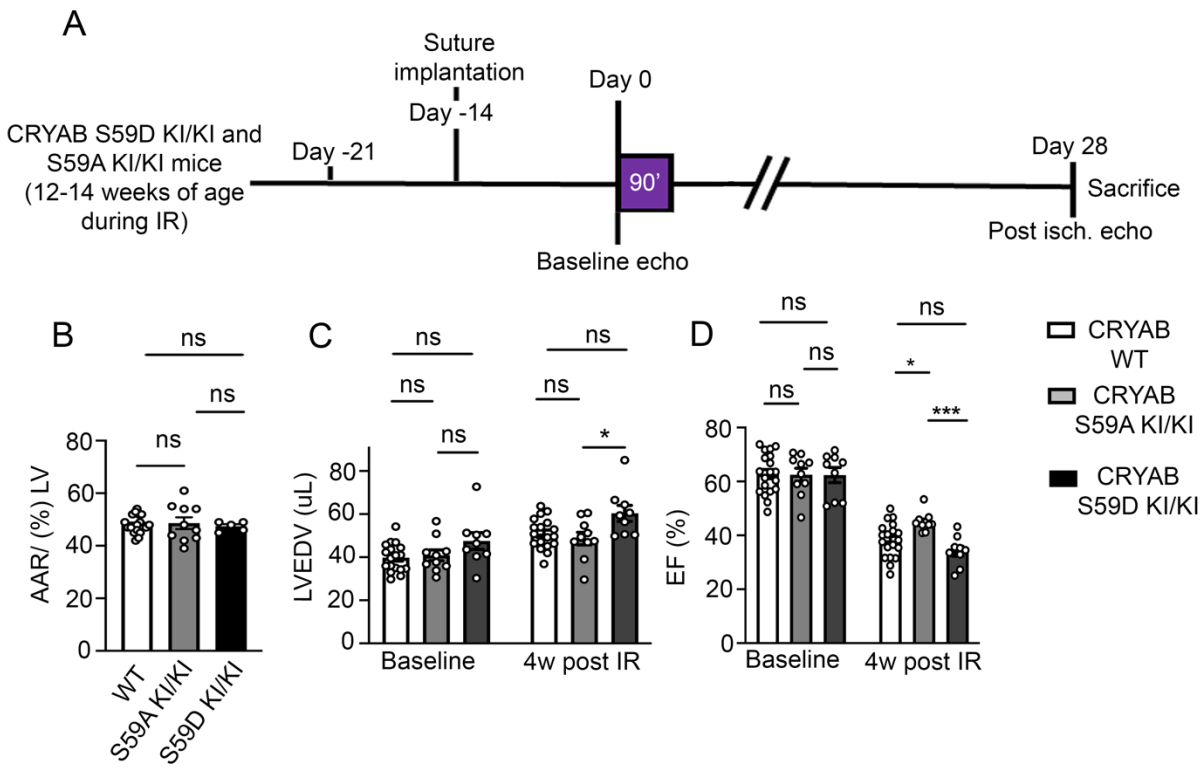

Figure 4.4: Preventing serine-59 phosphorylation in CRYAB rescues post-MI cardiomyopathy. A. Schematic depicting experimental strategy for closed-chest IR modeling in CRYAB wild-type, S59A KI/KI and S59D KI/KI mice. **B-D)** Quantitative analyses of area-at-risk (AAR, B), left ventricular end-diastolic volume (LVEDV, C), and LV ejection fraction (EF (%), D) before and at 4-weeks after IR injury in mice treated as in A. * denotes P< 0.05, *** denotes P <0.001 by one-way ANOVA. 'ns' indicates not significant.

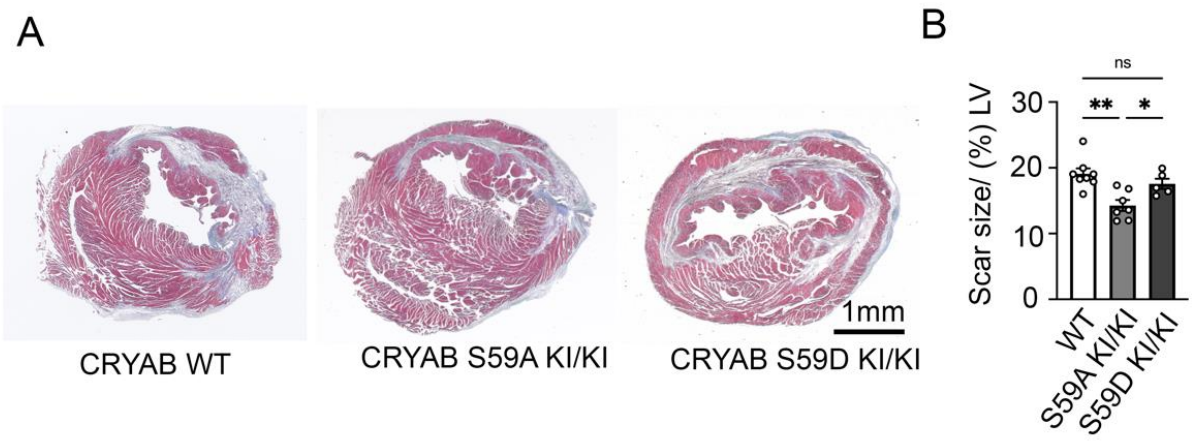

Figure 4.5: Preventing serine-59 phosphorylation in CRYAB shows reduces scar size post-MI. A, B) Representative Masson's trichrome images (A) and quantitation (B) of scar size from CRYAB WT and CRYAB S59A KI/KI mice subjected to closed chest IR modeling as in Figure 9A. * denotes P< 0.05, and ** denotes P< 0.01 by one-way ANOVA.

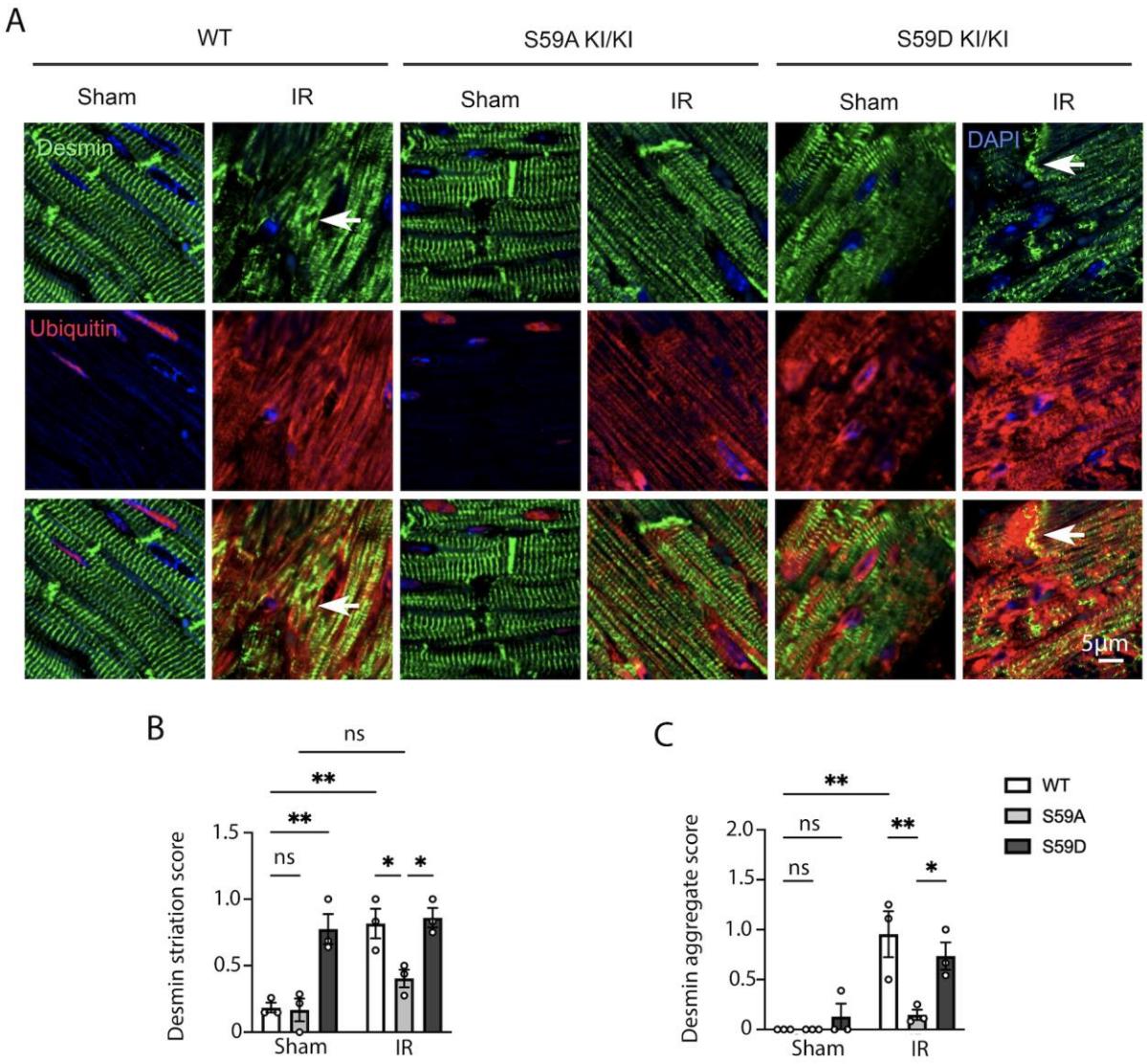

Figure 4.6: S59D KI/KI mice myocardium showed abnormal desmin striation in unstressed state. S59A KI/KI mice showed preserved desmin striation after ischemia-reperfusion injury. A-C) Representative immunohistochemical images (A) and quantitation (B, C) from remote myocardium of sham or IR-treated CRYAB wild-type, S59A KI/KI and S59D KI/KI mice that were stained for desmin, and polyubiquitin. Arrow points to desmin aggregates, which are mis-localized from their physiologic location (such as Z-discs and intercalated discs in donor myocardium for desmin to protein aggregates. Representative of n=3 hearts/group. * Denotes P< 0.05, and ** denotes P< 0.01 by one-way ANOVA. 'ns' denoted not significant.

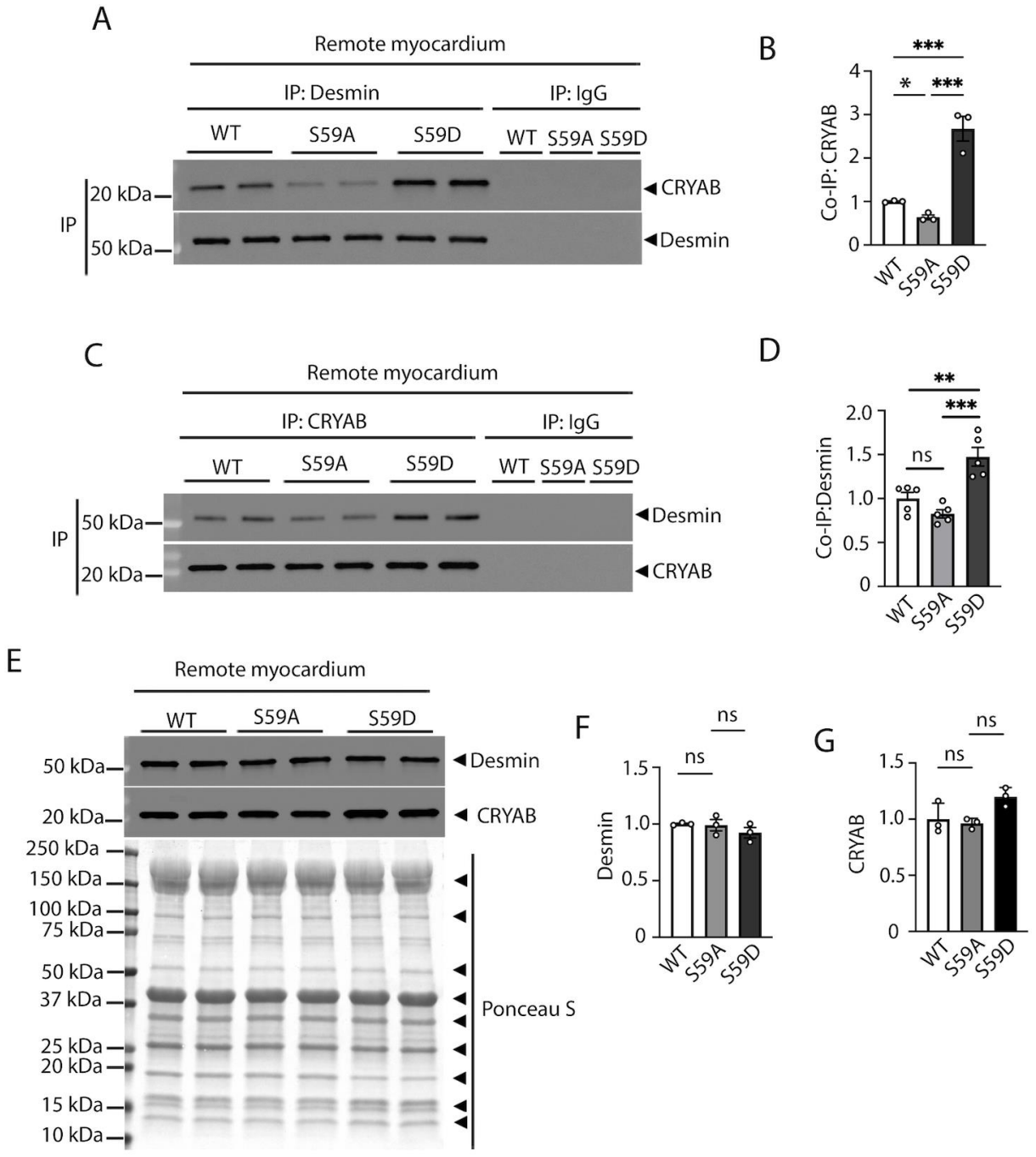

Figure 4.7: S59D KI/KI mice showed increased desmin-CRYAB interaction and S59A KI/KI mice showed decreased desmin-CRYAB interaction. A-D) Representative immunoblot (A, C) and quantitation (B, D) of Desmin or CRYAB when it was co-immunoprecipitated (co-IP) with CRYAB and Desmin respectively. Remote myocardium of CRYAB phospho-mimetic S59D and phospho-deficient S59A KI/KI mice of 10-11 weeks of age were used for this study where CRYAB WT was used as control. ** indicates p<0.01, *** denotes P <0.001by one-way

ANOVA. ‘ns’ denoted not significant. **E-G)** Representative immunoblot (E) and quantitation (F, G) of desmin and CRYAB when they were used as input for co-immunoprecipitation (co-IP) study. CRYAB phospho-mimetic S59D and phospho-deficient S59A KI/KI mice remote myocardium were used for this study where CRYAB WT was used as control. ‘ns’ denotes not significant by one-way ANOVA.

4.7 References

1. Dalakas MC, Park KY, Semino-Mora C, Lee HS, Sivakumar K, Goldfarb LG. Desmin myopathy, a skeletal myopathy with cardiomyopathy caused by mutations in the desmin gene. *NEnglJMed*. 2000;342:770-780. doi: 10.1056/NEJM200003163421104 [doi]
2. Goldfarb LG, Dalakas MC. Tragedy in a heartbeat: malfunctioning desmin causes skeletal and cardiac muscle disease. *JClinInvest*. 2009;119:1806-1813. doi: 38027 [pii];10.1172/JCI38027 [doi]
3. Vicart P, Caron A, Guicheney P, Li Z, Prevost MC, Faure A, Chateau D, Chapon F, Tome F, Dupret JM, et al. A missense mutation in the alphaB-crystallin chaperone gene causes a desmin-related myopathy. *NatGenet*. 1998;20:92-95. doi: 10.1038/1765 [doi]
4. Ito H, Okamoto K, Nakayama H, Isobe T, Kato K. Phosphorylation of alphaB-crystallin in response to various types of stress. *The Journal of biological chemistry*. 1997;272:29934-29941. doi: 10.1074/jbc.272.47.29934
5. Takagi H, Hsu CP, Kajimoto K, Shao D, Yang Y, Maejima Y, Zhai P, Yehia G, Yamada C, Zablocki D, et al. Activation of PKN mediates survival of cardiac myocytes in the heart during ischemia/reperfusion. *Circ Res*. 2010;107:642-649. doi: 10.1161/circresaha.110.217554
6. Cook SA, Sugden PH, Clerk A. Activation of c-Jun N-terminal kinases and p38-mitogen-activated protein kinases in human heart failure secondary to ischaemic heart disease. *Journal of molecular and cellular cardiology*. 1999;31:1429-1434. doi: 10.1006/jmcc.1999.0979
7. den Engelsman J, Gerrits D, de Jong WW, Robbins J, Kato K, Boelens WC. Nuclear import of {alpha}B-crystallin is phosphorylation-dependent and hampered by hyperphosphorylation of the myopathy-related mutant R120G. *The Journal of biological chemistry*. 2005;280:37139-37148. doi: 10.1074/jbc.M504106200
8. Javaheri A, Bajpai G, Picataggi A, Mani S, Foroughi L, Evie H, Kovacs A, Weinheimer CJ, Hyrc K, Xiao Q, et al. TFEB activation in macrophages attenuates postmyocardial infarction ventricular dysfunction independently of ATG5-mediated autophagy. *JCI Insight*. 2019;4. doi: 10.1172/jci.insight.127312
9. Ma X, Rawnsley DR, Kovacs A, Islam M, Murphy JT, Zhao C, Kumari M, Foroughi L, Liu H, Qi K, et al. TRAF2, an Innate Immune Sensor, Reciprocally Regulates Mitophagy and Inflammation to Maintain Cardiac Myocyte Homeostasis. *JACC Basic Transl Sci*. 2022;7:223-243. doi: 10.1016/j.jacbts.2021.12.002
10. Ma X, Mani K, Liu H, Kovacs A, Murphy JT, Foroughi L, French BA, Weinheimer CJ, Kraja A, Benjamin IJ, et al. Transcription Factor EB Activation Rescues Advanced alphaB-Crystallin Mutation-Induced Cardiomyopathy by Normalizing Desmin Localization. *Journal of the American Heart Association*. 2019;8:e010866. doi: 10.1161/JAHA.118.010866

4.8 Supporting materials

Table 4.1: Morphometric and M-mode echocardiographic data for CRYAB WT, S59A KI/KI, and S59D KI/KI mice at 10-11 weeks of age.

	CRYAB WT (n=6)	**CRYAB S59A (n=8)**	**CRYAB S59D (n=8)**
BW (g)	22.95 ± 1.61	22.28 ± 1.06	21.09 ± 1.39
HW/BW (mg/g)	4.53 ± 0.11	4.71 ± 0.16	4.78 ± 0.07
HW/TL (mg/mm)	6.50 ± 0.33	6.29 ± 0.18	6.36 ± 0.39
LVIDd (mm)	3.29 ± 0.09	3.13 ± 0.05	3.20 ± 0.09
LVIDs (mm)	1.76 ± 0.09	1.62 ± 0.04	1.75 ± 0.08
FS (%)	46.65 ± 1.66	48.43 ± 0.74	45.69 ± 1.11
LV mass (mg)	63.41 ± 2.73	57.37 ± 1.45	63.34 ± 4.13
HR (beats per min)	625± 13	593 ± 8	608 ± 10

Data represent mean ± SEM. No significant differences ($p>0.05$) were found between groups in ordinary one-way ANOVA by using Tukey's multiple comparison test. BW= Body Weight, HW= Heart Weight, TL= Tibia Length, LVIDd= Left Ventricular Internal Diameter End Diastole, LVIDs= Left Ventricular Internal Diameter End Systole, FS= Fractional Shortening,

LV mass= Left-Ventricular mass based on M-mode echocardiography measurements, HR= Heart rate.

Chapter 5: Pharmacological chaperone 25-hydroxycholesterol (25-HC) rescues post-MI cardiomyopathy by reducing toxic aggregate-prone pS59CRYAB.

5.1 Introduction

25-hydroxycholesterol (25-HC) is a derivative of cholesterol which is obtained by oxidation catalyzed by enzymes[1]. αB-crystallin is one of the most prevalent proteins in lens. When the soluble form of αB-crystallin becomes insoluble amyloid due to misfolding and aggregation, it forms cataract in humans[3]. Interestingly, 25-HC was discovered as a therapeutic chaperone in a study that screened a lot of small molecules which can protect against cataract formation[4]. 25-HC acts as a pharmacological chaperone in reducing aggregates in in-vitro model and refolding αB-crystallin in mouse model of cataract carrying R120G genetic mutation[4]. 25-HC improves the transparency of the lens when disaggregation was performed following aggregation induction[4]. Thus, the molecular mechanism of how CRYAB R120G aggregates can be rescued by 25-HC remains unknown. Later, in-silico molecular docking study was done to understand this phenomenon where it was found that 25-HC is able to bind in a groove in CRYAB native form forming multiple hydrogen bonds, but not the enantiomer of 25-HC[5]. In our study, we have observed that CRYAB interacts strongly with client proteins such as desmin and becomes aggregate-prone when it is phosphorylated by p38MAPK, and it induced cardiomyopathy associated adverse LV remodeling. Thus, we hypothesized that, treatment of 25-HC will be able to reduce CRYAB aggregates and total pS59CRYAB to rescue post MI-cardiomyopathy. In this study, we have first induced protein aggregate formation in NRCMs by

adenoviral transduction of CRYAB R120G and treated cells with 25-HC. We then subjected WT C57BL6J young adult male mice to ischemia-reperfusion injury, and injected 25-HC intraperitoneally to observe the effect in cardiac remodeling after IR.

5.2 Results

5.2.1 25-HC reduces pS59CRYAB and aggregates formed by an arginine to glycine (R120G) human disease-causing mutant in CRYAB

To examine the paradigm that overall reduction in pS59CRYAB may be beneficial, we turned to studies with 25-hydroxycholesterol (25-HC). This compound was uncovered in a screen focused on preventing aggregation of CRYAB-R120G in the lens of the eye to prevent cataract formation [4]. We tested the efficacy of 25-HC on serine-59 phosphorylation of CRYAB-R120G protein transduced in neonatal rat cardiac myocytes, followed by subcellular fractionation. As shown, 25-HC induced a dose-dependent reduction in pS59CRYAB levels in the detergent insoluble fraction (Fig. 5.1 B) with a significant reduction at the highest dose tested (Fig. 5.1 D) without a change its levels in the soluble fraction (Fig. 5.1 A, D) or in total CRYAB abundance (Fig. 5.1 A, B, E). This was accompanied by a reduction in p62 and polyUb proteins in the insoluble fraction (Fig. 5.1 B, F, G) but not the soluble fraction (Fig. 5.1 A, F, G) at the highest dose of 25-HC. 25-HC also induced a marked reduction in CRYAB-R120G aggregates detected with immunostaining (Fig. 5.1 C).

5.2.2 Altered phase separation of CRYAB R120G but not CRYAB S59D was rescued by 25-HC

To determine if 25-HC treatment alters phase separation of the CRYAB-R120G mutant protein, we expressed CRYAB-R120G optoIDR construct (as in Fig. 2.4 E-G) and treated the

cells with 40 μM 25-HC or diluent. 25-HC treatment reduced the number and size of CRYAB-R120G aggregates (Fig. 5.2 A-C) but did not result in a noticeable light-induced increase in condensate formation (Fig. 5.2 B, C). To examine the effect of 25-HC treatment on the fluidity of CRYAB-R120G condensates, we performed FRAP analyses. As shown (Fig. 5.2 D, E), the recovery of fluorescence was markedly increased in 25-HC-treated CRYAB-R120G mutant proteins post-bleach as compared with diluent-treated CRYAB-R120G. Taken together, these data indicate that 25-HC treatment reduces serine-59 phosphorylation to maintain fluidity of the resulting condensates and reduces the propensity for aggregate formation. To confirm if the mechanism of action of 25-HC was via S59 phosphorylation and whether 25-HC can affect the phase separation and dynamicity of phospho-mimetic S59D variant, we performed phase separation and FRAP analyses. We have observed that 25-HC is not able to alter phase separation (Fig. 5.3 A-C) or dynamicity (Fig. 5.3 D, E) of S59D variant. These findings predict a beneficial effect of 25-HC on post-MI remodeling by reducing the abundance of pS59CRYAB.

5.2.3 Attenuating serine-59 phosphorylation with 25-hydroxycholesterol rescues post-MI cardiac remodeling in-vivo

We set up a protocol, where mice were injected with 25-HC at the dose of 10 mg/kg beginning at day 4 after IR injury (Fig. 5.4 A). We chose this time point to avoid its effects on CRYAB phosphorylation during the acute phase of injury, where p38 kinase-mediated serine-59 phosphorylation may play a protective role [6,7]. Our data demonstrate a significant increase in LVEF (Fig. 5.4 C) with reduced LV dilation (Fig. 5.4 D) in 25-HC-treated mice. We examined the effect of 25-HC on pS59CRYAB and detected a decline in the insoluble fraction (Fig. 5.5 B-F) without an increase in the soluble fraction (Fig. 5.5 A, C-F), consistent with the effects

observed in neonatal rat cardiac myocytes (Fig. 5.1 A-D). We also have observed a reduction of polyubiquitinylated proteins in the insoluble fractions of the 25-HC injected mice, demonstrating a reduction of protein aggregates. As supportive evidence, we have observed 25-HC-treatment attenuated aggregates observed in the post-IR myocardium of wild-type mice (Fig. 5.6 A, B, C) with a trend towards reduction in scar size (Fig. 5.7 A, B), while the area-at-risk was similar between the two groups. Even though we observed decreased sequestration of pS59CRYAB in the insoluble fraction of the 25-HC injected mice, we saw a rescue in adverse LV-remodeling. Thus, we performed immunoblotting of pS59CRYAB using the crude extract of the remote myocardium of the diluent and 25-HC injected mice. We have observed a marked decrease of pS59CRYAB in 25-HC injected mice (Fig. 5.8 A, B). These data support the notion that attenuating overall levels of serine-59 phosphorylated CRAYB is an effective strategy to reduce the aggregation potential and toxicity of CRYAB under sustained stress, as observed in ischemic cardiomyopathy.

5.3 Discussion

CRYAB R120G is associated with cardiomyopathy and cataract formation with aggregate formation. As cardiomyopathy and cataract formation is associated with CRYAB aggregate formation, and 25-HC was found to rescue cataract formation by reducing protein CRYAB aggregates, we have planned to use 25-HC in our study. We have first performed a serial dosage of 25-HC in the NRCMs that had CRYAB R120G aggregates and have seen that 40 μM of 25-HC was able to reduce aggregates and abundance of pS59CRYAB in the insoluble fraction. We then modeled WT mouse of ischemia-reperfusion injury and treated 25-HC for three and a half weeks. We started administration of 25-HC four days after ischemia to reduce the confounding effect of immune cells that induce expression of 25-HC at the site of

inflammation. In our study, we observed a marked decrease of total pS59CRYAB in 25-HC injected mice in the crude extract. This demonstrate that the amount of pS59CRYAB after 25-HC injection reduces sufficiently to improve cardiac myocyte function after ischemia-reperfusion injury. However, future studies are needed to understand the molecular mechanisms.

5.4 Conclusion

The beneficial effect of reducing the overall abundance of pS59CRYAB with 25-hydroxychoesterol administration on post-MI remodeling indicates that reducing toxic aggregate-prone proteins such as pS59CRYAB, is an effective strategy to counter the pathogenesis of ischemic cardiomyopathy.

5.5 Materials and Methods

Neonatal cardiac myocyte isolation. Neonatal rat cardiac myocyte isolation was performed from C57BL6J young adult mice using a modification of the technique we have described with the Worthington Neonatal Cardiomyocyte Isolation System (CAT# LK003300) [8]. Hearts were harvested from one-day old neonatal mice and were subjected to trypsin digestion in a final concentration of 50 μg/ml in HBSS for 16-18 hours at 4°C after removal of the atria. Collagenase digestion (type II collagenase; 300 U/ml; Worthington) was conducted at 37°C for 45 min. Cardiomyocytes were seeded on collagen-coated four well chamber slides (Laboratory Tek) at a density of 10^5 cells per square cm. On the 2nd day, the culture medium was changed to the Rat Cardiomyocyte Culture Medium (Cell applications INC, CAT#R313-500) for at 3-5 days prior to immunofluorescence staining.

Adenoviral studies. Adenoviral vectors encoding for CRYAB-R120G were employed, as previously described[9]. We have treated the cells for 48 hours after adenoviral transduction and then treated with 25-HC for 24-hours.

Immunofluorescence analysis. We performed immuno-histochemistry on cells and myocardial tissues as we have previously described [10]. Primary cultures of neonatal mouse cardiac myocytes were fixed in 100% cold methanol for 20 minutes, followed by blocking with 1% normal serum in PBS for 1 hour at room temperature. Primary antibody used was as follows: anti–αB-crystallin polyclonal antibody (ENZO Life, ADI-SPA-223-F) with overnight incubation at 4°C. Paraffin-embedded heart sections (4 μm thick) were subjected to de-paraffinization using Xylene; serial 100%, 90%, 70% and 50% EtOH treatment followed by hydration using DI water and heat-induced epitope retrieval in Diva decloaker solution (Biocare medical, REF# DV2004MX). This was followed by blocking using 1% BSA (Sigma-Aldrich, CAT#A9647-100G), 0.1% Tween-20 (Sigma-Aldrich, CAT# P2287-500ML) in PBS (Corning, CAT# 21-040-CM) and 5% donkey serum. The slides were incubated overnight with primary antibody in 4°C. After serial washes, samples were stained with secondary antibody and mounted with fluorescent 4',6-diamidino-2-phenylindole mounting medium (Vector Labs, H-1200). Confocal imaging was performed on a Zeiss confocal LSM-700 laser scanning confocal microscope using 40×/1.3, and 63x oil immersion objectives, and images were processed using the Zen black software. Primary antibody used in these experiments were: anti-desmin (Santa Cruz Biotechnology, Inc, SC-7559), anti-actin (Millipore Sigma, A2066), anti-actinin (Abcam, ab9465).

Striation and aggregate scoring. We focused on mis-localization of CRYAB client proteins desmin, actin and α-actinin and the presence of aggregates in closed-chest ischemia reperfusion subjected C57BL6J WT mice that underwent diluent or 25-HC treatment to observe impaired protein quality control. At least three images were taken per sample for quantitation. Striation and aggregate scoring were performed following the protocol stated in chapter 3.

Biochemical fractionation into soluble and insoluble fractions. We have performed biochemical fractionation into soluble insoluble fractions of NRCMs and mouse remote cardiac tissue following the protocol described in the previous chapters.

Studies with optoDroplet constructs. CRYAB constructs were transfected into HEK 293A cells using Effectene transfection reagent (Qiagen, CAT#301425) and live-cell imaging was performed using 35-mm glass-bottom dishes at 24-hours after transfection using 40x oil immersion objective of the Nikon A1R confocal imaging system (equipped with 37°C stage) at the Center for Cellular Imaging (WUCCI) at Washington University in St. Louis School of Medicine. Cells were imaged with two laser wavelengths (488 nm for Cry2 activation and 561 nm for mCherry imaging) with laser power of 10% for the 488 nm. Various parameters were quantified using imageJ (NIH) by adjusting the threshold to ensure uniform cut-off values at the t=0 and t=300s time-point images. Average condensate area was determined by total area of the fluorescence signal divided by number of condensates before or after 300s of the blue light activation. Average number of condensates per cell was obtained by dividing total number of condensates divided by number of cells before or after 300s of the blue light activation.

Studies with fluorescence recovery after photobleaching (FRAP). FRAP was performed on OptoIDR constructs as described above while imaging with100x objective lens of the Nikon

A1R confocal imaging system, using 488nm laser at 50% intensity and 561 nm laser at 50% intensity for 1 minute selecting a region of interest of ~ 1 um in diameter; and fluorescence recovery was monitored. Intensity traces were collected using imageJ and normalized to pre-bleaching intensity (set at 100%). Only condensates with reduction in intensity to <10% (as compared to pre-bleach) post-photobleaching were selected for further analysis.

Immunoblotting. Immunoblotting was performed as previously described [10] with antibodies listed below: anti-SQSTM1/p62 antibody (Abcam, ab56416); αB-crystallin (CRYAB) polyclonal antibody (Enzo life sciences, CAT# ADI-SPA-223-F); Anti-Alpha B crystallin (pS59) antibody (Abcam, CAT#ab5577); Anti-ubiquitinylated proteins antibody, clone FK1 (Sigma-Aldrich, CAT#04-262) ; Anti-GAPDH antibody (Abcam, CAT#ab22555); Anti-Actin antibody (Sigma, CAT#A2066).

Closed-chest cardiac ischemia-reperfusion modeling and echocardiography. Described as before (Chapter 3)

Studies with 25-hydroxycholesterol. 25-hydroxycholesterol (CAT#H1015-100MG, Sigma-Aldrich) was dissolved in 100% ethanol (final concentration 20mg/mL) to make a stock solution. For in-vivo experiments, the stock solution was diluted in sterile PBS for injection. A dose of 10mg/kg or equivalent vehicle control was administered every other day via intraperitoneal injection beginning at day 4 after closed-chest ischemia-reperfusion injury for 3.5 weeks. Mice were weighed prior to injection and food intake was monitored through the experiment.

Scar size analyses. Scar area analysis was performed on Trichrome staining photographs from closed-chest ischemia-reperfusion subjected C57BL6J WT male mice that were diluent or 25-treated. The protocol is presented on chapter 4.

Statistical analyses. Data presented as mean±SEM. All measurements were obtained from separate biological replicates. Statistical analyses were performed in GraphPad Prism version 9. Data were tested for assumptions of normality with Shapiro-Wilk normality test. Statistical significance was assessed with unpaired two-tailed Student's t-test for comparison between two groups, or one-way or two-way ANOVA for assessing differences across multiple groups followed by post-hoc testing. A non-parametric test was performed if data were not normally distributed. A two-tailed P value of <0.05 was considered statistically significant.

Study approval. All animal studies were approved by the IACUC at Washington University School of Medicine.

5.6 Figures

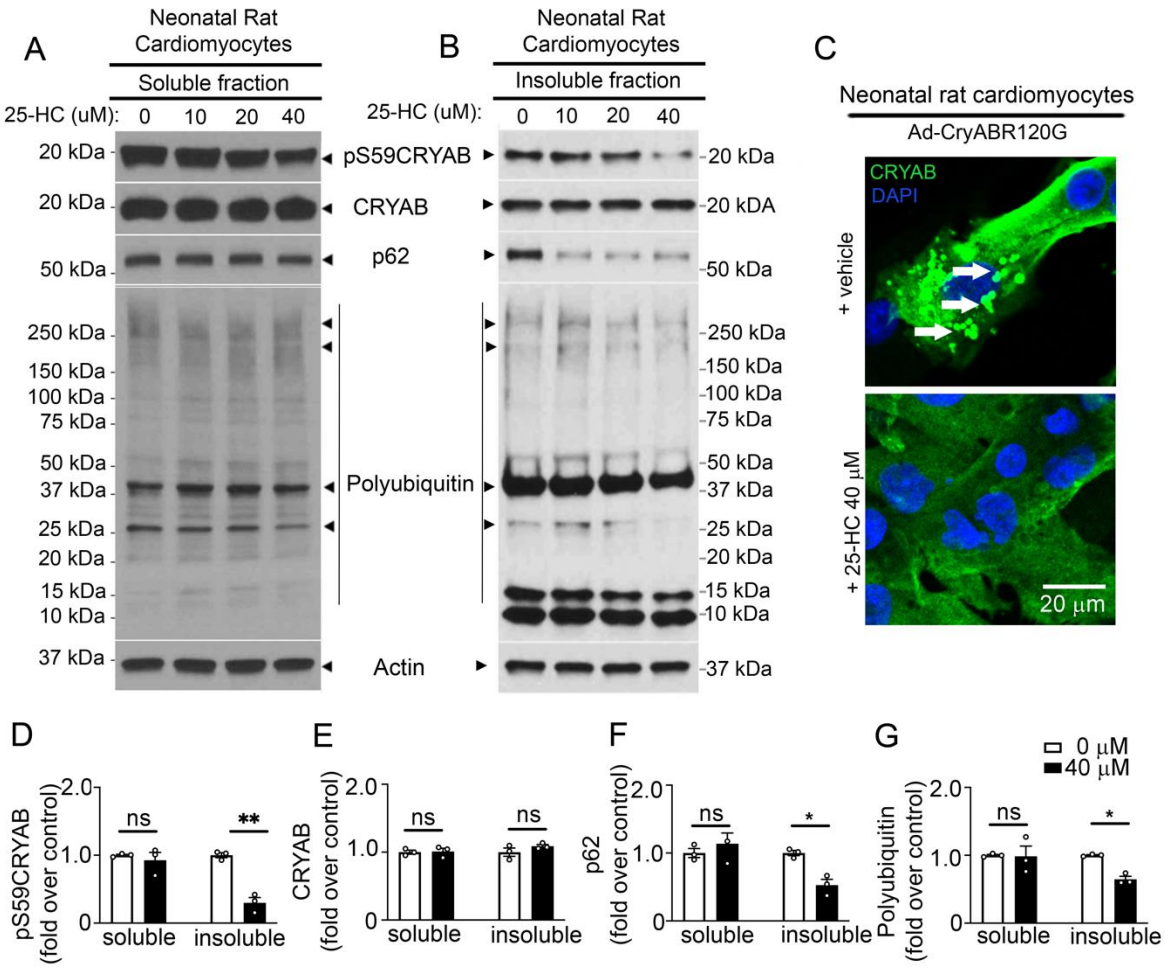

Figure 5.1: Treatment with 25-hydroxycholesterol reduces pS59CRYAB in the insoluble fraction and reduces aggregates. A, B) Representative immunoblots depicting total pS59CRYAB, CRYAB, p62 and polyubiquitinated proteins in NP40-detergent (A) soluble and (B) insoluble fractions from neonatal rat cardiomyocytes (NRCMs) transduced with adenoviral CRYAB-R120G (MOI=10) for 96 hours and treated with 0, 10, 20 and 40 μM 25-hydroxycholesterol for the final 72 hours. Actin is shown as loading control. **C.** Representative immunofluorescence images of NRCMs treated in A. Arrows point to GFP-positive aggregates. **D-G)** Quantitative assessment of pS59CRYAB (D), total CRYAB (E), p62 (F) and polyubiquitinated protein (G) expression in NP-40 soluble and insoluble fractions from NRCMs treated in A. * denotes P <0.05 and ** denotes P <0.01 by t-test.

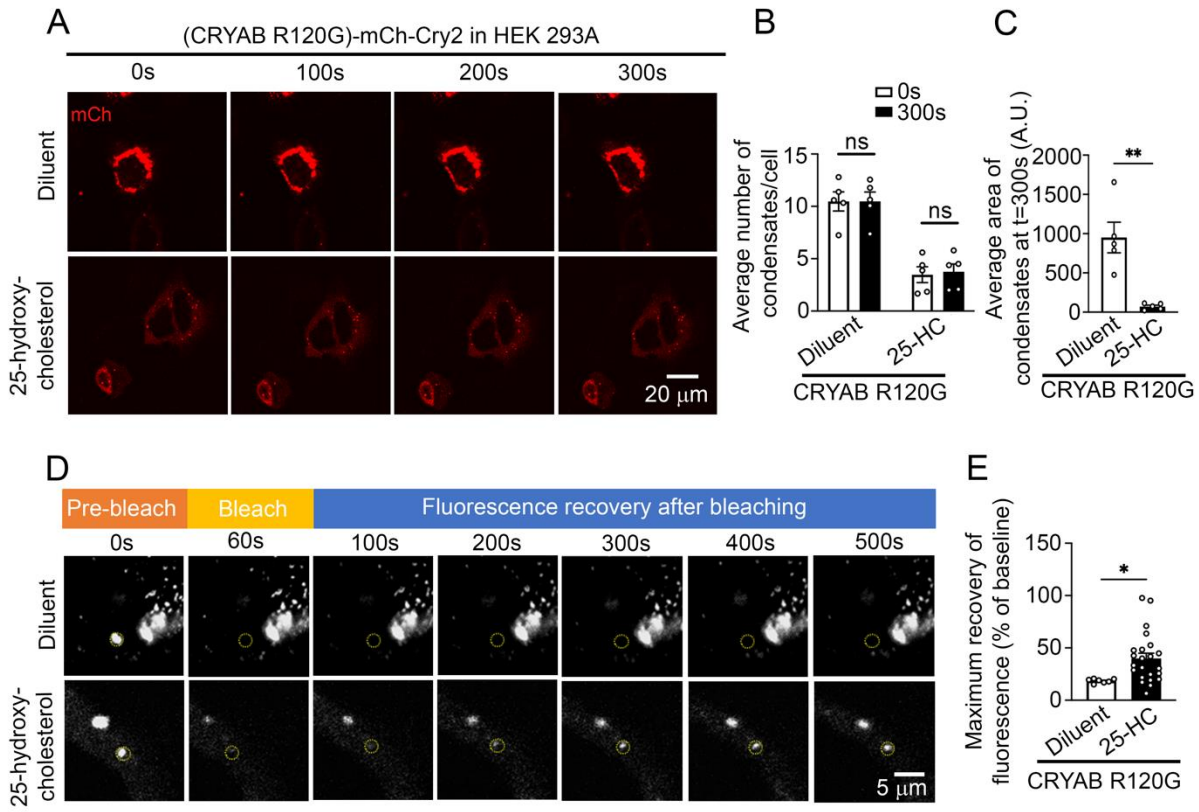

Figure 5.2: Treatment with 25-hydroxycholesterol alters the phase separation characteristics of CRYAB-R120G. A) Representative time-lapse images at t=0s, 100s, 200s, and 300s after light activation in HEK293A cells transfected with OptoIDR constructs generated with CRYAB-R120G as the 'IDR' protein and treated with diluent or 25-HC (20 μM). **B, C**) Average number (I) and area (J) of condensates/cell at t=0 vs. t=300s in cells treated as in H. ** indicates P<0.01 and *** indicates P<0.001 by t-test. **D)** Representative images demonstrating recovery of fluorescence after photobleaching in HEK 293A cells treated as in H. The area of photobleaching is marked with a dotted circle prior to (pre-bleach), and at 0, 100, 200, 300, 400 and 500 seconds (s) after photobleaching. **E)** Quantitation of fluorescence recovery in CRYAB variants indicated in K. * indicates P<0.05 by t-test.

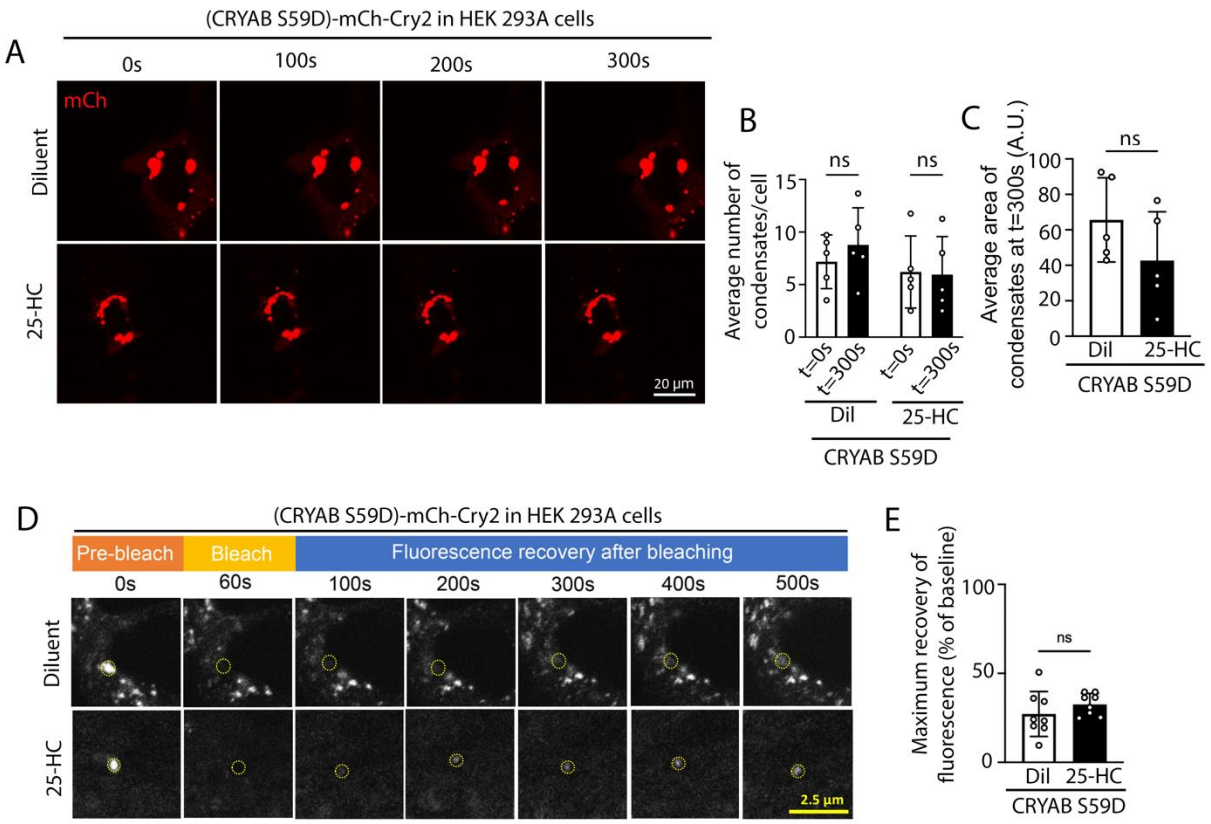

Figure 5.3: 25-HC does not affect phase separation or dynamicity of CRYAB S59D. A) Representative time-lapse images at t=0s, 100s, 200s, and 300s after light activation in HEK293A cells transfected with constructs generated with CRYAB S59D, the phospho-mimetic mutant as the 'IDR' in the optoIDR constructs. **B)** Average number of condensates/cells at t=0 vs. t=300s in cells treated as in A. 'ns' indicates not significant by t-test. **C)** Average area of condensates/cell at t=300s in cells treated in A. 'ns' indicates not significant by t-test. **D)** Representative images demonstrating recovery of fluorescence after photobleaching in HEK 293A cells transfected with mCherry-Cry2 fused optoIDR constructs generated with CRYAB S59D, the phospho-mimetic mutant. Representative images demonstrate area of photobleaching (marked with a dotted circle) prior to (pre-bleach), immediately after, and at 100, 200, 300, 400 and 500 seconds (s) after photobleaching was terminated. Intensity at various time points is depicted as a fraction of intensity prior to bleaching (set at 100%). **E)** Quantitation of

fluorescence recovery (maximum minus immediately post-bleach) in CRYAB S59D variants indicated in D.’ns’ indicates not significant by t-test.

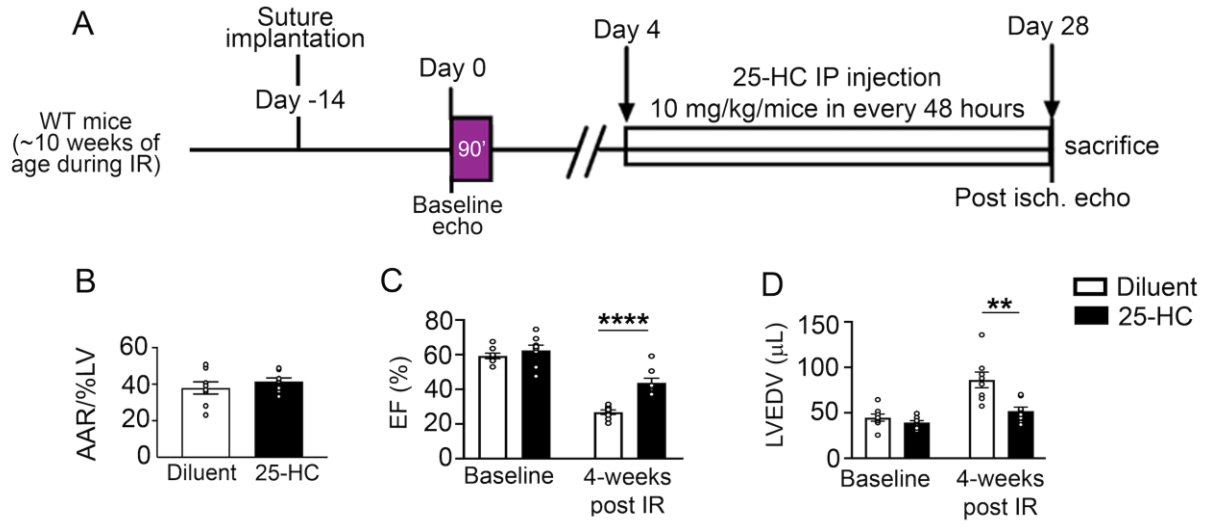

Figure 5.4: Treatment with 25-hydroxycholesterol rescues adverse LV remodeling after IR injury. A. Schematic depicting experimental strategy for closed-chest IR modeling in wild-type mice followed by intraperitoneal administration of 25 hydroxycholesterol (10 mg/kg/mouse in every 48 hours) or diluent, initiated as day 4 after IR injury. **B-D)** Quantitative analyses of area-at-risk (AAR, B), LV ejection fraction (EF (%), C) and left ventricular end-diastolic volume (LVEDV, D) prior to and at 4 weeks after IR injury in mice treated as in A. ** denotes P< 0.01 and **** denotes P <0.0001 by t-test. 'ns' indicates not significant.

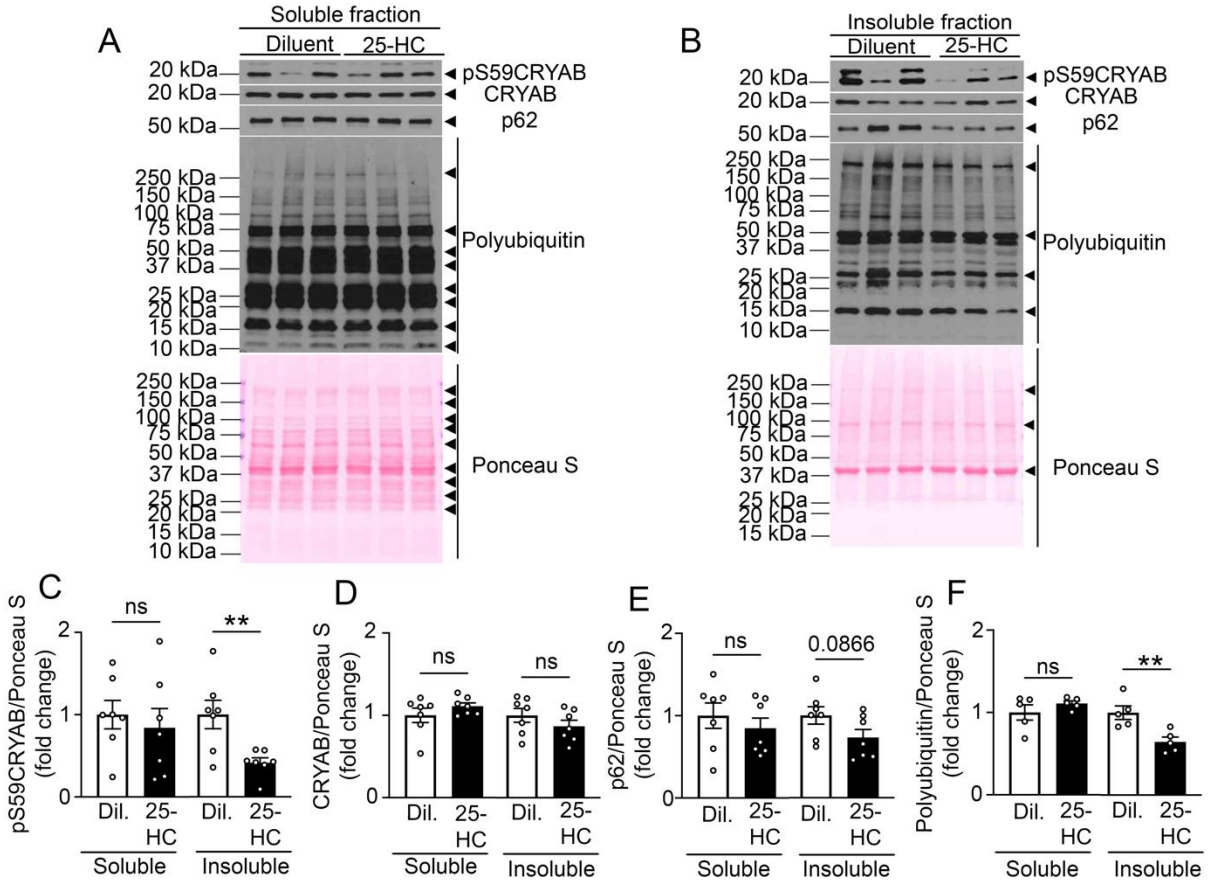

Figure 5.5: Treatment with 25-hydroxycholesterol reduces sequestration of pS59CRYAB in the insoluble fraction. A-F) Representative immunoblots (A, B) and quantitation (C-F) depicting total CRYAB, pS59CRYAB, p62 and polyubiquitinated protein expression in NP-40 soluble (A) and insoluble (B) fraction in myocardium of mice 4-weeks after IR injury and treated with diluent or 25-HC. ** indicates P<0.01 and 'ns' indicates not significant by t-test.

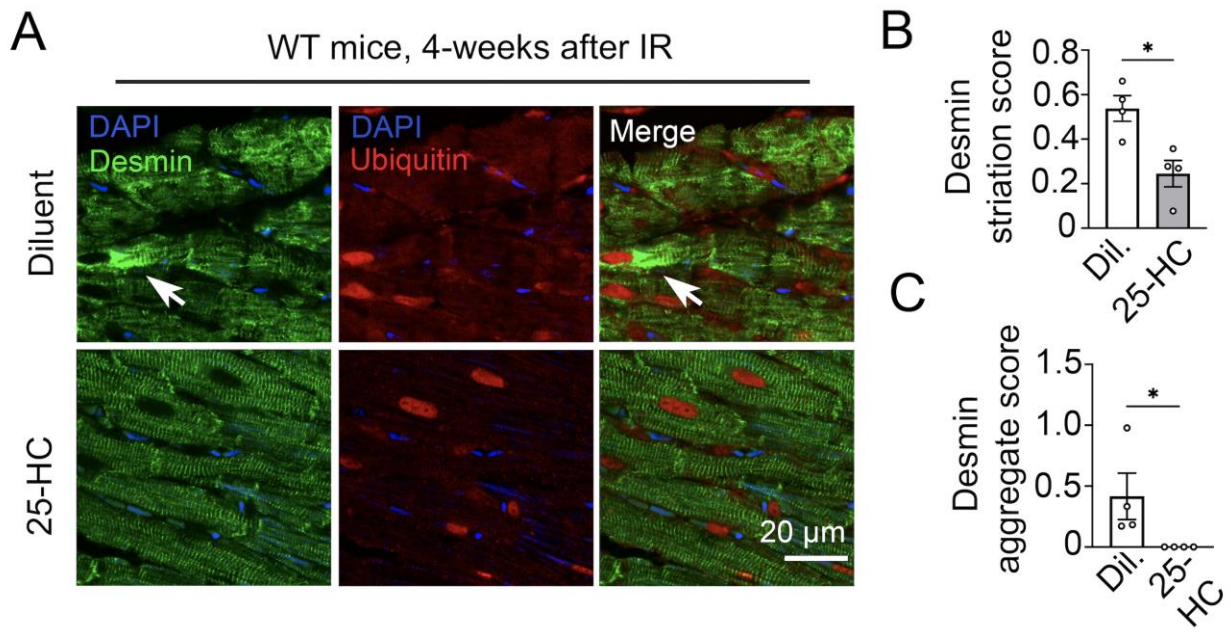

Figure 5.6: Treatment with 25-hydroxycholesterol reduces aggregates in the heart post-MI. A) Representative images depicting polyubiquitin, p62 and desmin staining on formalin fixed myocardial sections from WT mice 4-weeks after IR injury and treated with diluent or 25-HC. Representative of n=4 hearts per group. Arrows point to aggregates in cardiac myocytes. **B, C)** Representative Masson's trichrome images (B) and quantitation (C) of scar size from mice subjected to closed chest IR modeling followed by treatment with 25-hydroxycholesterol or diluent. P value shown is by t-test.

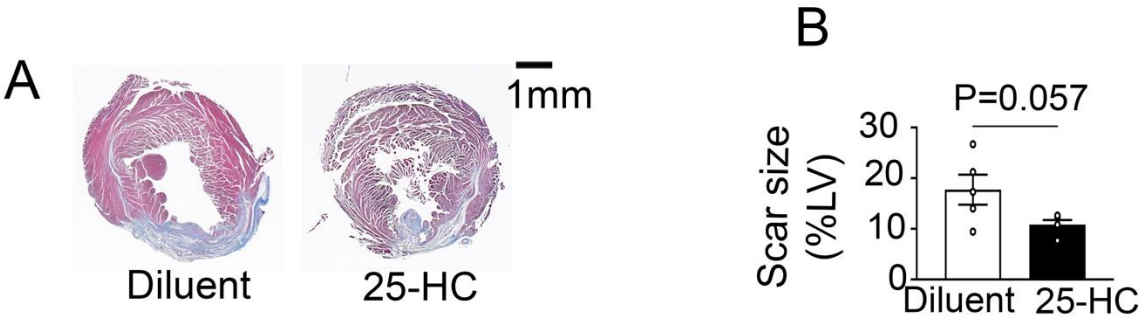

Figure 5.7: Treatment with 25-hydroxycholesterol reduces scar size post-MI. A, B) Representative Masson's trichrome images (A) and quantitation (B) of scar size from mice subjected to closed chest IR modeling followed by treatment with 25-hydroxycholesterol or diluent. P value shown is by t-test.

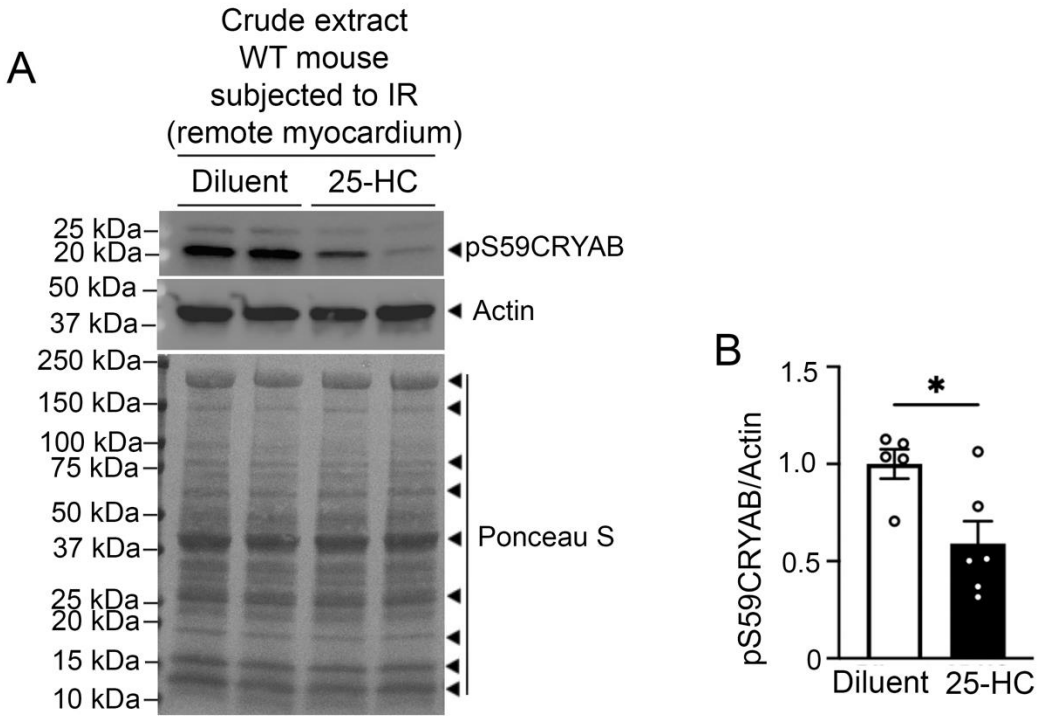

Figure 5.8: 25-HC treatment reduces overall pS59CRYAB in the WT C57BL6J mice post-MI. Representative immunoblot (A) and quantitation (B) of pS59CRYAB in crude extracts of remote myocardium from WT C57BL6J young adult male mice that were treated with 25-HC or diluent for ~3.5 weeks. * indicates $p<0.05$ by t-test. Actin and Ponceau S were used as loading controls.

5.7 References

1. Brown MS, Dana SE, Goldstein JL. Cholesterol ester formation in cultured human fibroblasts. Stimulation by oxygenated sterols. *J Biol Chem*. 1975;250:4025-4027.
2. Gold ES, Diercks AH, Podolsky I, Podyminogin RL, Askovich PS, Treuting PM, Aderem A. 25-Hydroxycholesterol acts as an amplifier of inflammatory signaling. *Proc Natl Acad Sci U S A*. 2014;111:10666-10671. doi: 10.1073/pnas.1404271111
3. Sacconi S, Féasson L, Antoine JC, Pécheux C, Bernard R, Cobo AM, Casarin A, Salviati L, Desnuelle C, Urtizberea A. A novel CRYAB mutation resulting in multisystemic disease. *Neuromuscul Disord*. 2012;22:66-72. doi: 10.1016/j.nmd.2011.07.004
4. Makley LN, McMenimen KA, DeVree BT, Goldman JW, McGlasson BN, Rajagopal P, Dunyak BM, McQuade TJ, Thompson AD, Sunahara R, et al. Pharmacological chaperone for alpha-crystallin partially restores transparency in cataract models. *Science*. 2015;350:674-677. doi: 10.1126/science.aac9145
5. Molnar KS, Dunyak BM, Su B, Izrayelit Y, McGlasson-Naumann B, Hamilton PD, Qian M, Covey DF, Gestwicki JE, Makley LN, et al. Mechanism of Action of VP1-001 in cryAB(R120G)-Associated and Age-Related Cataracts. *Invest Ophthalmol Vis Sci*. 2019;60:3320-3331. doi: 10.1167/iovs.18-25647
6. Morrison LE, Hoover HE, Thuerauf DJ, Glembotski CC. Mimicking phosphorylation of alphaB-crystallin on serine-59 is necessary and sufficient to provide maximal protection of cardiac myocytes from apoptosis. *Circ Res*. 2003;92:203-211. doi: 10.1161/01.res.0000052989.83995.a5
7. Morrison LE, Whittaker RJ, Klepper RE, Wawrousek EF, Glembotski CC. Roles for alphaB-crystallin and HSPB2 in protecting the myocardium from ischemia-reperfusion-induced damage in a KO mouse model. *American journal of physiology Heart and circulatory physiology*. 2004;286:H847-855. doi: 10.1152/ajpheart.00715.2003
8. Godar RJ, Ma X, Liu H, Murphy JT, Weinheimer CJ, Kovacs A, Crosby SD, Saftig P, Diwan A. Repetitive stimulation of autophagy-lysosome machinery by intermittent fasting preconditions the myocardium to ischemia-reperfusion injury. *Autophagy*. 2015;11:1537-1560. doi: 10.1080/15548627.2015.1063768
9. Ma X, Rawnsley DR, Kovacs A, Islam M, Murphy JT, Zhao C, Kumari M, Foroughi L, Liu H, Qi K, et al. TRAF2, an Innate Immune Sensor, Reciprocally Regulates Mitophagy and Inflammation to Maintain Cardiac Myocyte Homeostasis. *JACC Basic Transl Sci*. 2022;7:223-243. doi: 10.1016/j.jacbts.2021.12.002
10. Ma X, Mani K, Liu H, Kovacs A, Murphy JT, Foroughi L, French BA, Weinheimer CJ, Kraja A, Benjamin IJ, et al. Transcription Factor EB Activation Rescues Advanced alphaB-Crystallin Mutation-Induced Cardiomyopathy by Normalizing Desmin Localization. *Journal of the American Heart Association*. 2019;8:e010866. doi: 10.1161/JAHA.118.010866

Chapter 6: Preventing aggregate formation or forceful disaggregation worsens post-MI cardiomyopathy.

6.1 Introduction

Protein aggregates that form self-assemblies serve context-dependent beneficial or harmful roles in prokaryotes, fungi, and invertebrates[1,2]. However, in human diseases and in mammalian models, protein aggregates have been associated with 'proteotoxicity' and the mechanistic effect of protein aggregation remains unexplored. A rapidly fatal human cardiomyopathy results from a genetic mutation (Arginine to Glycine residue mutation at position 120, R120G) in a muscle enriched protein αB-crystallin. αB-crystallin is a chaperone protein that helps other cardiac proteins to fold and quality control. R120G mutation in αB-crystallin was studied in our lab in an MHC-Cre driven mice model which recapitulated cardiomyopathy associated aggregate formation[3]. When lysosomal degradative function was improved, clearance of the aggregate was achieved and desmin localization was restored[3]. Thus, we became interested to utilize the strategy to remove protein aggregates in the cardiac myocytes and see its effect in ischemia-reperfusion injury. We first planned a genetic approach and ablate protein aggregate formation and targeted p62. p62 or sequestosome was one of the first selective autophagy receptors discovered and it is comprised with LIR (LC3 interacting region) domain that binds with LC3 (ATG8) receptors of the autophagy cargo[4,5,6]. Human p62 is 440 amino acids long and contains N-terminal PB1 domain, zz domain, TRAF-6 binding domain (TB), Nuclear export signal (NES), bipartite nuclear localization signal (NLS), LC3 interacting region (LIR) and C-terminal Ubiquitin associated domain (UBA) crucial for autophagy and then Keap-interacting region (KIR)[7]. LIR domains have a conserved sequence containing W/F/Y-xx-L/I/V

which is crucial for the LIR-ATG8 interaction required for autophagy[7,8]. p62 is required for the protein aggregate formation in macrophages and these aggregates could show an anti-inflammatory role[9]. Protein aggregate formation requires dimerization of p62 in PB1 domain mediated by K7 and D69[8]. Thus, in order to ablate protein aggregate formation in the cardiac myocytes, we generated a perinatal cardiac specific p62 protein knockout mouse model with a goal to determine the role of the protein aggregates. We followed another parallel strategy to overexpress yeast disaggregase Hsp104 and selectively disaggregates protein aggregates in the heart. Hsp104 is a yeast chaperone protein of 104 kDa with a hexameric structure[10]. Amyloids are stable aggregate-like structure. Interestingly, they have been found in yeast mediating protective functions[11]. Hsp104 causes disaggregation of the amyloids by giving rise of linearized peptides that can be refolded to native conformations[12]. Engineered Hsp104 was observed to disaggregate neurodegenerative diseases associated protein aggregates such as alpha-synuclein[13,14] , TDP-43[14,15] and FUS[14]. Thus, the gain-of-function of Hsp104 disaggregase can be harnessed to work on diverse proteotoxic aggregations and thus have tremendous therapeutic potential in cases where aggregates are directly related with pathology. So, we have used the strategy of AAV9 mediated cardiac myotropic expression of HSP104 to disaggregate protein aggregates and determine its role in detail in ischemia-reperfusion injury.

6.2 Results

6.2.1 p62 ablation reduces CRYAB R120G aggregation in neonatal mouse cardiomyocytes

To examine the functional relevance of pS59CRYAB partitioning into aggregates with p62, we first performed loss-of-function modeling of p62 in cardiac myocytes to prevent protein aggregation. In prior data, p62 has been demonstrated to be critical for formation of protein-

aggregates in macrophages[9], and TRIM21-mediated ubiquitination of p62 at lysine 7 (K7) is essential in the process, whereby a lysine to arginine (K7R) mutation was sufficient to abolish its aggregation potential[16]. To determine if p62 affects CRYAB-R120G aggregates, we induced the aggregate formation in p62 floxed neonatal mouse cardiac myocytes (NMCMs). We then transduced the NMCMs with adenoviral Cre recombinase to induce p62 ablation (Figure 6.1 A, B). CRYAB-R120G formed protein-aggregates in Ad-LacZ control-treated cardiac myocytes (with intact p62), wherein desmin co-localized with p62 (Figure 6.1 A, B). Ablation of p62 markedly reduced formation of CRYAB-R120G protein-aggregates (Figure 6.1 A, B) and prevented desmin localization to aggregates, indicating that p62 is necessary for aggregate formation of CRYAB and desmin sequestration in cardiac myocytes.

6.2.2 Cardiac myocyte-specific p62 ablation in mice (p62cKO) did not result in altered cardiac structure and function in unstressed young adult mice

We generated and characterized mice carrying two *SQSTM1* alleles and a *Myh6*-Cre transgene (henceforth termed p62 cardiac myocyte knockout (p62cKO) mice). Young adult p62cKO mice demonstrated markedly reduced p62 levels in cardiac myocytes as compared with *SQSTM1* floxed (henceforth referred to as p62 floxed (p62fl/fl)) controls (Fig. 6.2 A) consistent with cardiac myocyte-specific ablation of p62. A previous study showed that p62 ablation in the cardiomyocytes cause mild cardiac dysfunction in normal conditions[28]. However, in this study p62cKO mice did not demonstrate any differences in cardiac structure or function as compared with floxed controls (Table 6.1). We also subjected Myh6-Cre mice to IR and assessed LVEDV and EF at 4-weeks (figure 3.5 A-D). We did not observe any effect of My6-Cre on cardiac function. Given that p62 also serves as an adaptor protein to facilitate sequestration of cargo in

autophagosomes, we examined autophagic flux in the myocardium using two approaches. Firstly, injection of chloroquine to inhibit lysosome acidification and prevent autophagosome-lysosome function demonstrated preserved myocardial flux through macroautophagy in p62cKO mice as compared with controls (Fig. 6.2 A-C). Moreover, the relative abundance of autophagosomes and autolysosomes, as assessed by dual fluorescent-tagged LC3 reporter was not different between p62cKO and controls (Fig. 6.2 A-E). Proteasome activity examined by a fluorometric assay was not altered in p62cKO myocardium as compared with controls (Fig. 6.2 F). We also observed no difference in p62cKO mice in trichrome, H&E and ultrastructure using transmission electron microscopy (Fig. 6.3 A, B). Given that various autophagy adaptors namely Optineurin, TAX1BP1, NDP52 and NBR1 function analogously as p62 in interacting with ubiquitinated protein and LC3, and bridging their engulfment in autophagosomes[17], we examined their expression in p62cKO mice. We did not detect any changes in their protein abundance (Fig 6.4 A-N) in p62cKO mice suggesting that redundancy between these adaptors and p62 maintains flux through macroautophagy despite loss of p62. Also, recent reports indicate a role of p62 in regulating mTOR activity and transcription factor EB (TFEB) in the myocardium[18]. Therefore, we examined phosphorylation of mTOR and its downstream substrate 4EBP1 and did not detect any differences (Fig. 6.4 K, M), or in levels of LAMP1 (Fig. 6.4 K, N), a TFEB target protein, in p62cKO mice as compared with control. Taken together, these observations support the application of p62cKO mice as a suitable model system to examine the relevance of pS59CRYAB partitioning by preventing aggregate formation in the setting of IR.

6.2.3 Reduced sequestration of pS59CRYAB in aggregates in p62cKO mice worsens post-MI cardiomyopathy

We next performed closed-chest ischemia-reperfusion modeling in p62cKO and floxed mice followed by evaluation of cardiac structure and function (Fig. 6.5 A). Notably, the presence of *Myh6*-Cre allele does not alter post-MI LV remodeling versus C57BL6J wild-type mice, whereby we employed p62 floxed mice as controls for subsequent studies. P62cKO mice did not demonstrate a difference in infarct size at 24 hours post injury (Fig. 6.5 B, C) but manifest a significant increase in scar size at 4 weeks (Fig. 6.5 D, E) despite comparable area-at-risk (Fig. 6.5 F) as compared with p62 floxed mice, suggesting infarct expansion in the setting of p62 ablation. We also observed a significant increase in LVEDV (Fig. 6.5 G) and a reduction in LVEF (Fig. 6.5 H) at 4 weeks post-IR injury in p62cKO versus p62 floxed controls. Importantly, loss of p62 resulted in a decline in pS59CRYAB abundance in the insoluble fraction post-IR vs. sham (Fig. 6.5 B, E) with a trend towards relative increase in the soluble fraction (Fig. 6.6 A, D) in p62cKO, suggesting the lack of sequestration of pS59CRYAB in the aggregates with loss of p62. Indeed, pre-amyloid oligomers were not detected in the p62cKO myocardium, while these were observed post-IR injury in the p62 floxed myocardium (Fig. 6.6 C). We previously observed decreased pS59CRYAB in the insoluble fraction showed improved post-MI cardiac remodeling (after 25-HC treatment in the WT mouse that underwent IR). However, In this experiment, we observed reduced pS59CRYAB in the insoluble fraction of the p62cKO mice after IR, but the post-MI cardiomyopathy is worsened. In order to determine whether this observance is due to total pS59CRYAB abundance change after IR in p62 cKO mice, we have performed immunoblotting in the crude extract in the remote myocardium of the p62 fl/fl and cKO groups. We have observed that pS59CRYAB does not reduce in expression in p62 fl/fl and

cKO mouse after IR (Fig. 6.7 A, B). which demonstrate that the adverse LV-remodeling in p62cKO mouse is primarily due to no reduction in the total pS59CRYAB in the crude extract. The reduction of pS59CRYAB in the insoluble fraction is just due to a shift from insoluble to soluble fraction. As total pS59CRYAB was reduced after 25-HC treatment in WT C57BL6J mouse after IR, we observed improved post-MI cardiac remodeling.

6.2.4. Reconstituting p62 by AAV9 expression in cardiac myocytes rescued post-MI cardiomyopathy

To examine the specific requirement for p62's role in protein aggregation in the observed phenotypes, we performed AAV9-mediated expression of wild-type p62 or its aggregation deficient K7R mutant [16] driven by the cardiac troponin T promoter in p62cKO mice and performed IR modeling (Fig. 6.8 A). Restoration of wild-type p62 but not the K7R mutant was sufficient to rescue the LV dilation (Fig. 6.8 B-D) and prevent the decline in LV systolic function (Fig. 6.8 E) in p62cKO mice at 4 weeks post-IR injury. The area-at-risk was similar between groups (Fig. 6.8 F). We also evaluated expression of Nrf2, a transcription factor that drives anti-oxidant signaling and is activated in a non-canonical fashion by p62-mediated sequestration of Keap1[19]; and did not detect changes in Nrf2 (which autoregulates its own expression) or its target genes in the myocardium in p62cKO or control mice after MI or sham surgery (Fig.6.10 A-D). To find out whether autophagy and mTOR pathway activation have an effect in the adverse-LV remodeling, we have performed immunoblotting for autophagy markers and mTOR complex. We have observed that LC3 II and mTOR complex is unaffected (Fig. 6.9 A-D) in the p62cKO mouse after IR. Taken together, these findings indicate that p62 promotes sequestration of pS59CRYAB in protein-aggregates, preventing which worsens ischemic cardiomyopathy.

6.2.5 Forcible disaggregation by AAV9-mediated expression of Hsp104 reduces pS59CRYAB in aggregates and worsens post-MI cardiomyopathy

As a second approach to examine the functional relevance of pS59CRYAB partitioning into aggregates in the setting of IR injury, we expressed Hsp104 (Fig. 6.11 A), a yeast protein, which is functional in disaggregating proteins in mammalian tissues by dis-aggregating protein-aggregates [14,20]. AAV9-Hsp104 expression via the CMV promoter resulted in detectable Hsp104 in myocardial extracts (Fig. 6.11 B) in wild-type mice, without affecting LVEF or LVEDV prior to IR injury (Fig. 6.11 C, D). In mice subjected to closed-chest IR injury, Hsp104 expression led to a significant decline in LVEF (Fig. 6.11 C) and worsening of LV dilation (Fig. 6.11 D), with a trend towards increased scar size at 4 weeks post-IR as compared with control (Fig. 6.11 F, G), while the area-at-risk was comparable (Fig. 6.11 E). Hsp104 expression resulted in decline of polyUb proteins and pS59CRYAB in the insoluble fraction (Fig. 6.12 A-D) with an increase in pS59CRYAB in the soluble fraction (Fig. 6.12 A-D). Taken together, these data demonstrate that Hsp104-induced forced disaggregation of protein-aggregates results in increased partitioning of pS59CRYAB to the soluble fraction accompanied by evidence for toxicity, i.e. worse post-MI remodeling.

6.3 Discussion

Our experiments demonstrate that p62 is essential to form cytoprotective protein-aggregates under stress, as restoration of wild-type p62 but not it's aggregation-deficient K7R variant [16] rescues the adverse consequences of its genetic ablation in cardiomyocytes, in progression of ischemic cardiomyopathy. p62 is a multifunctional protein comprised of a LIR (LC3-interacting region) domain that binds with LC3 (ATG8) to facilitate sequestration of

autophagic cargo in autophagosomes, and a PB1 domain that dimerizes via K7 and D69 residues to sequesters aggregate-prone proteins such as mutant huntingtin to prevent cytotoxicity [21]. Thus, we have employed the usage of K7R mutant in the AAV9 study to observe the role of p62 variant in the heart where p62 will be expressed but will not be able to form aggregates. Mice lacking TRIM21, a E3 ubiquitin ligase that ubiquitinates the K7 residue (which inhibits p62 dimerization), demonstrate marked attenuation of LV dilation and systolic dysfunction in response to pressure-overload modeling with increased p62 and polyUb containing protein-aggregates in cardiac myocytes [16]. These observations are consistent with a protective role for p62-mediated protein aggregation in the setting of ischemic cardiomyopathy that we have found in our study. In our study, we observed pS59CRYAB to be reduced in the insoluble fraction and a reduced signal of anti-oligomeric structures in the cardiac myocytes after IR (Fig. 6.6 C). This suggest that pS59CRYAB, which is aggregate-prone and toxic form of CRYAB, is less sequestered in the insoluble fraction, causing an adverse effect in LV remodeling after IR. This was further supported by the fact that, overall level of pS59CRYAB did not reduce in the p62cKO cardiac myocytes after IR in the crude extracts, (Fig. 6.7) it is only the shift in partitioning of pS59CRYAB in the soluble and insoluble fractions. Moreover, our observations with expression of Hsp104, a yeast disaggregase, also demonstrate worsened post-myocardial infarction LV systolic dysfunction with increased partitioning of pS59CRYAB to the soluble fraction as observed with cardiac myocyte p62 ablation (Fig. 6.11). In parallel, both of these studies showed similar outcome where decreased sequestration of CRYAB worsens cardiac remodeling after ischemia-reperfusion injury. Future studies will need to clarify whether protein-aggregates play a dual role in pathogenesis of disease.

6.4 Conclusion

The studies performed by ablation of p62 in the cardiac myocytes or forceful disaggregation of the protein aggregates in cardiac myocytes, show that there is decreased sequestration of pS59CRYAB in the insoluble fraction, where overall pS59CRYAB does not change in the crude extract. As we have seen worsening post-MI cardiomyopathy in both of those studies, we can conclude that, protein aggregates might play a protective role after IR by sequestering toxic and aggregate-prone pS59CRYAB.

6.5 Materials and Methods

Neonatal cardiac myocyte isolation. Neonatal mouse cardiac myocyte isolation was performed from p62 fl/fl mice using a modification of the technique we have described with the Worthington Neonatal Cardiomyocyte Isolation System (CAT# LK003300) [22]. Hearts were harvested from one-day old neonatal mice and were subjected to trypsin digestion in a final concentration of 50 μg/ml in HBSS for 16-18 hours at 4°C after removal of the atria. Collagenase digestion (type II collagenase; 300 U/ml; Worthington) was conducted at 37°C for 45 min. Cardiomyocytes were seeded on collagen-coated four well chamber slides (Laboratory Tek) at a density of 10^5 cells per square cm. On the 2nd day, the culture medium was changed to the Rat Cardiomyocyte Culture Medium (Cell applications INC, CAT#R313-500) for at 3-5 days prior to immunofluorescence staining.

Adenoviral studies. Adenoviral vectors encoding for CRYAB-R120G, LacZ [23] and Cre [24] were employed, as previously described [24].

Reagents and mice. We crossed mice homozygous for floxed *Sqstm1* alleles [25] (encoding for p62, annotated as p62*fl/fl*) with mice carrying the *Myh6*-Cre transgene [26] to generate mice with

perinatal cardiomyocyte-specific p62 ablation. C57BL6/J mice (strain #00664) and RFP-GFP-LC3 transgenic mice from JAX [24] were employed. All mice were maintained on a C57BL6/J background. Mice of both sexes were studied, unless otherwise specified. No significant differences were observed between sexes for the primary phenotype, whereby the data for both sexes were combined for presentation. All observers were blinded.

Closed-chest cardiac ischemia-reperfusion modeling and echocardiography. Described as before (Chapter 3)

Adeno-associated viral transduction, in vivo. Adeno-associated virus serotype 9 (AAV9) particles coding for p62 or its aggregation-deficient mutant construct (p62 K7R), or GFP (as control) driven by the cardiac troponin T (cTnT) promoter for conferring cardiac myocyte selective expression, and viral particles coding Hsp104 driven by CMV promoter were generated, using backbone constructs generously provided by Dr. Brent French at University of Virginia, Charlottesville, as previously described [24]. The Hsp104 viral plasmid DNA was provided by Dr. Meredith Jackrel from Department of Chemistry at Washington University in St. Louis. The viral particles were generated by the Hope Center viral vectors core. A one-time dose of 3.5×10^{11} particles (Hsp104 studies) and a dose of 7.0×10^{11} particles (p62 and p62-K7R studies) was administered to the mice by tail vein injection.

Biochemical fractionation into soluble and insoluble fractions. Described as before (chapter 3)

Autophagic flux assessment. We assessed autophagic flux by immunofluorescence examination of 10μM thick fresh frozen myocardial tissue from mice carrying the dual fluorescent red fluorescent protein (RFP)–green fluorescent protein (GFP)-LC3 reporter, as described [24]. Only

puncta associated with cells identified as myocytes based upon visualization of boxcar-shaped nuclei were counted. Assessment of autophagic flux, in vivo, was also performed with intraperitoneal injection of chloroquine (Sigma-Aldrich, CAT# C6628) at 60 mg/kg, 4 hours before euthanasia, as previously described[27].

Immunofluorescence analysis. We performed immuno-histochemistry on cells and myocardial tissues as we have previously described[23]. Primary cultures of neonatal mouse cardiac myocytes were fixed in 100% cold methanol for 20 minutes, followed by blocking with 1% normal serum in PBS for 1 hour at room temperature. Paraffin-embedded heart sections (4 μm thick) were subjected to de-paraffinization using Xylene; serial 100%, 90%, 70% and 50% EtOH treatment followed by hydration using DI water and heat-induced epitope retrieval in Diva decloaker solution (Biocare medical, REF# DV2004MX). This was followed by blocking using 1% BSA (Sigma-Aldrich, CAT#A9647-100G), 0.1% Tween-20 (Sigma-Aldrich, CAT# P2287-500ML) in PBS (Corning, CAT# 21-040-CM) and 5% donkey serum. Primary antibodies used were as follows: anti-desmin (Santa Cruz Biotechnology, Inc, SC-7559), anti–αB-crystallin polyclonal antibody (ENZO Life, ADI-SPA-223-F) and anti-p62/SQSTM1 (PROGEN Biotechnik, GP62-C), anti-actin (Millipore Sigma, A2066), anti-actinin (Abcam, ab9465) with overnight incubation at 4°C. After serial washes, samples were stained with secondary antibody and mounted with fluorescent 4’,6-diamidino-2-phenylindole mounting medium (Vector Labs, H-1200). For A11-staining (ThermoFisher, CAT#AHB005), the protocol was revised according to vendors instructions. The antigen retrieval solution was 0.1M glycine/PBS, at pH 3.5. Anti-oligomer A-11 antibody was used at 1-5 ug/mL concentration in 1:1mixture of blocking solution (1%BSA, 0.1% Tween-20 in PBS) and PBS. Confocal imaging was performed on a Zeiss

confocal LSM-700 laser scanning confocal microscope using 40×/1.3, and 63x oil immersion objectives, and images were processed using the Zen black software.

Scar size analyses: Scar area analysis was performed on Trichrome staining photographs from closed-chest ischemia-reperfusion (IR) subjected p62 floxed or cKO male and female mice. Similarly, we used closed-chest IR subjected C57BL6J WT male and female mice that were injected with either AAV-Hsp104 WT or AAV-GFP. The protocol is presented on chapter 4.

Quantitative PCR analyses. Assessment of *Nrf2, Nqo1*, *Mu1* and *Ho-1* transcript abundance was performed as previously described[3] using SYBR Green with primers stated as- Nrf2: Forward 5'- CTACTCCCAGGTTGCCCACA-3', Reverse 5'-CGACTCATGGTCATCTACAAATGG-3'; MmNqo1: Forward 5'-AGCGTTCGGTATTACGATCC-3', Reverse 5'-AGTACAATCAGGGCTCTTCTCG-3'; MmGstm1: Forward 5'-CTACCTTGCCCGAAAGCAC-3', Reverse 5'-ATGTCTGCACGGATCCTCTC-3'; HO-1: Forward 5'- GCTGGTGATGGCTTCCTTGTA, Reverse 5'- ACCTCGTGGAGACGCTTTACAT-3'.

Antibodies employed for immunoblotting: Specific antibodies employed are as follows: anti-SQSTM1/p62 antibody (Abcam, ab56416); αB-crystallin (CRYAB) polyclonal antibody (Enzo life sciences, CAT# ADI-SPA-223-F); Anti-Alpha B crystallin (pS59) antibody (Abcam, CAT#ab5577); Anti-Alpha B crystallin (pS45) antibody (Abcam, CAT#ab5598); Anti-ubiquitinylated proteins antibody, clone FK1 (Sigma-Aldrich, CAT#04-262) ; Anti-GAPDH antibody (Abcam, CAT#ab22555); LC3B antibody (Novus biologicals, CAT#NB100-2220SS); Anti-Actin antibody(Sigma, CAT#A2066); Hsp104 (yeast) polyclonal antibody (Enzo life sciences, CAT#ADI-SPA-1040-D); Recombinant anti-Optineurin antibody (Abcam, CAT#ab213556); TAX1BP1 (Abcam, CAT#ab176572); NBR-1 antibody (Novus biologicals,

CAT#NBP1-71703SS); anti-NDP52 antibody (GeneTex, CAAT#GTX115378); mTOR antibody (Cell signaling, CAT#2972); phospho-mTOR antibody (Cell signaling, CAT#5536S); 4EBP1 (Cell signaling, CAT#9644S); Phospho-4EBP1 (Cell signaling, CAT# 2855s); phospho-LAMP1 polyclonal antibody (Abcam, CAT#ab24170).

Proteosome activity assay. Ventricular tissues were homogenized with 0.5% NP-40 in PBS supplemented with proteinase inhibitor (cat#78442, Thermo scientific). The lysates were centrifuged at 4°C at 15,000 rcf for 10 min, and 20ug protein from the supernatant was used for the proteasome activity measurement using a Proteasome Activity Assay Kit (ab107921; Abcam, Cambridge, MA, USA) according to the manufacturer's protocol. Briefly, the lysates were incubated with proteasome substrate at 37 °C for 1 hour and the fluorescence intensity was measured by the kinetic reading using a Tecan microplate reader (excitation/emission = 350/440 nm). The values were analyzed in pmol/min/ug between two cycles within the linear range.

Statistical analyses. Data presented as mean±SEM. All measurements were obtained from separate biological replicates. Statistical analyses were performed in GraphPad Prism version 9. Data were tested for assumptions of normality with Shapiro-Wilk normality test. Statistical significance was assessed with unpaired two-tailed Student's t-test for comparison between two groups, or one-way or two-way ANOVA for assessing differences across multiple groups followed by post-hoc testing. A non-parametric test was performed if data were not normally distributed. A two-tailed P value of <0.05 was considered statistically significant.

Study approval: All animal studies were approved by the IACUC at Washington University School of Medicine.

6.6 Figures

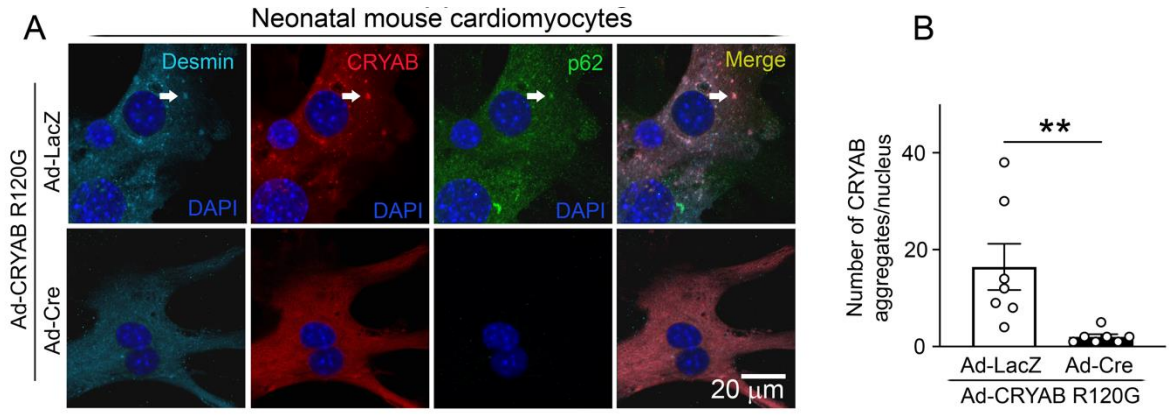

Figure 6.1: Loss of p62 impairs protein-aggregate formation. A, B) Representative immunocytochemical images depicting expression of expression of desmin, CRYAB and p62 (A) with quantitation for protein-aggregates (B, see arrow pointing to a representative aggregate) in neonatal mouse cardiomyocytes (NMCM) generated from p62 fl/fl mice treated with adenoviral (Ad)-Cre (to ablate p62) or with Ad-LacZ as control (all at MOI=10) for 24 hours. The cells were also transduced with adenoviral Ad-CRYAB R120G (MOI=10) to induce protein-aggregate formation and imaged 72 hours later. ** indicates $P< 0.05$ by Mann-Whitney test.

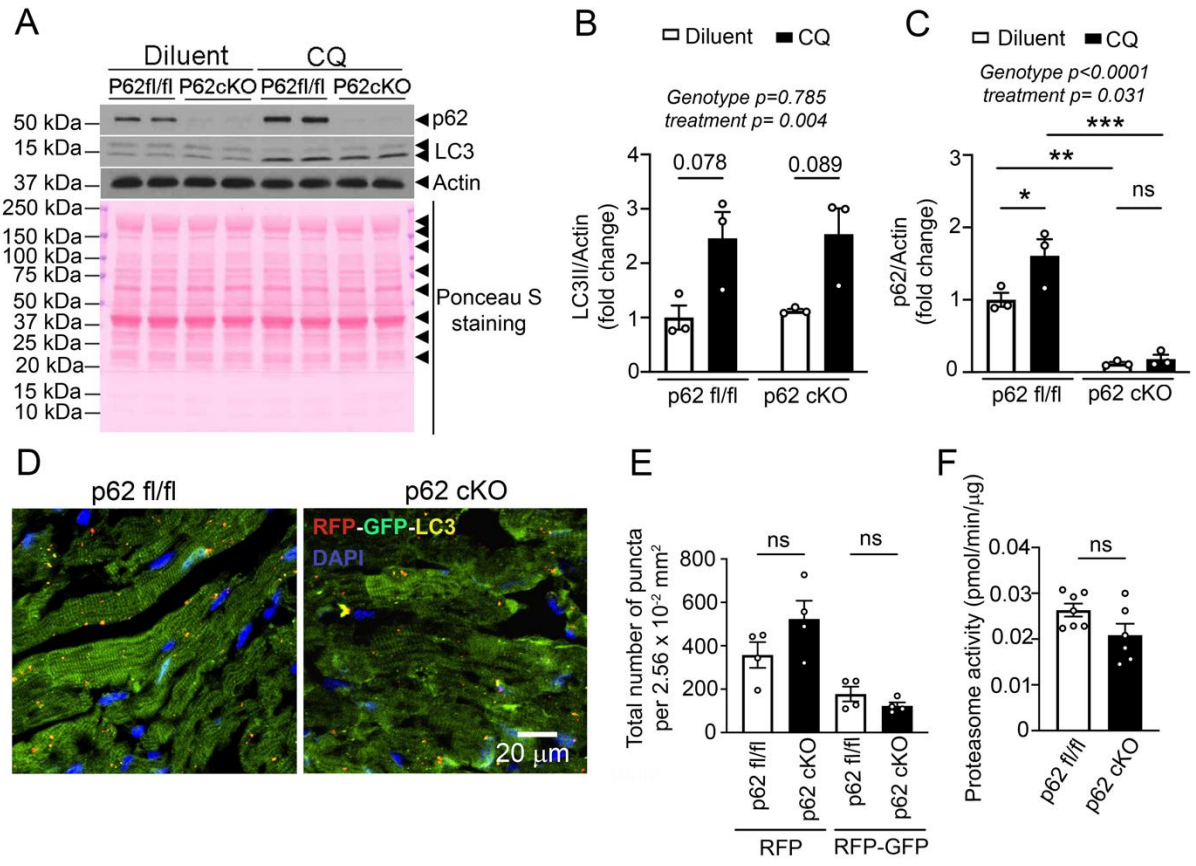

Figure 6.2: Loss of p62 does not affect autophagic flux or proteasome activity. A-F) Representative immunoblot (A) and quantitation depicting fold change of LC3II (B) and p62 (C) in p62 cKO or p62 fl/fl mouse myocardium, 6 hours after injection with 60 mg/kg CQ to evaluate autophagic flux. Actin and Ponceau S staining were performed as loading controls. Indicated P values on top of the panels (B, C) represent factor comparisons by 2-way ANOVA including genotype and treatment as fixed factors, followed by Tukey's post-hoc testing (indicated as P values in individual comparisons). **D-E**) Representative images (D) for visualization of dual fluorescent LC3 expression in p62 cKO and p62 fl/fl mice, with quantitative assessment (E) of autolysosomes (RFP expressing puncta) and total autophagosomes (RFP and GFP expressing puncta) per unit myocardial area. 'ns' indicates not significant by t-test. **F.** Quantitative assessment of proteasome activity in p62 cKO mouse myocardium as compared to p62 fl/fl mouse myocardium as controls. 'ns' indicates not significant by t-test.

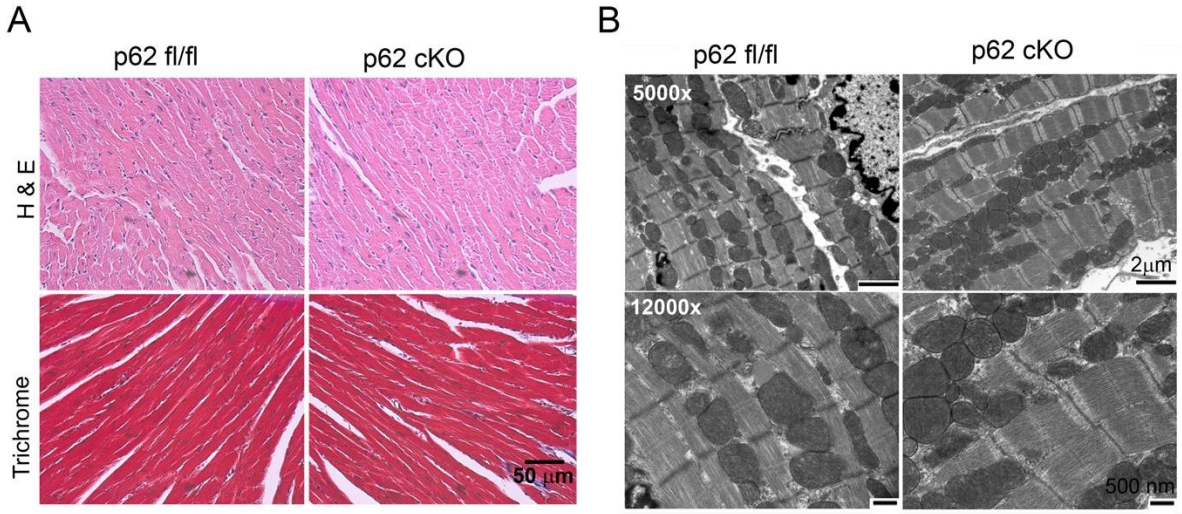

Figure 6.3: Loss of p62 does not affect myocardial structure. A. Representative hematoxylin and eosin-stained images (*top panel*), and Masson's trichrome stained images (*bottom panel*) of p62 cKO and p62 fl/fl mouse myocardium at 8 weeks of age. **B.** Representative transmission electron microscopy images to demonstrate myocardial ultrastructure in p62 cKO and p62 fl/fl mice at 8 weeks of age.

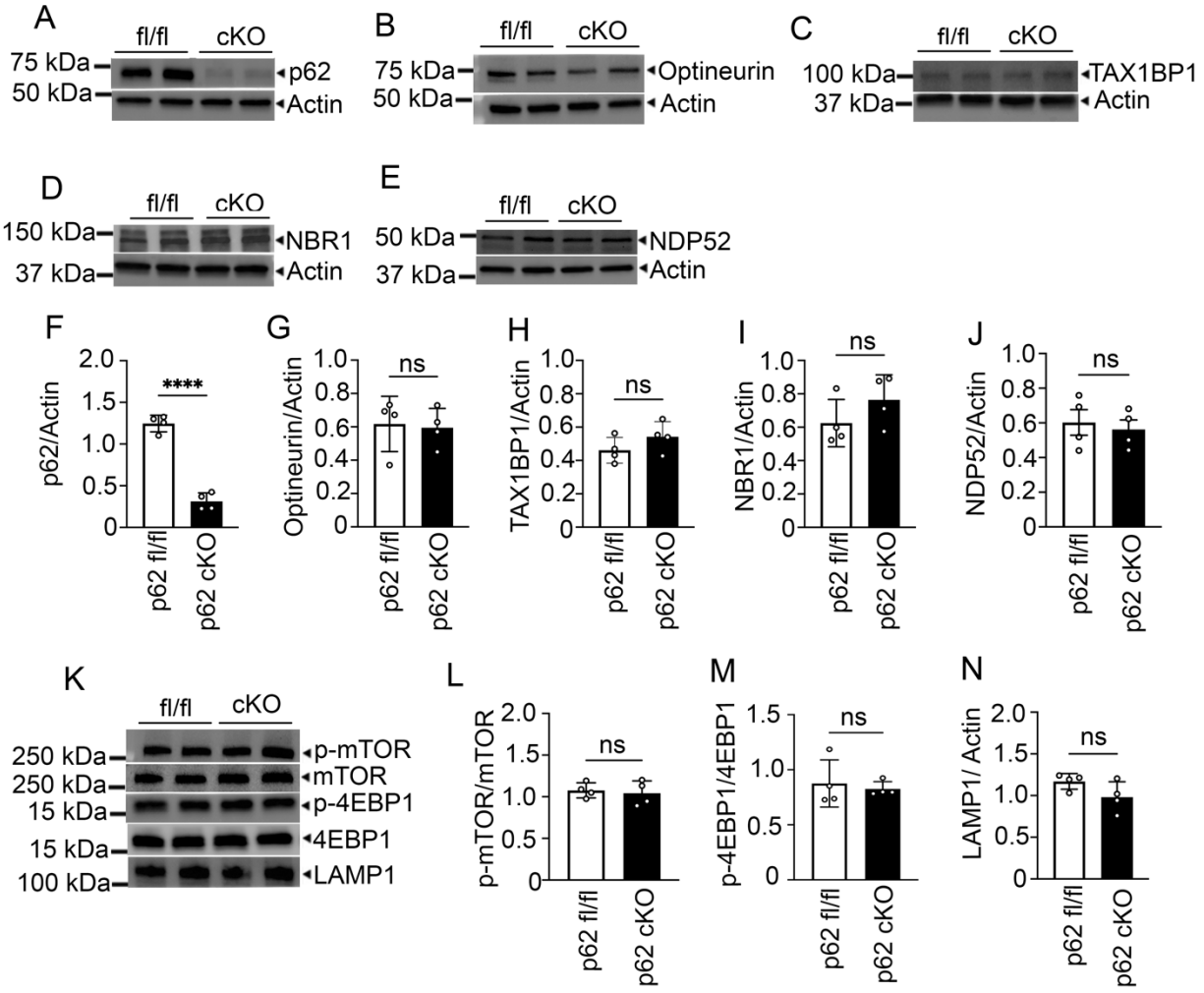

Figure 6.4: Expression of various autophagy adaptors, lysosomal proteins, and mTOR pathways is not significantly affected by cardiac myocyte p62 ablation in young adult mice. A-J) Representative immunoblots (A-E) and quantitation of p62 (F) and other autophagy adaptors optineurin (G), TAX1BP1 (H), NBR-1 (I) and NDP-52 (J) in the p62cKO young adult mice compared with p62 fl/fl mice as control. **** Indicates P<0.0001 by t-test. **K-N)** Representative immunoblot (K) and quantitation of phospho-mTOR (L), phospho-4EBP1 (M) and LAMP1 (N) in 62cKO young adult myocardium as compared with p62 fl/fl mice (as control). Statistical analyses were performed by t-test. 'ns' indicates not significant for all panels.

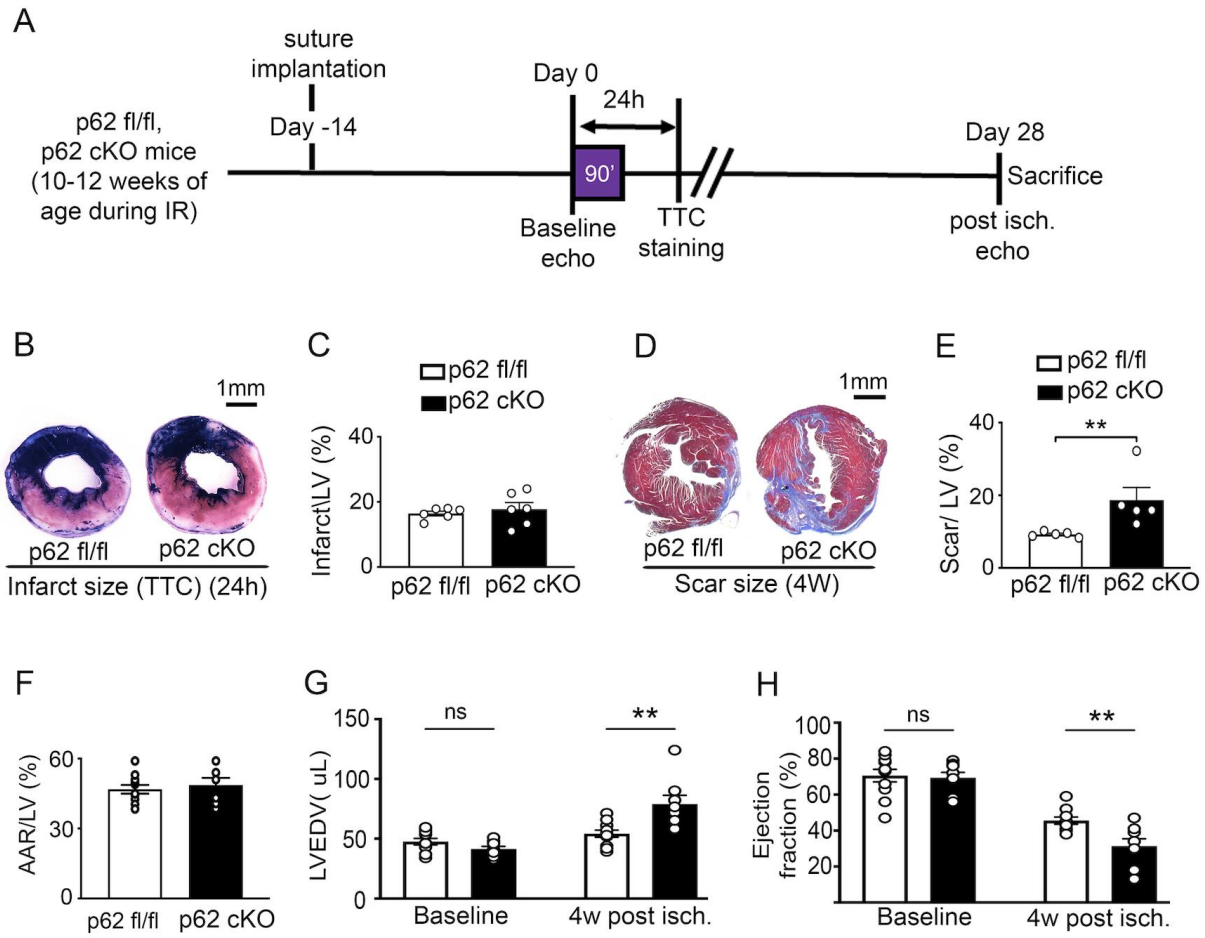

Figure 6.5: Cardiac myocyte p62 ablation worsens post-MI cardiomyopathy in mice. A) Schematic depicting experimental strategy for closed-chest IR modeling in p62cKO mice. **B, C)** Representative TTC-stained images (B) with quantitation of infarct area in young adult p62cKO and fl/fl mice hearts 24 hours (24h) post-IR injury. No statistically significant differences were detected by t-test. **D, E)** Representative Masson's trichrome-stained images (D) with quantitation of scar area (E) from p62cKO and fl/fl mice hearts at 4 weeks (4W) post-IR injury. ** indicates P value <0.01 by t-test. **F-H)** Quantitative analyses of area-at-risk (AAR, F) during LAD occlusion; and left ventricular end-diastolic volume (LVEDV, G) and LV ejection fraction (E,F, H) at baseline (i.e. prior to) and at 4 weeks after IR injury. ** denotes P < 0.01 by t-test. Echocardiographic parameters at baseline and 4 weeks post-IR injury are analyzed separately as they were performed under different anesthetic regimens.

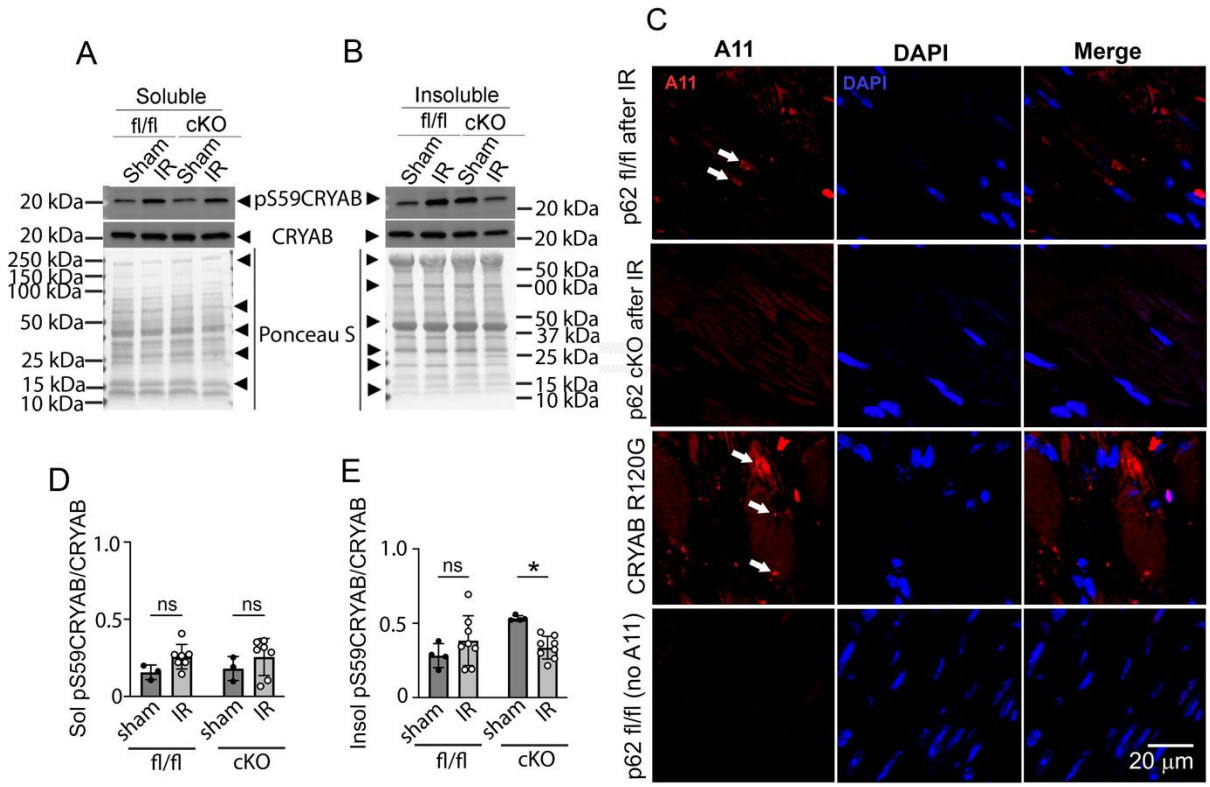

Figure 6.6: Cardiac-myocyte p62 ablation impairs sequestration of pS59CRYAB in aggregates. A-B, D-E) Representative immunoblot (A, B) depicting CRYAB and pS59CRYAB expression and quantitation (D, E) of fold change in pS59CRYAB over total CRYAB in NP40-detergent soluble (A, D) and insoluble (B, E) myocardial fractions from IR vs sham-treated p62cKO or fl/fl mice at 4-weeks after IR injury. Ponceau S staining is shown as loading control. *denotes P value <0.05 and by t-test. 'ns' indicates not significant. **C.** Representative images depicting anti-oligomeric antibody staining in p62cKO or fl/fl mice at 4-weeks after IR injury. Representative of n=5 hearts per group. Myocardial sections from a CRYAB-R120G transgenic mouse at 48 weeks of age with and without incubation with anti-oligomer antibody are shown as positive and negative controls, respectively. Arrows point to pre-amyloid oligomers in cardiac myocytes.

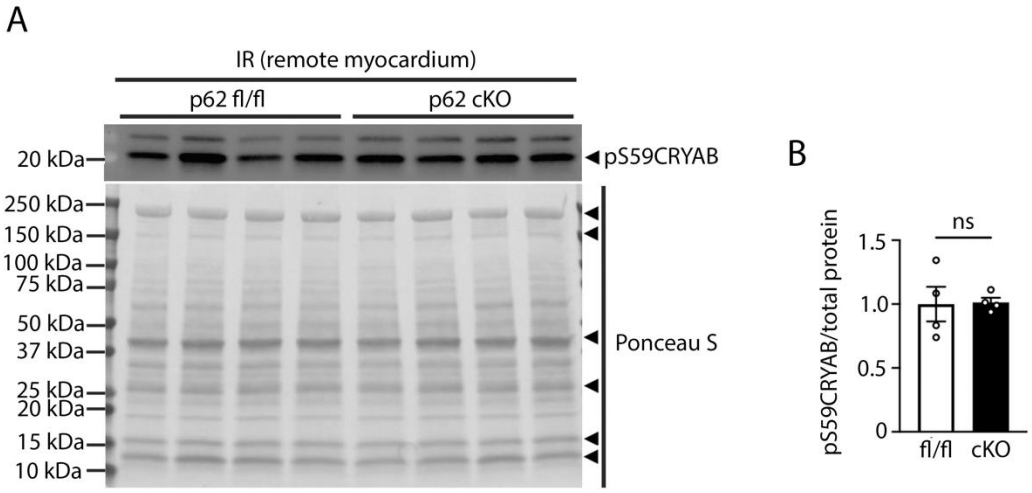

Figure 6.7: Total pS59CRYAB is unaffected in p62cKO mice after IR. A, B) Representative immunoblot (A) and quantitation (B) depicting total pS59CRYAB in crude extracts of remote myocardium from p62 cKO young adult mice of both sexes compared with floxed controls. 'ns' denotes not significant by t-test.

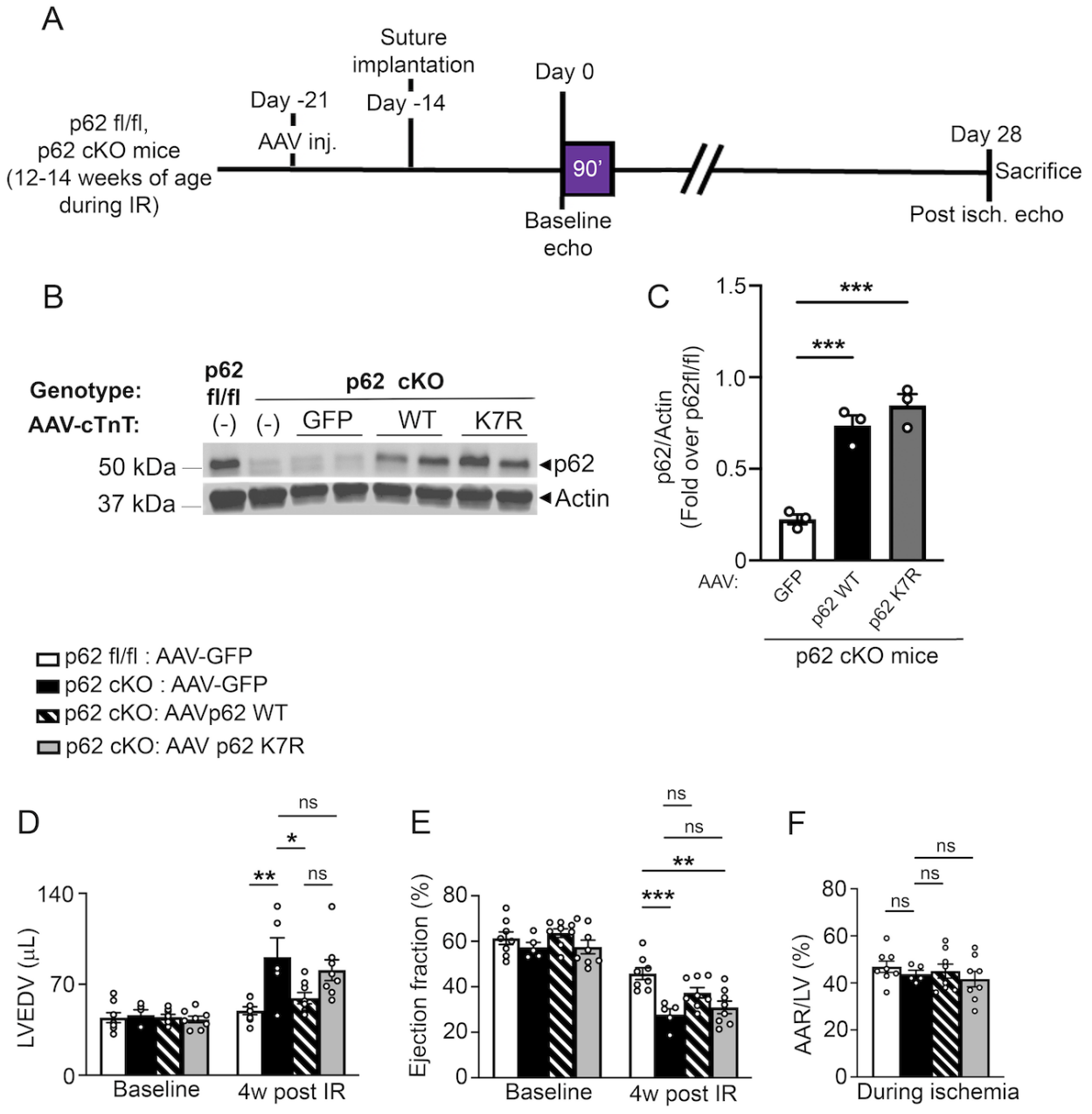

Figure 6.8: AAV9-cTnT promoter-driven restoration of p62 but not its aggregation-deficient K7R variant rescues post-MI cardiac remodeling in p62cKO mice. A) Schematic depicting experimental strategy for closed-chest IR modeling in p62cKO mice transduced with AAV9-cTnT-GFP (n=5), AAV9-cTnT-p62 WT (n=8) and AAV9-cTnT-p62 K7R (n=8) versus p62 fl/fl mice transduced with AAV9-cTnT-GFP (n=8). **B-C**) Representative immunoblot (B) and quantitation (C) of p62 expression in mice treated as in A. * denotes P <0.05 by Tukey's post-hoc test after one-way ANOVA. **D-F)** Quantitative analyses of left ventricular end-diastolic

volume (LVEDV, D) and LV ejection fraction (EF (%), E) at baseline (i.e. prior to) and at 4 weeks after IR injury. Quantitative assessment of area-at-risk (AAR, F) during LAD occlusion in mice treated as in A.* denotes $P < 0.05$, ** denotes $P < 0.01$ and *** denotes $P < 0.001$ by Tukey's post-hoc testing after one-way ANOVA. Echocardiographic parameters at baseline and 4-weeks post-IR injury are analyzed separately as they were performed under different anesthetic regimens.

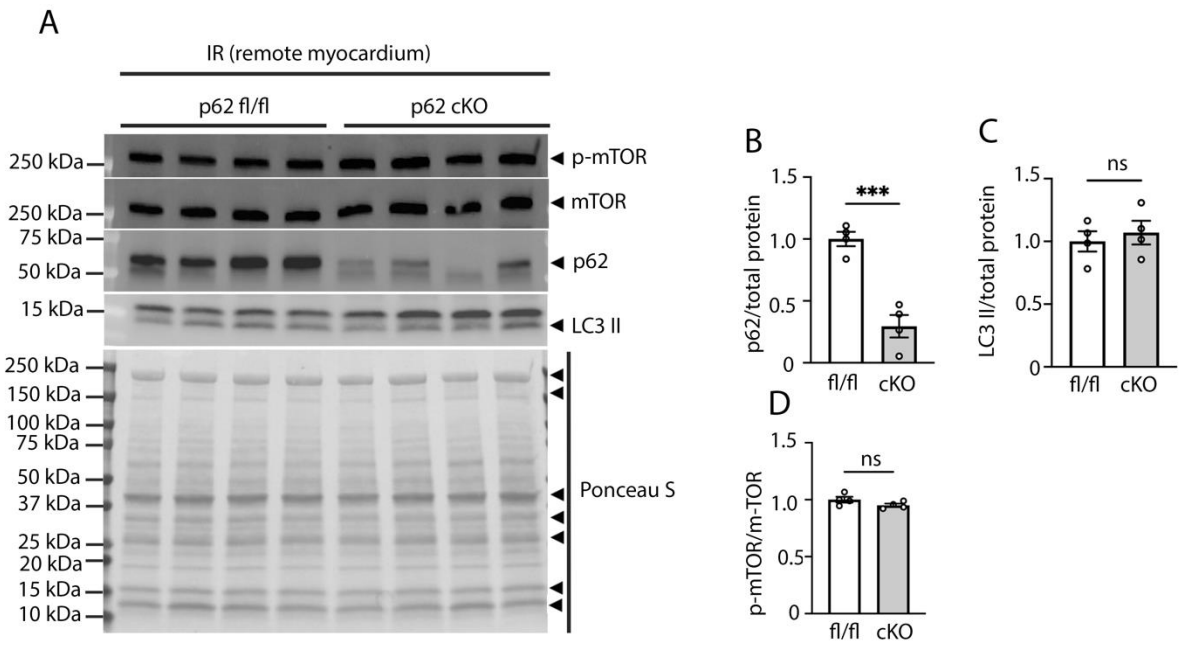

Figure 6.9: Autophagy marker proteins and mTOR pathway is not changed in p62cKO mice post-MI. A-D) Representative immunoblot (A) and quantitation (B-D) of p62 (B), LC3 II (C), phospho-mTOR/mTOR (D) depicting total proteins in crude extracts of remote myocardium from p62 cKO young adult mice of both sexes compared with floxed controls. *** indicates $p<0.001$ and 'ns' denotes not significant by t-test.

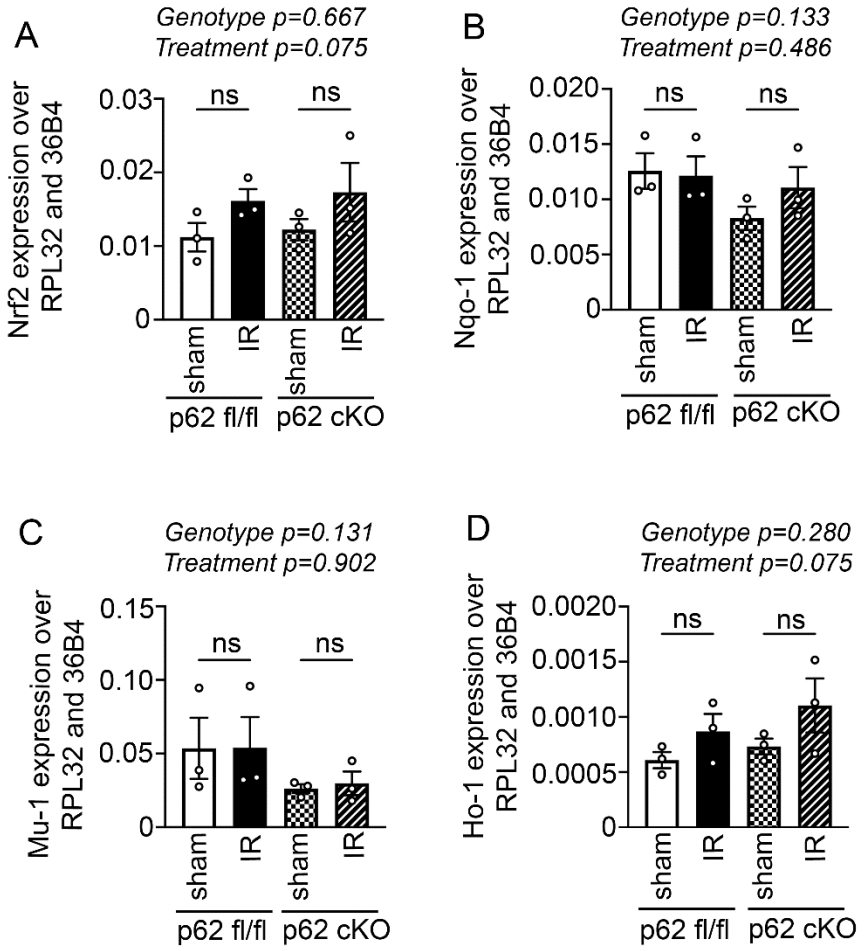

Figure 6.10: Cardiac myocyte ablation of p62 does not alter expression of Nrf2 or its target transcripts at 4 weeks post-MI. A-D) Quantitative PCR analyses for expression of *Nrf2* (A) transcripts and the transcripts for its target genes, namely *Nqo-1* (B), *Mu-1* (C) and *Ho-1* (D) in the myocardium from p62 cKO and p62 floxed mice at 4 weeks after IR injury. Indicated P values on top of the panels represent factor comparisons by 2-way ANOVA including genotype and treatment as fixed factors, followed by Tukey's post-hoc test, where 'ns' indicates 'not significant'.

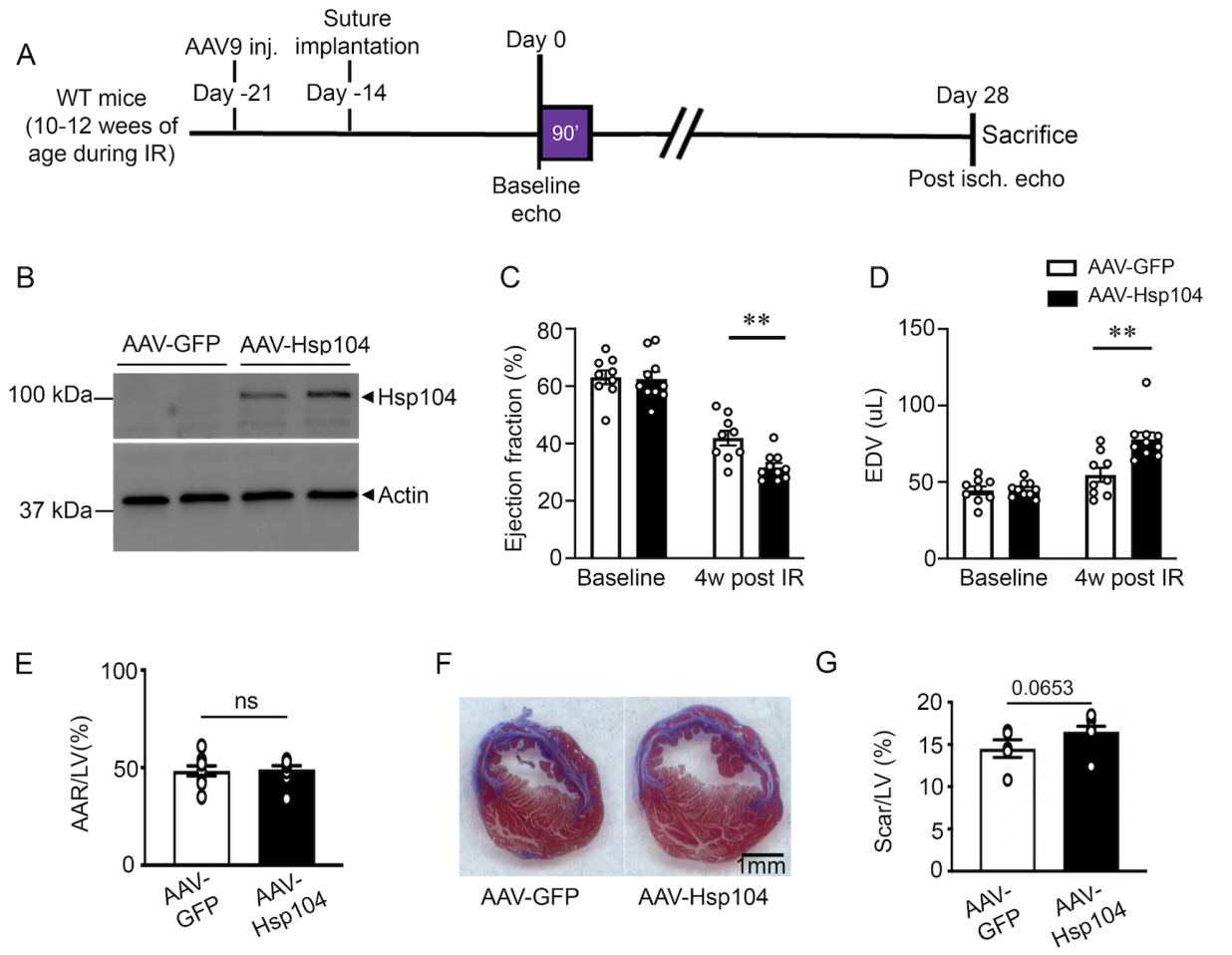

Figure 6.11: AAV9-mediated expression of fungal disaggregase Hsp104 worsens post-MI cardiomyopathy. A) Schematic depicting experimental strategy for closed-chest IR modeling in C57BL6/J wild-type mice transduced with AAV9-CMV-Hsp104 or AAV9-CMV-GFP. **B)** Representative immunoblot of Hsp104 expression in C57BL6J wild-type mouse myocardium prior to IR modeling. Actin is shown as loading control. **C-E)** Quantitative analyses of LV ejection fraction (EF (%), C), left ventricular end-diastolic volume (EDV, D) prior to and at 4 weeks after IR injury, and area-at risk (E) in wild-type mice transduced with AAV9-Hsp104 (or AAV9-GFP as control). Echocardiographic parameters at baseline and 4 weeks post-IR injury are analyzed separately as they were performed under different anesthetic regimens. ** denotes P <0.01 by t-test in C and by Mann-Whitney test in D. **F, G)** Representative Masson's trichrome stained images (F) and quantitation of scar size (G) 4 weeks after IR injury. P value is by t-test.

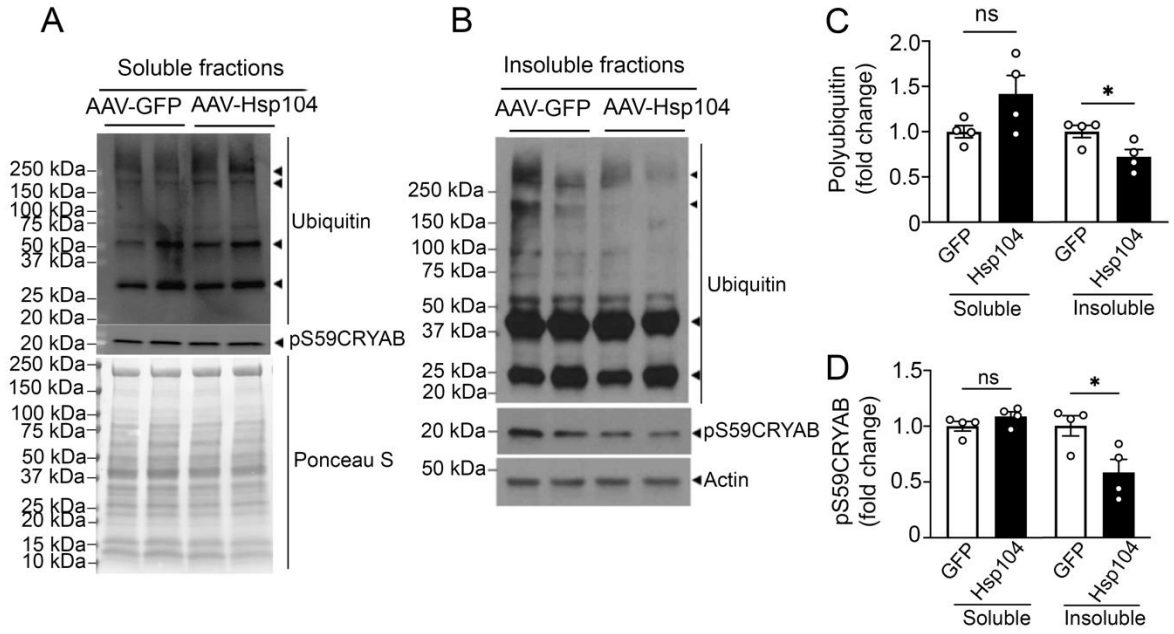

Figure 6.12: AAV9-mediated expression of fungal disaggregase Hsp104 impaired sequestration of pS59CRYAB in the aggregate-rich insoluble fraction. A, B) Representative immunoblots depicting total polyubiquitinated proteins and pS59CRYAB expression in NP40-detergent soluble (A) and insoluble (B) fractions in the myocardium at 4 weeks after IR injury. Ponceau S staining and Actin are shown as loading controls, respectively. **C, D)** Quantitation of total polyubiquitinated proteins (C) and pS59CRYAB (D) in NP40-detergent soluble and insoluble fractions from the myocardium of C57BL6J mice transduced with AAV9-Hsp104 (or AAV9-GFP as control) after closed-chest IR injury as in A. * denotes $P < 0.05$ by t-test.

6.7 References

1. Mogk A, Ruger-Herreros C, Bukau B. Cellular Functions and Mechanisms of Action of Small Heat Shock Proteins. *Annu Rev Microbiol*. 2019;73:89-110. doi: 10.1146/annurev-micro-020518-115515
2. Walther DM, Kasturi P, Zheng M, Pinkert S, Vecchi G, Ciryam P, Morimoto RI, Dobson CM, Vendruscolo M, Mann M, et al. Widespread Proteome Remodeling and Aggregation in Aging C. elegans. *Cell*. 2015;161:919-932. doi: 10.1016/j.cell.2015.03.032
3. Ma X, Mani K, Liu H, Kovacs A, Murphy JT, Foroughi L, French BA, Weinheimer CJ, Kraja A, Benjamin IJ, et al. Transcription Factor EB Activation Rescues Advanced αB-Crystallin Mutation-Induced Cardiomyopathy by Normalizing Desmin Localization. *J Am Heart Assoc*. 2019;8:e010866. doi: 10.1161/jaha.118.010866
4. du Pré BC, Dierickx P, Crnko S, Doevendans PA, Vos MA, Geijsen N, Neutel D, van Veen TAB, van Laake LW. Neonatal rat cardiomyocytes as an in vitro model for circadian rhythms in the heart. *J Mol Cell Cardiol*. 2017;112:58-63. doi: 10.1016/j.yjmcc.2017.08.009
5. Bjørkøy G, Lamark T, Brech A, Outzen H, Perander M, Overvatn A, Stenmark H, Johansen T. p62/SQSTM1 forms protein aggregates degraded by autophagy and has a protective effect on huntingtin-induced cell death. *J Cell Biol*. 2005;171:603-614. doi: 10.1083/jcb.200507002
6. Pankiv S, Clausen TH, Lamark T, Brech A, Bruun JA, Outzen H, Øvervatn A, Bjørkøy G, Johansen T. p62/SQSTM1 binds directly to Atg8/LC3 to facilitate degradation of ubiquitinated protein aggregates by autophagy. *J Biol Chem*. 2007;282:24131-24145. doi: 10.1074/jbc.M702824200
7. Birgisdottir Å B, Lamark T, Johansen T. The LIR motif - crucial for selective autophagy. *J Cell Sci*. 2013;126:3237-3247. doi: 10.1242/jcs.126128
8. Pan JA, Sun Y, Jiang YP, Bott AJ, Jaber N, Dou Z, Yang B, Chen JS, Catanzaro JM, Du C, et al. TRIM21 Ubiquitylates SQSTM1/p62 and Suppresses Protein Sequestration to Regulate Redox Homeostasis. *Mol Cell*. 2016;61:720-733. doi: 10.1016/j.molcel.2016.02.007
9. Sergin I, Bhattacharya S, Emanuel R, Esen E, Stokes CJ, Evans TD, Arif B, Curci JA, Razani B. Inclusion bodies enriched for p62 and polyubiquitinated proteins in macrophages protect against atherosclerosis. *Sci Signal*. 2016;9:ra2. doi: 10.1126/scisignal.aad5614
10. Vashist S, Cushman M, Shorter J. Applying Hsp104 to protein-misfolding disorders. *Biochem Cell Biol*. 2010;88:1-13. doi: 10.1139/o09-121
11. Chernova TA, Wilkinson KD, Chernoff YO. Prions, Chaperones, and Proteostasis in Yeast. *Cold Spring Harb Perspect Biol*. 2017;9. doi: 10.1101/cshperspect.a023663
12. Sweeny EA, Shorter J. Mechanistic and Structural Insights into the Prion-Disaggregase Activity of Hsp104. *J Mol Biol*. 2016;428:1870-1885. doi: 10.1016/j.jmb.2015.11.016
13. Mack KL, Kim H, Barbieri EM, Lin J, Braganza S, Jackrel ME, DeNizio JE, Yan X, Chuang E, Tariq A, et al. Tuning Hsp104 specificity to selectively detoxify α-synuclein. *Mol Cell*. 2023;83:3314-3332.e3319. doi: 10.1016/j.molcel.2023.07.029
14. Jackrel ME, DeSantis ME, Martinez BA, Castellano LM, Stewart RM, Caldwell KA, Caldwell GA, Shorter J. Potentiated Hsp104 variants antagonize diverse proteotoxic misfolding events. *Cell*. 2014;156:170-182. doi: 10.1016/j.cell.2013.11.047

15. Torrente MP, Chuang E, Noll MM, Jackrel ME, Go MS, Shorter J. Mechanistic Insights into Hsp104 Potentiation. *J Biol Chem*. 2016;291:5101-5115. doi: 10.1074/jbc.M115.707976
16. Pan JA, Sun Y, Jiang YP, Bott AJ, Jaber N, Dou Z, Yang B, Chen JS, Catanzaro JM, Du C, et al. TRIM21 Ubiquitylates SQSTM1/p62 and Suppresses Protein Sequestration to Regulate Redox Homeostasis. *Molecular cell*. 2016;62:149-151. doi: 10.1016/j.molcel.2016.03.015
17. Kirkin V, Rogov VV. A Diversity of Selective Autophagy Receptors Determines the Specificity of the Autophagy Pathway. *Molecular cell*. 2019;76:268-285. doi: https://doi.org/10.1016/j.molcel.2019.09.005
18. Pan B, Li J, Parajuli N, Tian Z, Wu P, Lewno MT, Zou J, Wang W, Bedford L, Mayer RJ, et al. The Calcineurin-TFEB-p62 Pathway Mediates the Activation of Cardiac Macroautophagy by Proteasomal Malfunction. *Circ Res*. 2020. doi: 10.1161/CIRCRESAHA.119.316007
19. Silva-Islas CA, Maldonado PD. Canonical and non-canonical mechanisms of Nrf2 activation. *Pharmacological research*. 2018;134:92-99. doi: 10.1016/j.phrs.2018.06.013
20. Lo Bianco C, Shorter J, Régulier E, Lashuel H, Iwatsubo T, Lindquist S, Aebischer P. Hsp104 antagonizes alpha-synuclein aggregation and reduces dopaminergic degeneration in a rat model of Parkinson disease. *J Clin Invest*. 2008;118:3087-3097. doi: 10.1172/jci35781
21. Bjorkoy G, Lamark T, Brech A, Outzen H, Perander M, Overvatn A, Stenmark H, Johansen T. p62/SQSTM1 forms protein aggregates degraded by autophagy and has a protective effect on huntingtin-induced cell death. *The Journal of cell biology*. 2005;171:603-614. doi: 10.1083/jcb.200507002
22. Godar RJ, Ma X, Liu H, Murphy JT, Weinheimer CJ, Kovacs A, Crosby SD, Saftig P, Diwan A. Repetitive stimulation of autophagy-lysosome machinery by intermittent fasting preconditions the myocardium to ischemia-reperfusion injury. *Autophagy*. 2015;11:1537-1560. doi: 10.1080/15548627.2015.1063768
23. Ma X, Mani K, Liu H, Kovacs A, Murphy JT, Foroughi L, French BA, Weinheimer CJ, Kraja A, Benjamin IJ, et al. Transcription Factor EB Activation Rescues Advanced alphaB-Crystallin Mutation-Induced Cardiomyopathy by Normalizing Desmin Localization. *Journal of the American Heart Association*. 2019;8:e010866. doi: 10.1161/JAHA.118.010866
24. Ma X, Rawnsley DR, Kovacs A, Islam M, Murphy JT, Zhao C, Kumari M, Foroughi L, Liu H, Qi K, et al. TRAF2, an Innate Immune Sensor, Reciprocally Regulates Mitophagy and Inflammation to Maintain Cardiac Myocyte Homeostasis. *JACC Basic Transl Sci*. 2022;7:223-243. doi: 10.1016/j.jacbts.2021.12.002
25. Harada H, Warabi E, Matsuki T, Yanagawa T, Okada K, Uwayama J, Ikeda A, Nakaso K, Kirii K, Noguchi N, et al. Deficiency of p62/Sequestosome 1 causes hyperphagia due to leptin resistance in the brain. *The Journal of neuroscience : the official journal of the Society for Neuroscience*. 2013;33:14767-14777. doi: 10.1523/jneurosci.2954-12.2013
26. Agah R, Frenkel PA, French BA, Michael LH, Overbeek PA, Schneider MD. Gene recombination in postmitotic cells. Targeted expression of Cre recombinase provokes cardiac-restricted, site-specific rearrangement in adult ventricular muscle in vivo. *The Journal of clinical investigation*. 1997;100:169-179. doi: 10.1172/JCI119509

27. Bhuiyan MS, Pattison JS, Osinska H, James J, Gulick J, McLendon PM, Hill JA, Sadoshima J, Robbins J. Enhanced autophagy ameliorates cardiac proteinopathy. *J Clin Invest*. 2013;123:5284-5297. doi: 10.1172/jci70877
28. Ghosh R, Fatahian AN, Rouzbehani OMT, Hathaway MA, Mosleh T, Vinod V, Vowles S, Stephens SL, Chung SD, Cao ID, Jonnavithula A, Symons JD, Boudina S. Sequestosome 1 (p62) mitigates hypoxia-induced cardiac dysfunction by stabilizing hypoxia-inducible factor 1α and nuclear factor erythroid 2-related factor 2. Cardiovasc Res. 2024 Apr 30;120(5):531-547. doi: 10.1093/cvr/cvae023. PMID: 38332738; PMCID: PMC11060490

6.8 Supporting Materials

Table 6.1: Morphometric and echocardiographic assessment of p62 fl/fl and p62 cKO young adult mice between 6-8 weeks of age.

Group	BW (gm)	HW/TL (mg/mm)	LVIDd (mm)	LVIDs (mm)	%FS	IVSd (mm)	LVPWd (mm)	LVM (mg)	r/h	HR (per min)
p62 fl/fl (M=6, F=3)	21.4 ± 1.0	8.8 ± 0.1	3.58 ± 0.07	1.81 ± 0.07	49.5 ± 1.2	0.67 ± 0.01	0.63 ± 0.02	73.7 ± 2.9	2.75 ± 0.08	601.84 ± 11.10
p62 cKO (M=6, F=10)	21.1 ± 0.80	7.7 ± 0.4	3.69 ± 0.07	2.03 ± 0.08	45.2 ± 1.6	0.62 ± 0.02	0.59 ± 0.01	70.8 ± 3.2	3.07 ± 0.08	613.54 ± 10.80

All data are shown as Mean ± SEM. No statistically significant differences were noted between groups. Abbreviations are as follows: ‘M’ indicates male, ‘F’ indicates female, ‘BW’ indicates body weight, ‘HW/TL’ indicates heart weight indexed to tibial length, ‘LVIDd’ indicates left ventricular internal diameter in diastole, ‘LVEDs’ indicates left ventricular internal diameter in systole, ‘%FS” indicates percent endocardial fractional shortening, ‘IVSd’ indicates interventricular septum thickness in diastole, ‘LVPWd’ indicates left ventricular posterior wall thickness in diastole, ‘LVM, indicates left ventricular mass, ‘r/h’ indicates ratio of left ventricular radius to wall thickness, and ‘HR’ indicates heart rate.

Chapter 7: Conclusion and future studies

7.1 Conclusion

Our study showed impaired protein quality control in ischemic cardiomyopathy human patients and in mouse hearts undergoing post-myocardial infarction cardiac remodeling. We demonstrated it by showing mis-localization and presence of aggregates of CRYAB clients desmin, actin, and α-actinin and increased pS59CRYAB in the insoluble fraction. We also showed CRYAB undergoes phase separation in our study that demonstrate how a cardiac chaperone protein might perform its function by forming condensates. Phosphorylation in CRYAB (phospho-mimetic variant S59D and disease-associated R120G) alters its phase separation properties by reducing dynamicity. Introducing the phospho-deficient S59A mutation, but not the phospho-mimetic S59D mutation, at the CRYAB locus in mouse rescued adverse left ventricular remodeling after post-MI. S59D mouse does not show cardiac function abnormality at baseline without stress but shows impaired protein quality observed by increased polyubiquitinated proteins. This shows that impaired protein quality at 10-11 weeks of age might not be sufficient to cause cardiac function abnormality, and also abnormal protein quality control occurs prior to cardiac dysfunction. S59A mouse showed reduced interaction with desmin. Perhaps, this reduced interaction between desmin and CRYAB is protective in post-MI cardiac remodeling because we observed reduced mis-localization and aggregates of desmin in S59A mouse than S59D or WT mouse. Pharmacological chaperone 25-Hydroxycholesterol reduces total serine-59 phosphorylation, rescues post-myocardial infarction cardiac dysfunction and reduces scar size. Preventing aggregate formation by ablating p62 expression in the cardiac myocytes or promoting disaggregation by overexpressing Hsp-104 exacerbated post-myocardial

infarction cardiomyopathy by reduced sequestration of pS59CRYAB in the insoluble fraction and by not reducing the total pS59CRYAB in the crude extract after IR. This showed that reduction of total pS59CRYAB is sufficient to cause protection after IR, and there could be a contextual based protective role of protein aggregates by sequestering toxic aggregate-prone proteins after IR. However, future studies are needed to further demonstrate the mechanism of reduced sequestration of pS59CRYAB in the insoluble fraction. Also, we could perform experiments to determine how CRYAB client proteins, desmin, actin and α-actinin are localized in p62cKO mice after IR demonstrating the protein quality control in absence of p62 in cardiac myocytes.

7.2 Future studies

Our study showed a novel condensatopathy mechanism to demonstrate how abnormal condensate formation of CRYAB worsens post-MI cardiomyopathy. However, certain area remains unexplored. Nature has selected serine-59 as the crucial phosphorylation site in CRYAB function, and specifically p38 MAPK phosphorylates it. Further experiments could be done to explore if there is an acute vs persistent stress difference in CRYAB S59 phosphorylation and its interaction with client proteins. Evaluating cardiac functions in both S59D and S59A mouse models in acute vs persistent stress can be explored in this regard showing whether there could be a contextual-based role of CRYAB phosphorylation. We can also perform future studies to have alternate explanations of how S59A mouse shows protective effect after MI and reduced scar size at 4-weeks. We can perform single-cell RNAseq studies in WT, S59A and S59D mouse after IR and determine if there are any differences in specific cellular pathways and cell populations that might contribute to the protective effect of S59A. Our study was based on

mostly male ICM human heart samples. Subsequent investigations could focus on expanding the inclusion of more female ischemic cardiomyopathy (ICM) samples to observe whether female hearts also have similar pathological outcome. An important consideration in this study was the absence of a stable cell line expressing CRYAB variants that we used for in vitro phase separation experiment using optoIDR constructs[1]. As desmin is not sufficiently expressed in HEK cells, further studies could also be done using iPSC-cardiomyocytes model to observe how desmin expression and interaction with CRYAB is affected by altered CRYAB phase separation. To better replicate physiological conditions, future experiments could also be done utilizing purified CRYAB and client proteins and conduct mixing studies. This will help to construct phase diagrams of protein condensate formation and determine how saturation concentration of CRYAB is affected by phosphorylation or disease-associated mutation. It is also important to explore if there are additional stress such as aging that can worsen cardiac function when CRYAB is phosphorylated. CRYAB S59D KI/KI mice can be compared to S59A KI/KI and WT mice in this aspect. Additionally, elucidating the mechanism by which 25-Hydroxycholesterol (25-HC) reduces total CRYAB levels, whether through targeting p38 MAPK itself or by binding and stabilizing CRYAB from p38 phosphorylation, could be explored. We focused on desmin-CRYAB abnormal interaction in this study as the potential mechanism of desmin mis-localization upon stress and to represent impairment in protein quality control. Investigating the potential interactions between CRYAB and other client proteins such as α-actinin, and actin could be done that as well can demonstrate a wide-range of disarray of CRYAB client protein and impaired protein quality control. These avenues of inquiry will further our understanding of CRYAB dynamics in ischemic cardiomyopathy.

7.3 Concluding remarks

Our study demonstrated abnormal condensate properties upon phosphorylation as the mechanistic link between proteotoxicity and protein-aggregates in the more common ischemic cardiomyopathy by focusing on CRYAB, the most abundant cardiac chaperone protein.

7.4 References

1. Shin Y, Berry J, Pannucci N, Haataja MP, Toettcher JE, Brangwynne CP. Spatiotemporal Control of Intracellular Phase Transitions Using Light-Activated optoDroplets. *Cell*. 2017;168:159-171.e114. doi: 10.1016/j.cell.2016.11.054